Active Noise Control of Supersonic Impinging Jet using Pulsed Microjets

by

Seung Hyuck Hong

B.S., Seoul National University (2007)

Submitted to the Department of Mechanical Engineering
in partial fulfillment of the requirements for the degree of

Master of Science in Mechanical Engineering

at the

MASSACHUSETTS INSTITUTE OF TECHNOLOGY

February 2009

Author .....
Department of Mechanical Engineering
Jan 15, 2009

Certified by .....
Anuradha M. Annaswamy
Senior Research Scientist
Thesis Supervisor

Accepted by .....
David E. Hardt
Chairman, Department Committee for Graduate Students

Active Noise Control of Supersonic Impinging Jet using Pulsed Microjets

by

Seung Hyuck Hong

Submitted to the Department of Mechanical Engineering
on Jan 15, 2009, in partial fulfillment of the
requirements for the degree of
Master of Science in Mechanical Engineering

Abstract

This thesis concerns an active noise control of supersonic impinging jet flow using unsteady microjet injection. Supersonic impinging jet involves several problems such as lift loss, ground erosion, significant noise pollution, and sonic fatigue, all of which are dominated by impinging tones mainly caused by well-known phenomenon, the feed back loop. The main goal of this study is to achieve uniform and consistent noise reduction in the entire range of jet operating condition, by means of intercepting this feed back loop. Experimental investigations on ideally expanded Mach number 1.5, supersonic impinging jet flow were carried out at the scaled supersonic experimental facility. The actuator used for active control is composed of pulsed microjets, utilizing a fraction of mass flow rate needed with steady microjets. Two means of producing pulsed microjet were introduced; one with a rotating cap, pulsing at 16 - 100Hz, and the other developed based on the principle of Hartmann tube, pulsing at 4.4 - 6.1kHz, referred to as *high frequency actuator*. Control parameters related to pulsed microjet injection with rotating cap were varied to evaluate their effects on suppression of impinging tones, whereas the effect of high frequency actuator is shown only as an initial step and needs further investigation in the future. For pulsed microjet with rotating cap, mass flow rate, directly proportional to the supply pressure of microjet, is found to be the most important parameter amongst all and *saturated supply pressures* for steady and pulsed microjet are demonstrated. It is demonstrated that pulsed microjet gives more noise reduction than steady microjet with the same mass flow rate, at certain range of supply pressure, and also that pulsed microjet could be as effective on suppression of impinging tones as steady microjet with less mass flow rate. In addition, the effect of pulsed microjet on hot temperature impinging jet was examined since the jet is much hotter than ambient air in reality. The concept of extremum control strategy is introduced to more efficiently find an optimal pulsing condition for uniform and consistent noise reduction.

Thesis Supervisor: Anuradha M. Annaswamy
Title: Senior Research Scientist

Acknowledgments

First and foremost, I would like to thank Dr. Anuradha Annaswamy, my thesis advisor, for her guidance, support, patience, enthusiasm and attention to detail. Owing to her leadership, I have learned to see a bigger picture, changing my way of thinking.

None of the works in this thesis would have been possible without the help of several people at Florida State University. I would like to thank Professor Farrukh Alvi and Dr. Rajan Kumar for their guidance, enthusiasm and dedication to this study. I would also like to thank Dr. Brent Greska for his valuable advices and help regarding the experimental works. Bobby Avant, the lab machinist deserves special mention for providing professional skill in fabrication of experimental facility and related hardware; his prompt advice and help to design and fabricate hardware for experiment enabled me to conduct some crucial tests. I would also like to thank Sladana Lazic, Alex Wiley for their help to conduct experiments, and John Solomon for his invaluable advice and help regarding *high frequency actuator* .

I would like to thank my colleagues of Active Adaptive Control Laboratory at MIT, especially Dr. Jinho Jang, Paul Ragaller, and Dr. Jae Jeen Choi, for their invaluable advices and support. I also thank to the colleagues of Advanced Aero Propulsion Laboratory at Florida State University, for refreshments at the daily coffee hour.

Special thanks to my family, father, Dr. Chang-Sun Hong, my mother, Soon-Hee Lee, my sisters, Janet and Helen, and their husbands, Kyemoo and Jungho, for their unlimited mental support during my life at MIT. Thanks to all of my friends for their mental support.

The help and consideration of all those mentioned above are sincerely appreciated.

Contents

List of Figures

Chapter 1

Introduction

1.1 Flow Control

1.1.1 Overview

Flow control, in general, is an attempt to alter the character or disposition of a flow field favorably. The science of flow control originated with a well-known scholar, Prandtl (1904), who introduced the boundary layer theory and explained the physics of the separation phenomena [8]. He also described several experiments in which a boundary layer was controlled. An overview of flow control and specific examples of each kind of flow control are given in section 1.1[1], where more details can be found in [8].

Realizing efficient flow-control systems has many potential benefits such as not only saving billions of dollars in annual fuel costs for land, air, and sea vehicles, but also achieving economically and environmentally more competitive industrial processes involving fluid flows. Since flow control goals are strongly, often adversely, interrelated, a particular control strategy may vary depending on the kind of flow and specific control goal to be achieved. Presence or lack of walls, Reynolds and Mach numbers, and the character of the flow instabilities are all important considerations when one should choose the type of control to be applied. Altering flow

[1]Section 1.1 as a whole refers to [8] and briefly describes an overview of flow control.

characteristic may be to delay or advance transition, to suppress or enhance turbulence, or to prevent or provoke separation. By these attempts, our expected and desired result can be: drag reduction, lift enhancement, mixing augmentation, and flow-induced noise suppression.

Control strategies to achieve a desired effect can be classified based on the presence of energy expenditure and control loop involved [8]. If a control device requires no auxiliary power and no control loop, it is referred to be passive control. On the other hand, active control refers to requiring energy expenditure. Moreover, active control may require a control loop and can be further divided into predetermined or reactive categories. Predetermined control includes the application of steady or unsteady energy input without regard to the particular state of the flow. The control loop in this case is open loop, and no sensors are required for feedforward or feedback. Reactive control is a special class of active control in which the control input is continuously adjusted based on measurements of some kind. The control loop in this case can either be an open feedforward one or a closed feedback loop. Classical control theory deals, for the most part, with reactive control. The distinction between feedforward and feedback is particularly important when dealing with the control of flow structures that convect over stationary sensors and actuators. In the feedforward control, the measured variable and the controlled variable differ. For example, the pressure or velocity can be measured at an upstream location and the resulting signal is used together with an appropriate control law to trigger an actuator, which in turn influences the velocity at a downstream position. Feedback control, on the other hand, necessitates that the controlled variable be measured, fed back, and compared with a reference input. Reactive feedback control can be further classified into four categories: adaptive, physical-model-based, dynamical systems-based and optimal control - these naming can vary.

Flow control may involve passive or active devices to effect a beneficial change in wall-bounded or free-shear flows. The challenge is to achieve a goal using a simple device that is inexpensive to build as well as to operate, and the most important, has minimum side effects. In the following section, some of the flow controls in the

literature will be introduced.

1.1.2 Examples of Flow Controls

(1) Transition control

To delay or advance transition could be a good example of altering the characteristic of the flow field. Delaying laminar-to-turbulence transition of a boundary layer, to be more specific, has many obvious advantages; the skin friction drag in the laminar state can be as much as an order of magnitude less than that in the turbulent condition. This can be beneficial in that the aircraft or underwater body can have longer range, with less fuel cost, and with increased speed. Moreover, flow induced noise from the pressure fluctuations in the turbulent boundary layer is absent when the flow is laminar. However, turbulent flow can also have some good aspects, as an efficient mixer in terms of mass, momentum and heat transfer. Therefore, one can enhance heat transfer rate by advance laminar-to turbulent transition, as desired in heat exchangers or combustors.

One of examples of transition control is wall heating or cooling. Linke [9] observed that the drag of a flat plate placed in a wind tunnel increases by a large amount when the plate is heated. Motivated by Linke, both Frick and McCullough [10] and Liepmann and Fila [11] showed that the transition location of a flat-plate boundary layer in air at low subsonic speeds is moved forward when the surface is heated. Lees [12] also confirmed these observations, and moreover, showed that cooling has the exact opposite effects. All of these works are such good examples of active flow control.

(2) Separation control

The performance of many practical devices is often limited by the separation location of the flow, due to the large energy losses associated with boundary layer separation. For example, if separation is postponed, the pressure drag of a bluff body is decreased, the circulation and hence the lift of an airfoil at high angle of attack is enhanced,

and the pressure recovery of a diffuser is improved. On the other hand, the high lift capabilities of delta wings are achieved by provoking separation and forming leading-edge vortices.

Schubaur and Skramstad [13] observed that sound at particular frequencies and intensities could enhance the momentum exchange within a boundary layer and could, therefore, advance the transition location. Moreover, Collins and Zelenevitz [14] introduced the external acoustic excitation technique to enhance the lift of an airfoil and Ahuja et al. [15] successfully demonstrated that sound at certain frequency and sufficient amplitude can postpone the separation of a turbulent boundary layer developing on an airfoil in both pre- and post-stall regimes.

One of the recent developments of flow separation control is vortex generators. Streamwise vortex generation via discrete blowing or injection could lead to turbulence or Reynolds stress amplification, and thus, can actively add a momentum to the flow field. This supply of additional energy to the near-wall fluid particles that are being retarded in the boundary layer - that is about to be separated- can delay separation of the flow. Papell [16] addressed vortex generation within the injection jet itself. Also, Bradley and Wray [17] tried spanwise injection along the leading edges of swept wings for upper surface separation control. Moreover, Johnston and Nishi [18] employed spanwise arrays of small, skewed, pitched jets from holes on the surface, and have shown that the jets can produce longitudinal vortices strong enough to reduce or eliminate a large stalled region of turbulent separated flow. Although it is clear that discrete jets will generate vortices and thereby delay separation, the optimal condition of jet injection - such as spacing, geometry and size of individual hole, velocity and pressure - should be more investigated.

(3) Noise reduction

Noise, in this context, is referred to be an undesired sound particularly generated by a fluid flow. Noise suppression generally involves the reduction of noise sources' efficiency and ability to convert kinetic energy to sound power, the interruption of sound transmission, the accelerated dissipation of acoustic energy into heat, or the

active cancelation of sound waves using out-of-phase waves. These strategies can be implemented by a variety of passive, active, and reactive devices ranging in complexity from simple ear plugs to complicated anti-sound systems; in general, by reducing the vibrations of solid surfaces, eliminating or suppressing turbulence, or by appropriate management of certain flow instabilities and coherent structures.

For cold subsonic flows, in such a specific case, small scale turbulence fluctuations and unsteady flow oscillations, either in free shear modes or interacting with solid surfaces, provide the primary sources for the flow-induced sound energy. For hot supersonic flows, on the other hand, the interaction of the turbulent large eddies with the flow is the dominant noise source. In either case, controlling the flow modulates the sound field favorably or adversely. As in these examples, controls of flow characteristics are not individual, but correlated to one another.

In section 1.1, an overview of flow control has been introduced with several examples. The present study deals with the specific case of flow control, a noise control in supersonic impinging jet flow. The primary objective is to reduce noise in supersonic impinging jet problem, which can be easily seen in Short Take Off and Vertical Landing (STOVL) aircraft. Microjet array located at the periphery of the main jet nozzle exit is used to suppress the noise in the impinging jet flow field. Therefore, it can be classified to be an active flow control. Also, it is yet an open loop control since the corresponding output - noise level in this case - is not fed back to the condition of microjet injections. From the following section, more details of noise reduction in supersonic impinging jet will be discussed.

1.2 Supersonic Impinging Jet

1.2.1 Background and Motivation

When STOVL aircraft operates in hovering mode, in close proximity to the ground, it produces lift force by a downward pointing impinging jet. The impinging jet here

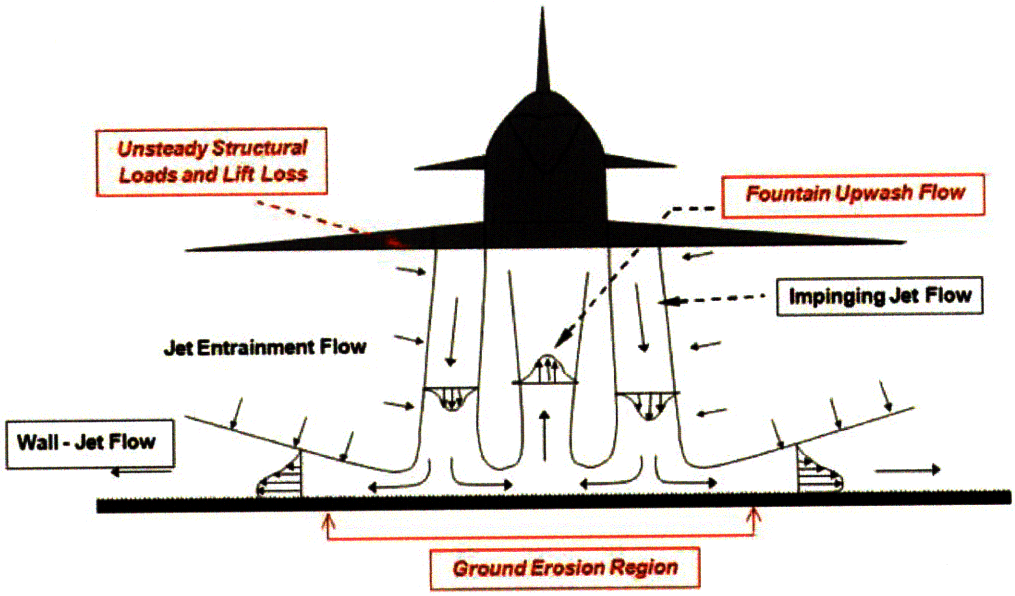

Figure 1.1: Schematic of a STOVL aircraft in hovering mode

refers to the jet flow that impinges on a solid surface - ground for STOVL aircrafts. During taking off and landing - as referred to be a hovering mode, the impinging jet also generates several unfavorable effects as well as a lift force.

First of all, as shown in Figure 1.1, significant lift loss is induced by the flow entrainment from an ambient air. As the jet comes out from the nozzle exit and it forms a shear boundary layer, the difference of velocities between the jet and of the ambient air results in the flow entrainment from the ambient air into the shear layer, thereby resulting in a suck down force which is led to a lift loss. Second, from an environmental point of view, the impinging jet causes significant ground erosion by the wall jet composed of hot gas. In addition, impinging tones - discrete tone of the impinging jet - make significant near-field noise pollution, which can be a serious problem to personnel in vicinity; guiding the aircraft on the deck. Moreover, since the increased acoustic noise, when associated with highly unsteady pressure field by the impingement on the ground, is dominated by discrete tone frequency which could match the resonance frequency of aircraft body, it could make the sonic

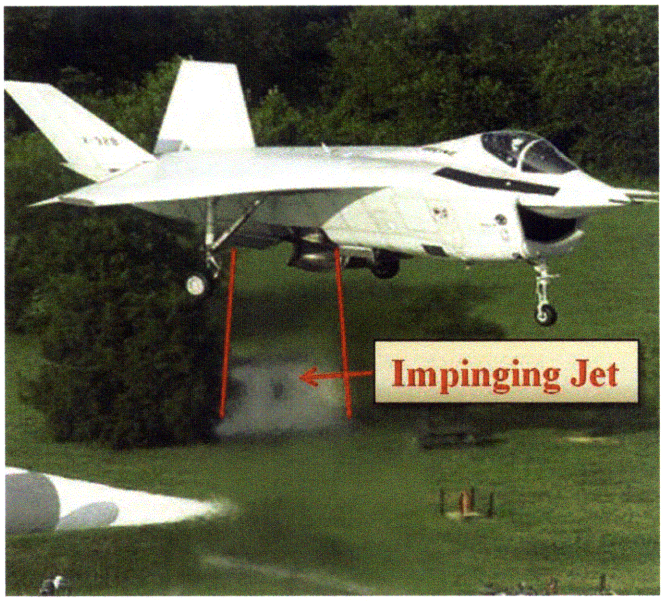

Figure 1.2: JSF X-32B in hovering mode

fatigue problem more crucial. Sonic fatigue problem can become more serious for the supersonic STOVL aircraft such as JSF (Joint Strike Fighter, see Figure 1.2).

Due to many problems caused by the strong interaction between the flow field and acoustic noise as described above, the flow field properties of a supersonic impinging jet have been investigated for a long time. A number of studies [19, 20, 21] demonstrate that the impinging jet flows are dominated by discrete impinging tones. The impinging tones are caused by well-known phenomena, the feedback loop (see Figure 1.3). To briefly explain the feedback loop, one could start with that the large scale vortical structure in the shear layer impinges on the ground. Upon impinging on the ground, high amplitude of the unsteady pressure fluctuation produces the acoustic wave which propagates up to the nozzle exit and excites the shear layer. This excitation generates enhanced instability wave in the shear layer near the nozzle exit and the instability wave grows into a large scale vortical structure as it travels downstream, and finally impinges on the ground, thereby closing the feedback loop. Figure 1.3 shows a schematic that describes the feedback loop phenomenon. More details of the feedback loop can be found in [19, 20, 21, 22]. In order to reduce acoustic noise level as well as the unfavorable effects, one should be able to intercept this feedback loop. For example, one could intercept upcoming acoustic wave or shield the shear layer so

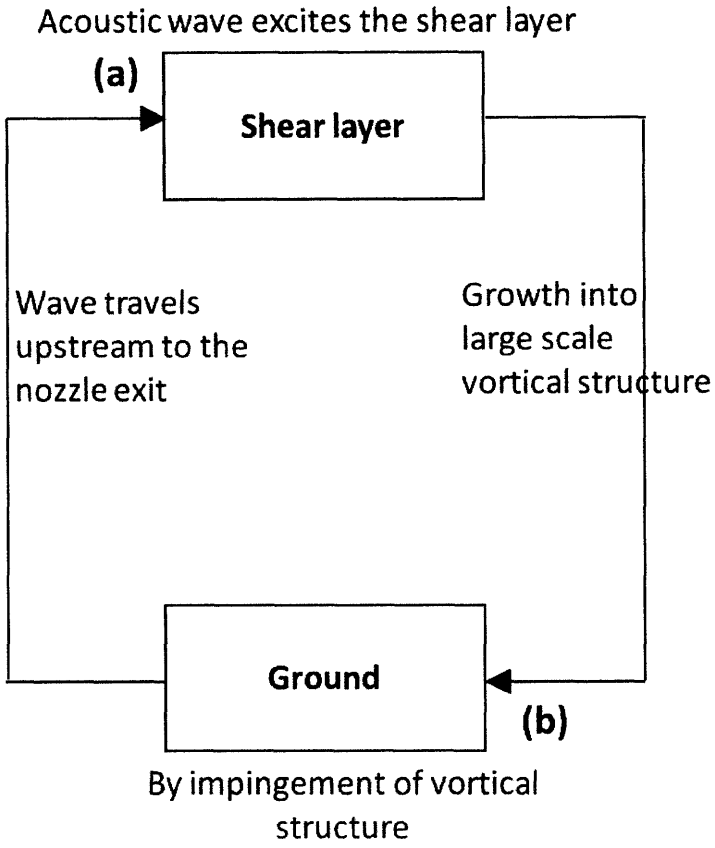

Figure 1.3: Schematic of the feedback loop in supersonic impinging jet

that the shear layer does not get excited by the upcoming acoustic wave, or simply disrupt the coherent interaction between acoustic wave and flow instabilities. There have been many attempts that introduce passive and active flow control methods to suppress the impinging tones, which will be following in the next section.

1.2.2 Previous Research (Literature Survey)

A number of previous researches have made efforts to interrupt the feedback loop with passive or active flow control method. Sheplak and Spina [23] attempted to reduce the noise by protecting the shear layer from incoming acoustic wave utilizing co-flow near the main jet. They could successfully reduce near-field broadband noise level up-to 10 dB with appropriate ratio of the main jet velocity to co-flow exit velocity,

and also could significantly suppress impinging tones. Similarly, Shih et al. [24] used counter-annular-flow around the main jet flow to successfully suppress screech tones of non-ideally expanded jets, that is, over/under expanded jets. Additionally, they could reduce noise level by approximately 3$\sim$4 dB. Although these approaches are effective, they have some limitations such as: 1) the flow used for control (such as co-flow and counter flow) through the annular nozzle requires large amount of mass flow rate, approximately 20$\sim$25% of the main jet flow, 2) they would need some major modification of aircraft design for application, thus to be impractical. Elavarasan et al. [25], a good example of passive control, employed a semi-circular plate as a baffle to block the upcoming acoustic wave, thereby intercepting the interaction between acoustic wave and unsteady flow field in the shear layer. This approach brought significant noise reduction by up-to 13 dB compared to the case without a baffle - referred to as uncontrolled case, which is a promising result. However, this method is also impractical in that the additional plate gives a constraint on the design of aircraft or needs a significant modification of the aircraft design, and also in that it could generate another adverse effect such as drag or thrust loss.

More recently, Alvi et al. [26] introduced microjet array around the nozzle exit for active control of supersonic impinging jet problem. By flushing high-momentum microjets into the shear layer at the main jet nozzle exit, a noticeable amount of noise has been reduced, accompanied with recovery of the lift loss as well. Microjets could also significantly suppress or eliminate impinging tones. Since the diameter of microjet is very small scale - 400μm, the required mass flow rate for the active control is very small compared to the previous methods; approximately 0.5% of the main jet, thereby to be more practical for application. Moreover, microjet injection does not diminish other aircraft performances such as lift force or thrust. However, the effect of microjets varied depending on operating conditions of the main jet, which implies that more consistent and uniform control method of impinging jet problem should be further investigated.

Choi et al. [27] were motivated to make an attempt to modulate the microjet array, thereby introducing the unsteady microjet injection - referred to as *pulsed microjet*.

The rationale of pulsed microjet is that unsteady flow is able to deliver higher momentum than steady flow with the same mass flow rate [5]. They showed, as expected, pulsed microjet is as effective as steady microjet with less mass flow rate [27], and in some particular case, pulsed microjet generates more noise reduction than steady microjet even with less mass flow rate. In this method, pulsed microjet involves some control parameters such as pulsing frequency, duty cycle, phase difference, and supply pressure (for more details, see section 2.3). It is also demonstrated by Choi et al. [28] that dominant control parameters are pulsing frequency and duty cycle; their experiment results show that phase difference does not affect much on noise reduction, and also that there is a saturated supply pressure for pulsed microjet where the effect of pulsed microjet gets saturated beyond certain supply pressure. Additionally, Choi et al. [29] claimed the existence of the low frequency mode in the supersonic impinging jet flow field; in the spectra plot, they found a peak at about 20Hz and considered this peak as one of the dominant modes along with the peak at an impinging tone frequency (a few kilohertz). Considering the noise level of impinging jet flow field is very sensitive to the change of jet operating condition, it is needed to realize uniform and consistent noise reduction regardless of changing operating condition. Clarifying this low frequency mode may be important to step forward to achieve the fundamental goal; to get uniform and consistent noise reduction in overall jet operating conditions.

In this section, previous researches on supersonic impinging jet problem have been briefly discussed. The present study is along the extension of [5]; the active noise control of supersonic impinging jet using pulsed microjet. The main objectives of this study includes: (1) to find an optimal pulsing parameters that delivers uniform and consistent noise reduction by means of more experiments, (2) to clarify the low frequency mode, (3) to apply pulsed microjet injection for hotter temperature main jet, and (4) to develop high frequency pulsing actuator if needed. More specific aspects of these objectives are discussed in section 2.4. This thesis includes up-to-date experiment results and analysis of data, and also describes the future work.

Chapter 2

Experiments

2.1 Test Facility and Configuration

All experiments were carried out at the supersonic STOVL jet facility of Advanced Aero Propulsion Laboratory (AAPL) located at Florida State University. This facility is used primarily to inspect jet-induced phenomenon on STOVL aircraft in hovering mode [26]. The schematic diagram of facility and its picture are shown in Figure 2.1. This section briefly describes the facility and experiment procedures, where more details can be found in [30] and [31].

2.1.1 High pressure air supply

In order to simulate supersonic impinging jet, the high pressure air should be supplied[1]. The schematic diagram of high pressure air supply is shown in Figure 2.2. There are two four-stage-high displacement reciprocating air compressors, each of them made by CompAir MAKO (model 5436-60E3), Bauer (model I-280), respectively. One storage tank is $5m^3$, where other three tanks have a combined volume of $5m^3$.

The air is compressed by the compressors up-to 2000psig. Since compressed air straight from the compressor contains moisture from the atmosphere, although some

[1]This section refers to [1, 2].

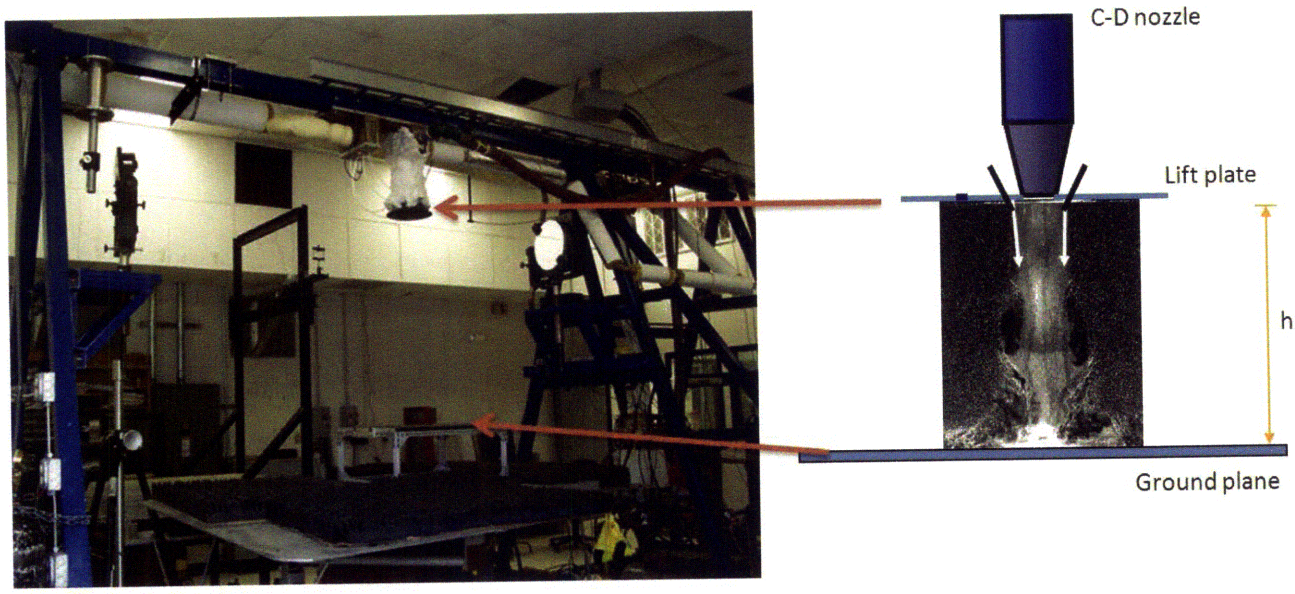

Figure 2.1: STOVL supersonic facility at AAPL, FSU

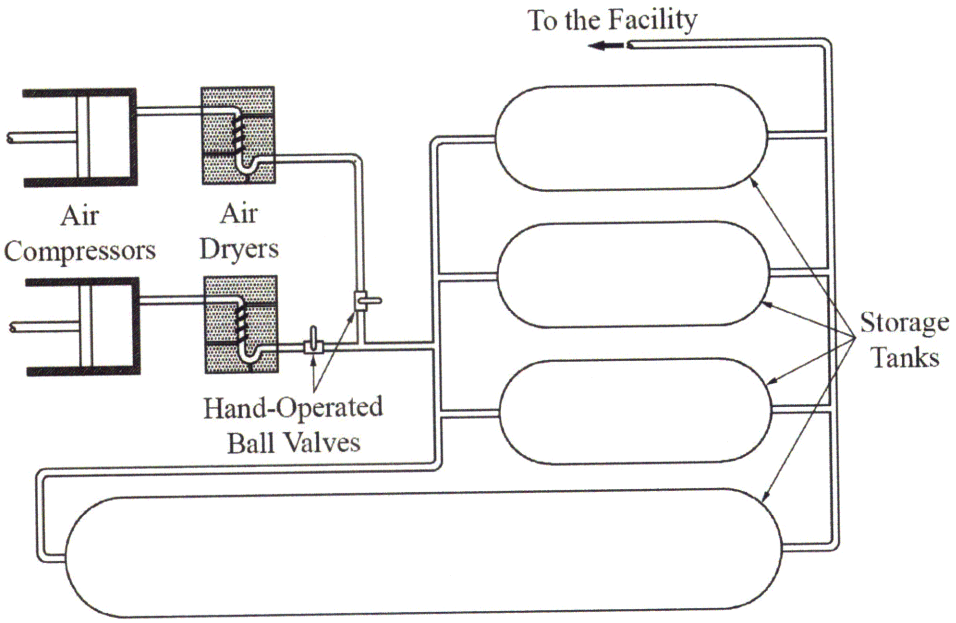

Figure 2.2: Schematic of the high pressure air supply [1]

water is removed during the inter-cooler and after-cooler stages, the compressed air could be not dry enough, may condensate, and eventually make the pressure lower in the storage tank. In order to remove water content in the air nearly completely, the air is then passed through a set of refrigerated air dryers. After then, the air is passed through the filter in order to remove any dust or oil particles. Four storage tanks with a combined volume of $10m^3$, as described above, are used to store this compressed air. This storage capacity allows the experimental run for up-to 30$\sim$40 minutes, depending on the jet operating conditions.

This compressed air enters STOVL facility through a series of valves as shown in Figure 2.3. A dome regulator (Tescom^{TM}) - first valve - installed in series aft the solenoid valve is used to reduce the high pressure of the compressed air to appropriate value for each experiment. The regulator is designed such that an input pressure is provided via an additional nitrogen tank, set to balance the output pressure, thus equal to the input pressure. The output pressure of the regulator was chosen between 150 and 300psi, depending on the jet operating condition, and once the pressure was set to be a certain value, it was kept constant throughout the single run of the main jet. For example, in the present study, when the jet was operated ideally expanded and at the ambient temperature, the pressure was set to be 200psi throughout the single run. The air aft the regulator is passed through a Fisher^{TM} low pressure valve - second valve - for more precise control of the main jet pressure, to ensure that the jet is operated at the constant, appropriate pressure. These two pressure control valves can be controlled in the control room via LabView^{TM} based flow control program. Additionally, two relief valves are used in the system for the safety reasons. The air is then passed through the flow heater to adjust its temperature to appropriate value, the details of which are following in the next section.

2.1.2 The inline flow heater

In order to assure that each experiment has repeatability, jet operating condition in each run should be remained nominally constant. The heater is used throughout the experiment to maintain isothermal condition as well as to heat up the main jet for hot

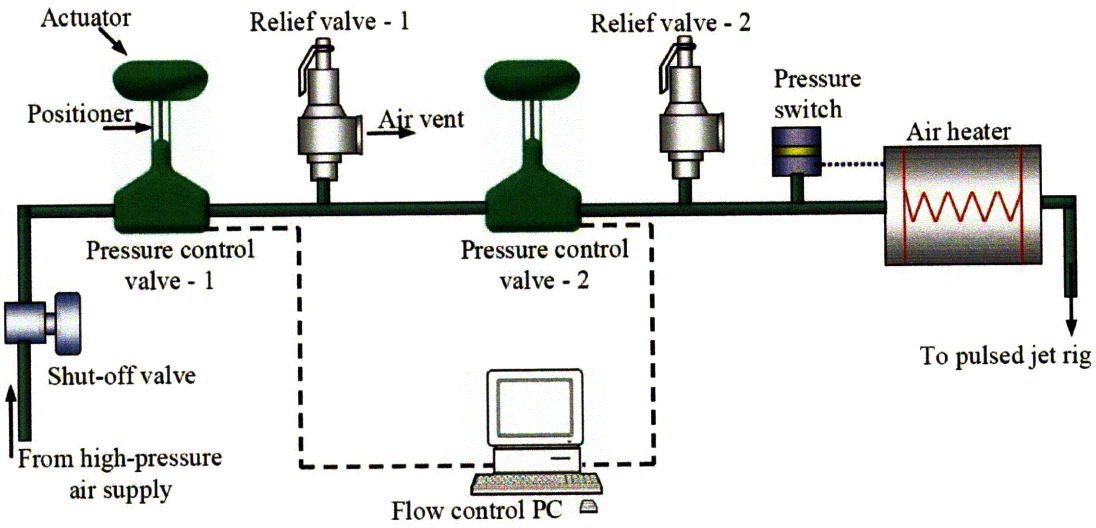

Figure 2.3: Schematic of the air flow control [2]

temperature jet experiment[2]. In the present study, the flow heater manufactured by Osram Sylvania was used (see Figure 2.4). The air heater system consists of one 192-kW inline flanged heater capable of heating air with flow rates of 600-scfm at 150-psi to 800 °F. It employs a closed-loop heater control system composed of a temperature controller and thermocouples to provide a constant output temperature, regardless of temperature changes in the air flow. At the core of the air heater are serpentine heating elements designed for efficient heat transfer between the heater and the air stream. The inlet to the heater is designed in such a way that the air entering the heater is distributed uniformly over the entire inlet cross sectional area [2]. This is realized by a smooth expansion of sufficient length from a 3-inch diameter pipe to the 8-inch diameter inlet of the heater. This design, at the same time, eliminates localization of the flow, thereby prevents any damage to the external part of the heater. For additional safety, a pressure switch is also located at the upstream of the heater to prevent the heating elements from burning out; cut off the electrical power for heater in case of loss of air supply. This electric air heater is capable of

[2]This section refers to [2].

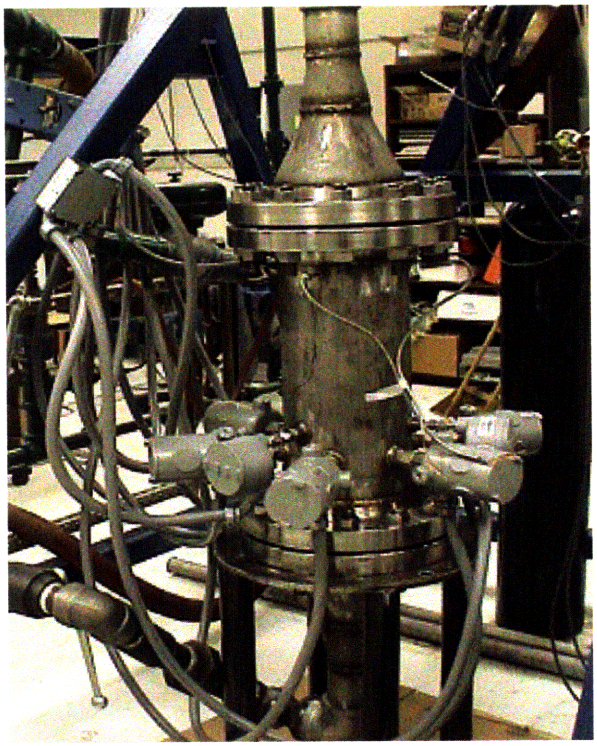

Figure 2.4: The inline flow heater [2]

maintaining temperatures to an accuracy of ±1 °F.

After passing through the heater, the air arrives at the stagnation chamber. The role of stagnation chamber is to ensure that supplied air is a laminar flow, before entering the nozzle, with the condition of desired pressure and temperature. The stagnation chamber employs a thermocouple and an Omega^{TM} pressure transducer (model PX219-200A5V) which constantly monitor the temperature and the pressure of the main jet, thereby to enhance the accuracy of experiment.

2.1.3 Nozzle

Since the current study concerns supersonic impinging jet problems, all experiment data were obtained at supersonic conditions using a C-D (convergent-divergent) nozzle. To briefly explain a C-D nozzle, the inside-wall of the inlet converges to a minimum area - also known as the throat of the nozzle, and the wall-contour diverges aft the throat up-to the nozzle exit (see Figure 2.5). The convergent region of the nozzle accelerates the subsonic flow to sonic conditions at the throat, and then this sonic

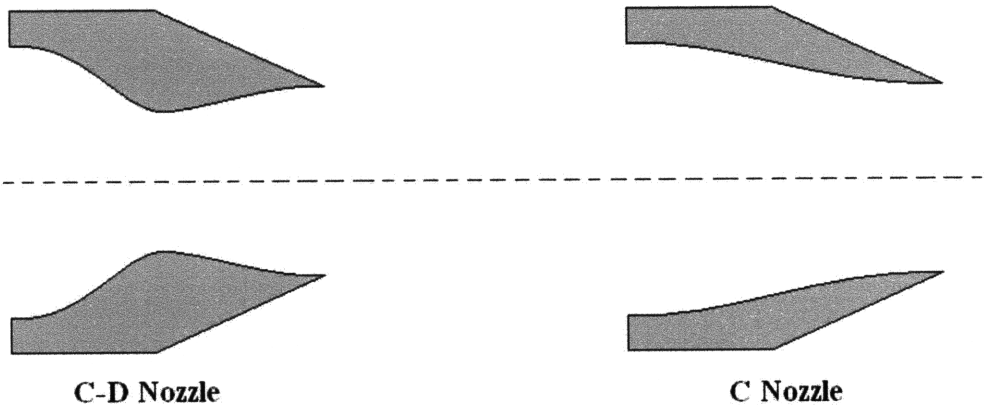

Figure 2.5: Schematic of the inside of C-D nozzle [3]

flow is further accelerated until it reaches the nozzle exit to supersonic speed in the divergent region. The design Mach number at the exit depends on the ratio of the nozzle exit area to the throat area. An individual design of the nozzle determines its own ideal condition, Nozzle Pressure Ratio (NPR, where NPR is defined as the ratio of stagnation pressure to the ambient pressure). If the jet is operated at the design condition - design NPR of the nozzle, it is called ideally expanded jet; otherwise, it is called off-design jet, that is, over- or under-expanded jet. When the jet is operated at off-design condition, the screech tone is observed due to the presence of shock wave, which does not exist in the ideally expanded jet [32].

In the present study, the air leaves the stagnation chamber and passes through a C-D axisymmetric nozzle. The diameters of throat and exit area are 2.54cm and 2.75cm, noted as d and d_e, respectively. The design Mach number is 1.5 and the diverging section of the nozzle is straight walled with 3° divergence angle from the throat to the nozzle exit. The design NPR for this nozzle is 3.7 to generate ideally expanded jet.

2.1.4 Lift plate

The circular plate is flush mounted with the nozzle exit as shown in Figure 2.6, representing the aircraft body (referred to as *lift plate*). The diameter of the lift

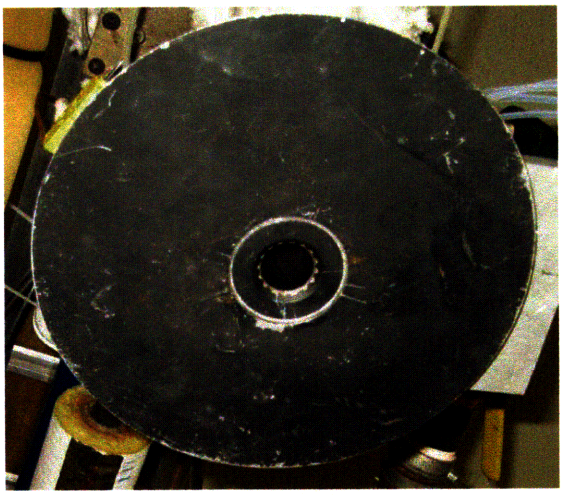

Figure 2.6: Lift plate

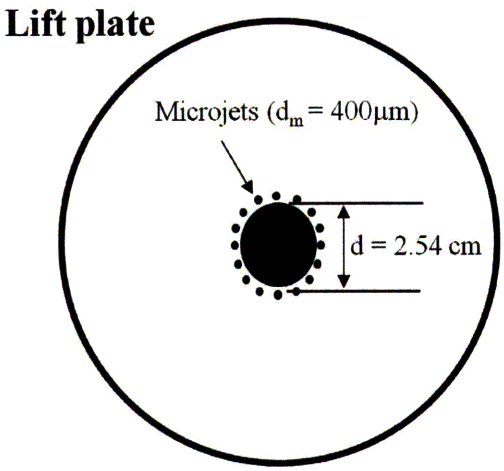

Figure 2.7: Schematic of the lift plate with microjets

plate is 25.4cm (10 times of the nozzle throat diameter, d), which has a central hole of the same diameter as the nozzle exit so that the nozzle and the lift plate could be combined (flush mounted) together. For the present study, an actuator is also mounted on the lift plate; that is, microjets and the motor are mounted in order to produce pulsed microjets (see Figure 2.7). In the following section, more details of microjets are discussed.

2.1.5 Microjets

In order to perform an active flow control, microjets were used as an actuator. Microjets here refer to the jet with a micro scale diameter. The number of microjet and its diameter could be chosen arbitrarily, however, total sixteen microjets with diameter of 400μm were uniformly distributed on the periphery of the nozzle exit, based on [33]. Nitrogen was supplied to the microjet actuator. Leaving the compressed nitrogen cylinder, nitrogen gas arrives primarily at the stagnation chamber. The role of stagnation chamber here is similar as the one for the main jet; the microjets are settled in the stagnation chamber and the pressure of stagnation chamber is always monitored by Omega^{TM} pressure transducer (model PX303-200G5V), in order to precisely control the supply pressure of the microjet. Nitrogen gas is then passed through micrometer-sized filter to prevent the micro-nozzles from being clogged. Then it is connected to four secondary plenum chambers through four solenoid valves[3]. The secondary plenum chamber ensures that microjet flow is free from unsteadiness as possible. Each one of these secondary chambers is connected to the stainless steel tubes, which are mounted on the lift plate. The stainless steel tubes are mounted with a 30° inclination angle from the main jet axis. The supply pressure of the microjets is controlled by adjusting the wheel-valve regulator in the control room. Figure 2.8 shows a schematic of the microjet control. The primary stagnation chamber and secondary plenum chambers are shown in Figure 2.9.

2.1.6 Ground plane

In order to simulate hovering mode of STOVL aircraft, the planar plate was set up to represent a landing surface of the aircraft. A 1m × 1m × 25mm aluminum plate (referred to as *ground plane*) was mounted on a hydraulic lift as shown in Figure 2.10, so that it can move up and down, thereby simulates hovering mode of STOVL aircraft at different ground-to-aircraft distances. The hydraulic lift enables the ground plane-to-nozzle exit distance - referred to as *height*, h - to be varied from $2d$ to $35d$.

[3]The solenoid valve allows to control each group of four microjets individually, however, in the present study, all microjets are activated synchronously

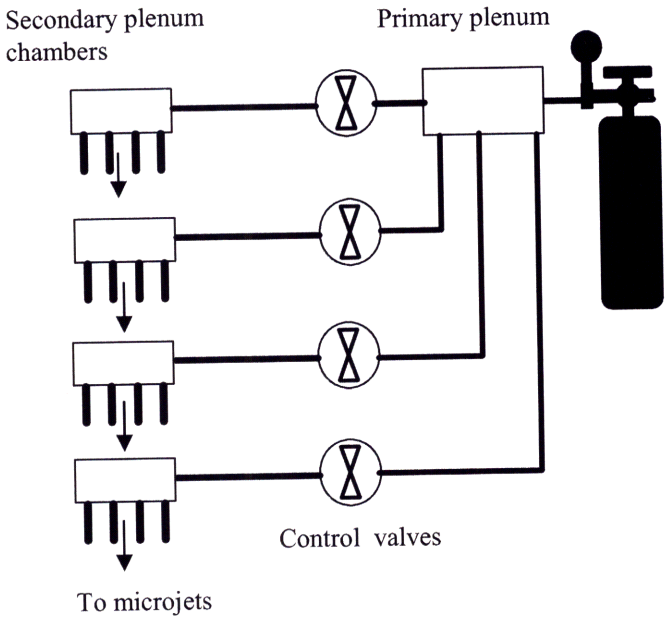

Figure 2.8: Schematic of microjet control [4]

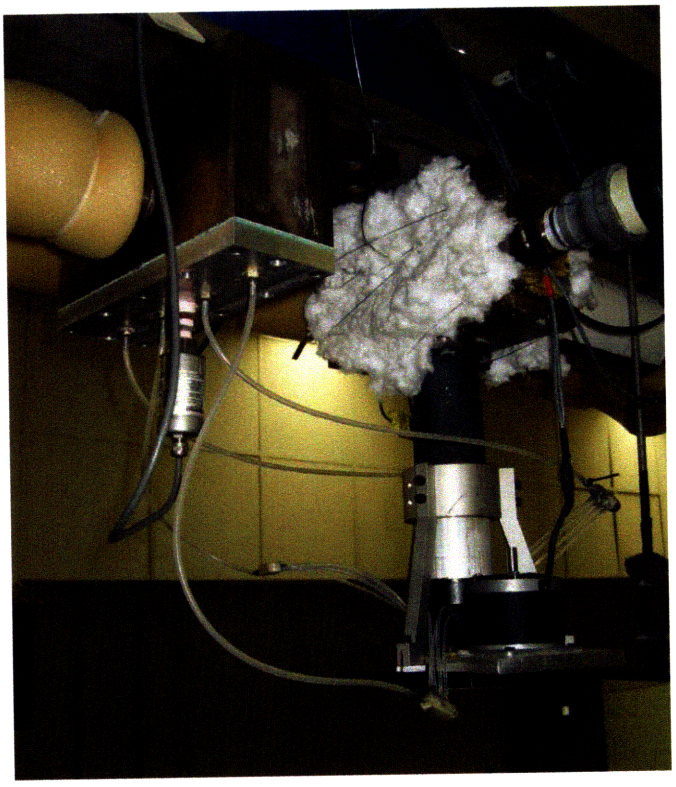

Figure 2.9: Microjets flow through the primary stagnation chamber and secondary plenum chambers

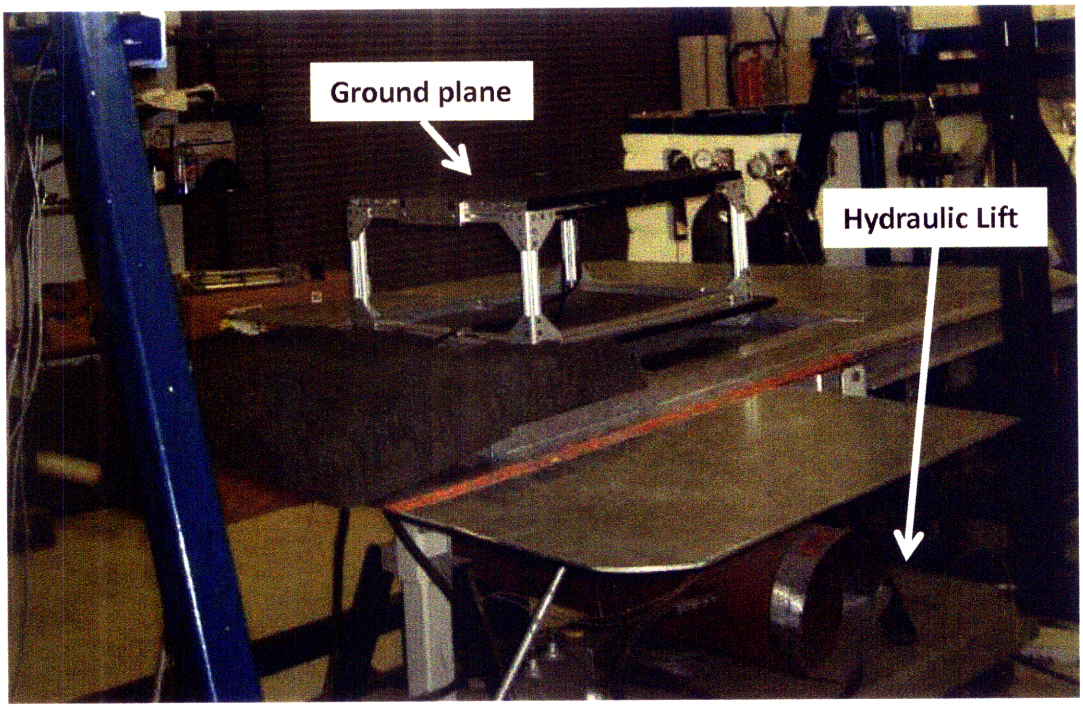

Figure 2.10: The ground plane mounted on a hydraulic lift

The hydraulic controller (Rexroth model DLC-100) was used to control the vertical motion of the ground plane, connected to the computer in the control room so that the height can be remotely controlled during the main jet running. In order to investigate the unsteady pressure fluctuation on the ground, Kulite^{TM} pressure transducers were mounted on the ground plane; more details are discussed in section 2.2.2.

2.2 Measurements

2.2.1 Test conditions

In the present study, the main jet was operated at NPR of 3.7 using a C-D nozzle with the design Mach number of 1.5, which corresponds to a nearly ideally expanded jet flow. The main reason for operating the jet at ideally expanded condition is to isolate the effect of impinging tone from the screech tone which is observed at under/over expanded jet [26, 32]. Most of experiments were conducted with jet stagnation temperature of 300K, about the same as the ambient temperature, where

the jet was heated up to 360K for a few cases - corresponding to the Temperature Ratio (TR, where TR is defined as the ratio of the stagnation temperature to the ambient temperature) of 1.2. Since the impinging jet in reality is much hotter than the ambient air, one should examine the effect of an actuator on hot temperature jet for the application to reality. The test Reynolds number based on the main jet velocity at the nozzle exit and the nozzle diameter of main jet was 7.5×10^5. Mostly in the present study, height was varied from $3.5d$ to $4.5d$ since $h/d = 3.5$ has been a troublesome case, thereby to be our interest [5]. The supply pressure of microjets was varied from 40 psi to 190 psi; the total mass flow rate of steady microjets is less than 1 % of the main jet. More details of microjet actuation are discussed in section 2.4.

2.2.2 Unsteady pressure and near field noise measurement

In order to measure unsteady pressure field on the ground plane generated by the impinging jet, two high-frequency 100-psi Kulite^{TM} pressure transducers (model XTEH-10L-190-100A) are mounted on the ground plane as shown in Figure 2.11. One was located at the impingement point (at the jet center line, $x/d = 0$) and another at about 50mm away from the centerline ($x/d = 2$). The near field acoustic noise was measured using a 0.635cm-diameter B&K microphone (model 2633) placed at 25cm ($\sim10d$) away from the nozzle exit, oriented 90° to the main jet axis, and flush mounted with the lift plate (see Figure 2.11). In order to minimize the sound reflections during the near field acoustic measurements, nearby exposed metal surfaces were covered with thick acoustic foam. Both Kulite^{TM} pressure transducer and microphone were frequently calibrated before experiments.

2.2.3 Data acquisition and processing

The acoustic, unsteady pressure signals were acquired through National Instruments digital data acquisition board (PC-MIO-16E-1) using LabView^{TM} software. The transducer outputs were conditioned using Stanford Research System low-pass fil-

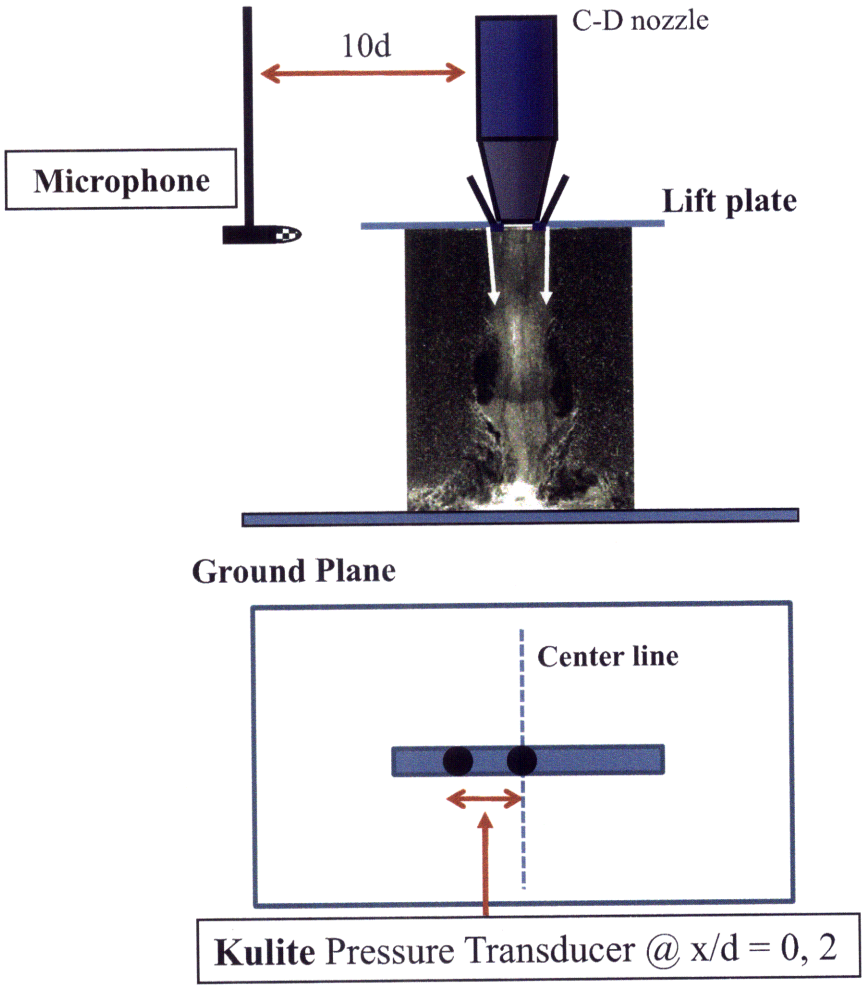

Figure 2.11: Sensors: two Kulite^{TM} pressure transducer on the ground plane and a microphone flush mounted with the lift plate

ters (model SR 640) and simultaneously sampled at 70kHz with cut-off frequency of 30kHz, which satisfies Nyquist criteria and thereby keep it from aliasing. The voltage data read by the sensors were primarily transferred to the pressure values based on calibration.

In order to represent the total noise level measurement, a scalar value would be needed; denoted as Overall Sound Pressure Level (OASPL), where it is defined as the following:

$$OASPL(p) = 20\log_{10}(P_{rms}/P_{ref})$$

where $P_{rms} = \lim_{T\to\infty}\sqrt{\frac{1}{T}\int_0^T p(t)^2 dt}$, and $P_{ref} = 20\mu Pa$. In order to obtain spectra in frequency domain and to calculate OASPL from these measurements, standard FFT (Fast Fourier Transform) analysis was used. Total number of 409,600 points were recorded (for about 6 second) for each signal. The spectral content of the unsteady signals was obtained by segmenting each data record into 100 subgroups with 4096 samples each, and a FFT with a frequency resolution of 17Hz was computed for each segment. The 100 FFT's thus obtained were averaged to obtain a statistically reliable estimate of the narrow-band noise spectra.

2.2.4 Measurement uncertainties

The estimated uncertainty associated with each measurement, for the worst-case scenario, is described in this section. For the unsteady pressure measurement on the ground plane, the intensities of the pressure measured from the Kulite^{TM} transducer are accurate within ±0.2psi (or ±1378.95Pa). As the data are acquired through analog to digital (A/D) card, the resolution of the card should be also taken into account as well. A 12-bit NI PCI-MIO-16E-1 card has been used through all experiments, and DAQ resolution is constant (12 bit). The gain for Kulite^{TM} is 0.878mV/Pa, the gain of amplifier is set to be 50, and thus the gain is $\frac{0.878mV/Pa\times 50}{1000mV/V} = 0.0439V/Pa$. For ±5V range, therefore, the uncertainty in pressure can be obtained by the following [3]:

$$\epsilon_p = \frac{1}{2}\cdot\frac{range}{resolution\cdot gain} = \frac{1}{2}\cdot\frac{10V}{4096\cdot 0.0439V/Pa} = 0.028Pa$$

This value is relatively small - in terms of an order of magnitude - thereby negligible. If we express the unsteady pressure in decibel unit, the same error in psi unit can be expressed as different in decibel unit, depending on the overall value of P_{rms}. The P_{rms} value on the ground plane for the range of interest is near 180dB, thereby its uncertainty to be about 0.6dB. The estimated uncertainty of acoustic noise measured by microphone signal can be similarly obtained. Since the microphone response is taken into account in the data acquisition program, and factored even before saving, the uncertainty associated with the card and the amplifier is calculated as the following: DAQ resolution is constant (12 bit), the gain is set to be either 3.16mV/Pa or 1mV/Pa. For the worst-case scenario, the uncertainty based on 1mV/Pa is calculated. Therefore, for the input range of ±10V, the uncertainty is

$$\epsilon_p = \frac{1}{2}\frac{range}{resolution \cdot gain} = \frac{1}{2}\frac{20V}{4096 \cdot 1mV/Pa} = 2.4414Pa$$

Since sound pressure level of our interest is near 140~150dB, the value in Pa corresponds in decibel unit to maximum ±0.1dB.

2.3 Pulsing Actuator with Rotating Cap

Choi et al. [27] introduced the modulation of the microjets - referred to as *pulsed microjet* - as an active control method. The pulsed microjet was realized using a rotating cap, as shown in Figure 2.12 and 2.13. To briefly describe the pulsed microjet using a rotating cap, a saw-teeth-shaped rotating cap is attached to the lift plate, also connected to the motor - which is mounted on the lift plate - via a pulley belt. The rotating cap rotates as the motor rotates, and thereby the teeth of rotating cap periodically block and unblock microjets at the microjet exit, which simulate microjets' ON/OFF position, and thus producing a pulsed microjet. There are control parameters associated with pulsed microjets that should be considered; pulsing frequency, duty cycle, phase, and supply pressure [5]. Pulsing frequency is controlled by the speed of the motor and supply pressure is directly controlled by the pressure

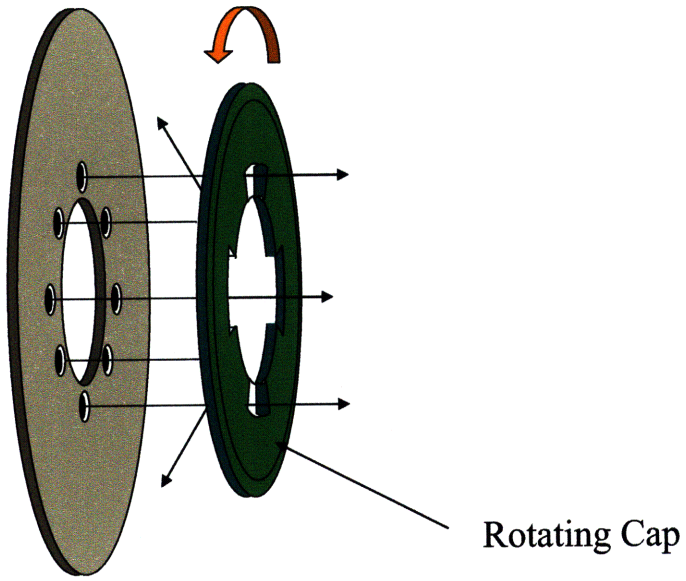

Figure 2.12: Schematic of generating pulsed microjet via rotaing cap [5]

regulator, where duty cycle and phase are dependent on the design of rotating cap. Duty cycle is defined as the time ratio of when microjets are at ON position to the one pulsing period. Therefore, duty cycle could be determined by the size of holes on the rotating cap (see Figure 2.14), where phase is controlled by the number of holes on the rotating cap (see Figure 2.15). More details of pulsing parameters can be found in [5].

In the present study, the attempt to find optimal conditions of pulsing parameters, in order to make a consistent and maximum noise reduction, have been made. Based on [5, 28], most of experiments were focused on pulsing frequency and supply pressure, where a few tests were for duty cycle due to the limited time of the study. More details of each experimental description are discussed in section 2.4.

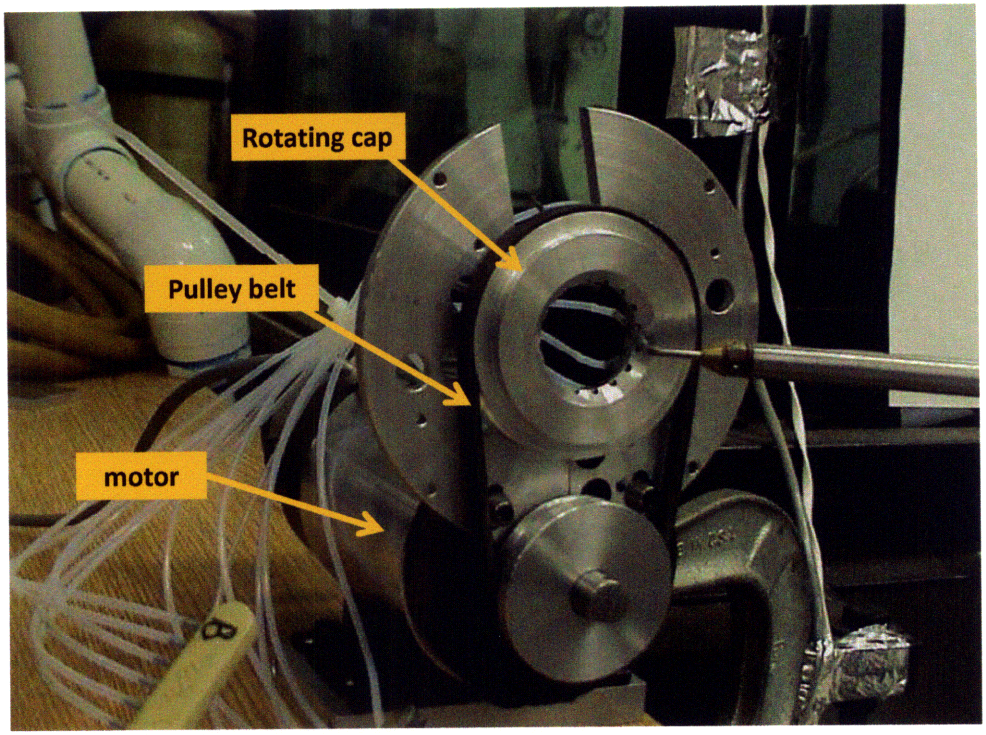

Figure 2.13: Pulsed microjet generated by the rotaing cap connected to the motor via pulley belt [5]

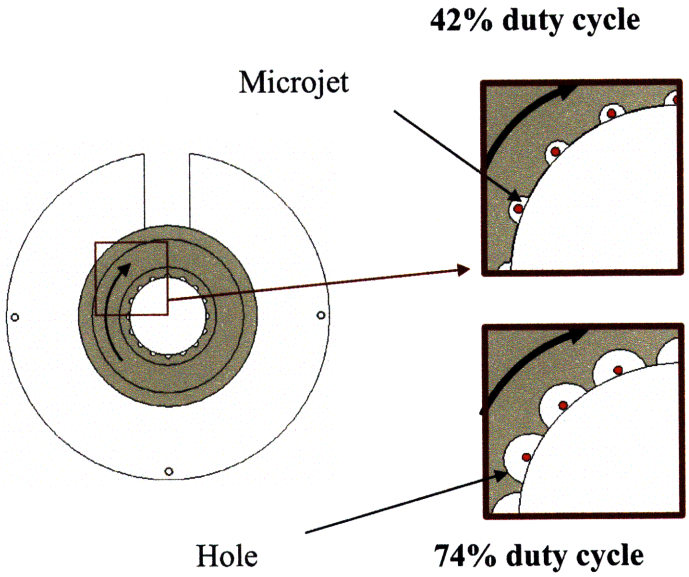

Figure 2.14: Schematic of a pulsing parameter - altering duty cycle [5]

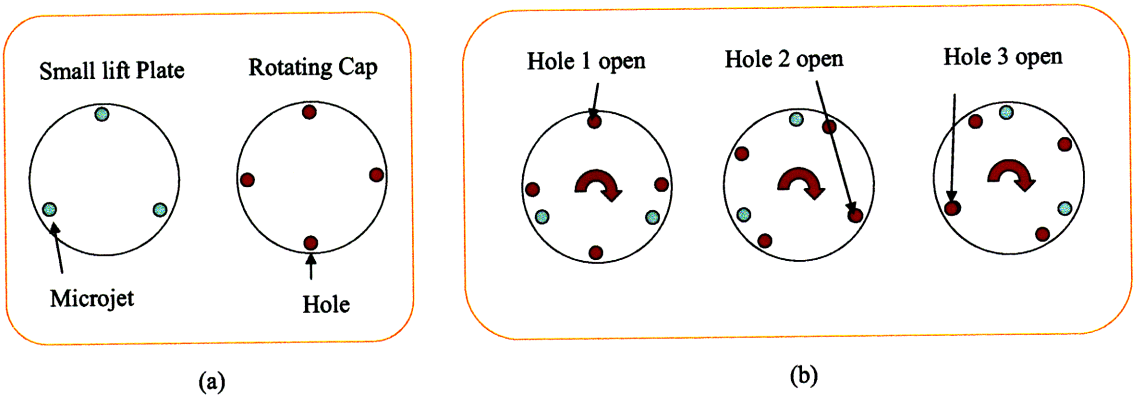

Figure 2.15: Schematic of a pulsing parameter - altering phase [5]

2.4 Experimental Description

In this section, the detailed experimental procedure and planned test matrices, based on the objectives of the present study, are described. It should be again noted that the primary objectives of current study include the followings: (1) to find an optimal pulsing parameters that delivers uniform and consistent noise reduction, (2) to clarify the low frequency mode, (3) to apply pulsed microjet injection for the hotter temperature main jet, and (4) to develop high frequency pulsing actuator if needed, all of which are along the extension of [5].

First of all, since the impinging jet noise level is a nonlinear function of height and NPR and furthermore it is sensitive to even small change of jet operating condition, it is necessary to find optimal pulsing parameters which can generate consistent and maximum noise reduction in overall jet operating condition. Choi et al. [28] claimed that pulsing frequency and duty cycle are dominant control parameters amongst all; They observed increased noise reduction by 1 $\sim$ 2dB with very low frequency pulsing ($\sim$ 20Hz), which was referred to as the low frequency mode. Also, it was reported that pulsed microjet generates more noise reduction than steady microjet with certain duty cycle at certain height. On the other hand, Choi [5] observed that noise reduction gets saturated with beyond certain supply pressure, and that phase difference of microjets does not have significant effect on noise reduction. Based on [5, 28], the present study concerns finding optimal combinations of pulsing parameters

(pulsing frequency, duty cycle) to generate consistent and maximum noise reduction, and also concerns clarifying the low frequency mode, which refer to objectives (1) and (2) above, respectively.

On the other hand, as the previous experiment data and [5] were carefully reviewed, it was found that most of experiments were conducted with supply pressure of 100 psi for microjets - for both steady and pulsed microjets. Choi [5] also stated that noise reduction gets saturated at the mass flow rate of $0.8\dot{m}_{100}$ (where $\dot{m}_{100}$ stands for the mass flow rate of steady microjet at the supply pressure of 100psig). Recalling the mass flow rate is directly proportional to supply pressure [5], it should be noted for convenience that the supply pressure at which noise reduction gets saturated will be referred to as a *saturated supply pressure*. By simple calculation, the corresponding saturated supply pressure for pulsed microjet (with duty cycle of 56%) to $0.8\dot{m}_{100}$ is 153psi. Therefore, it can be inferred that pulsed microjet may produce more noise reduction with higher supply pressure than 100psi, since noise reduction is not saturated yet in this case with supply pressure of 100psi, based on the statement of [5]. The experiment in the present study, with this inference, was planned to also vary the supply pressure of microjets, although supply pressure was not reported as a dominant pulsing parameter in [28].

For all experiments, the baseline case and steady microjet control case were conducted together with pulsed microjet control case for the sake of comparison; the baseline case refers to the primary jet operating without any control attempt made, and steady/pulsed microjet control case refer to the primary jet operating with steady/pulsed microjet activated at the nozzle exit. The experimental procedure consists of the following steps: (1) measure the noise (OASPL) at the baseline case (2) with steady microjet on, vary the supply pressure (from 40psi to 190psi, by increment of 10 or 20psi) of microjets to find a saturated supply pressure for steady microjet, (3) with the motor on (to activate pulsed microjet), vary a pulsing frequency (from 16Hz to 100Hz, by increment of 5 or 10Hz) at the saturated supply pressure found in the previous step, in order to find the effect of pulsing frequency, (4) with the pulsing frequency at which the maximum noise reduction was generated

in the previous step, vary a supply pressure again as in step (2) in order to find a saturated supply pressure for pulsed microjet. Repeating (1) $\sim$ (4) for different heights and with different duty cycle of rotating cap, it may be possible to find optimal pulsing parameters that could generate maximum noise reduction. However, it should be noted that since there was a limited time to conduct all experiments, some experiments could not be conducted completely. In order to get useful data as much as possible with limited time, the experiments were conducted at h/d of 3.5, 4, 4.5, at which noise was previously, hardly reduced [5]. Since changing rotating cap on the lift plate (in order to alter duty cycle) needs much of time consumption, most of experiments were focused on altering pulsing frequency and supply pressure, with duty cycle of 56%, and a few tests were conducted with duty cycle of 74% due to the limited time. Supply pressure was varied up-to 190psi, which is definitely above the saturated supply pressure for pulsed microjet reported in [5], and also within the range of operating limitation (up-to 200psi) of the pressure transducer at the primary stagnation chamber.

In order to clarify the low frequency mode, it should be first confirmed if the low frequency mode really exists, by means of pulsing frequency sweep tests. Once it is confirmed, the flow mechanism should be explored by means of PIV experiment and flow visualization via shadow graph image. Choi et al. [29] suggested that stagnation bubble in the impingement region of primary jet flow structure may be responsible for the low frequency mode; it was observed that stagnation bubble repeats to appear and to disappear with a time scale of 20Hz, which is about the same frequency range of interest.

Also, considering the reality of supersonic impinging jet problem in hovering mode of STOVL aircraft, since the primary jet is much hotter than the ambient air, it is necessary to examine the effect of pulsed microjet on the hot temperature impinging jet. The previous work in [5] includes only the effect of steady microjet for the case of TR = 1.3 (390K), and the effect of steady microjet on the hot temperature impinging jet for up-to TR = 1.6 can be found in [34]; therefore, the present study made an attempt to clarify the effect of pulsed microjet on the hot temperature impinging jet.

As the motor mounted on the lift plate to produce pulsed microjet should not be exposed to hot ambient temperature for normal operation, guided by its manual, the temperature of the impinging jet was heated up to TR = 1.2 (360K). Although the temperature of the main jet, due to the limitation by the motor, could not be heated up enough, for example up-to TR = 1.6 or so, this experiment could be still useful since it can be inferred from the result how the effectiveness of pulsed microjet varies as the main jet gets hotter.

Chapter 3

Results and Discussion: Active Control using Pulsed Microjets

3.1 Description of A New Motor and Controller

As described in section 2.3, duty cycle of pulsed microjet can be varied via the size of hole on the rotating cap. In the experimental set up, changing rotating cap requires a lot of time consumption since it needs many steps to incorporate another rotating cap with lift plate; fist of all, lift plate should be disassembled from the main nozzle, and after rotating cap is changed inside the lift plate, the lift plate should be assembled to the main nozzle again. Moreover, as stated before, impinging jet flow field is very sensitive to even slight change of jet operating condition, one may not want to repeat assembling/disassembling the lift plate every time varying duty cycle. Therefore, an attempt to vary a duty cycle without changing rotating cap has been made.

Based on that there are opening time and closing time of microjets as the rotating cap rotates - which correspond to microjets' ON and OFF positions, respectively - in every pulsing period, the basic idea is to control the opening and closing time of microjets, so thereby varying duty cycle. If a motor is rotating at a constant speed, the size of hole on the rotating cap determines duty cycle. However, if one could stop at the moment when microjets are at ON position and furthermore the motor rotates faster when microjets are closed, the opening time of microjets would

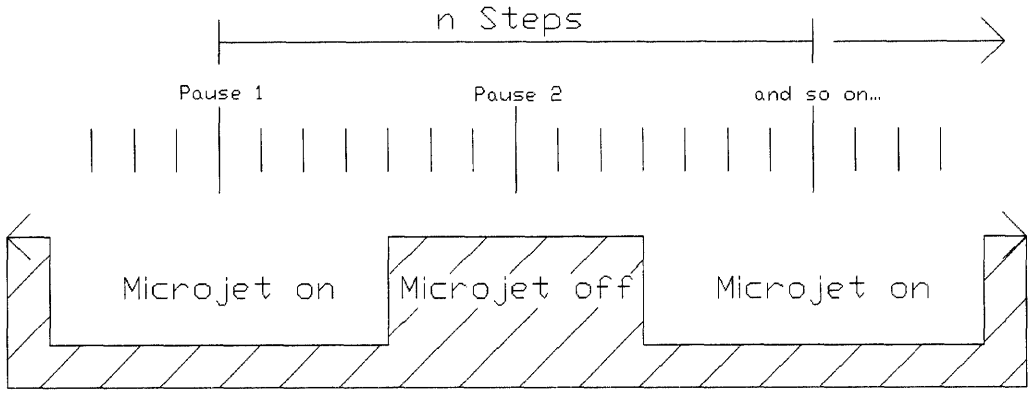

Figure 3.1: Schematic of the concept of varying duty cycle by pausing microjets at ON/OFF position

increase per the same pulsing period and thereby duty cycle is increased. In order to realize this idea in the experimental set up, the motor was replaced to a stepper motor (PacSci, H31NRHP-LNK-M2-00) and appropriate motor controller was used (Jova Inc. TIMS-0201 Stepper Motor Controller).

Figure 3.1 shows a schematic of this rationale. Pulsing frequency (f) determines one pulsing period ($1/f$), where the desired duty cycle (DC) could further determine the opening and closing time of microjets. Then the step rate (R, the rotating speed of stepper motor for one step) and pausing time for each ON and OFF position (P_1 and P_2, respectively) can be determined from the relation between parameters (see Figure 3.2). One pulsing period is composed of the time while microjets are actually pulsing and the time while the rotating cap is stopped momentarily at microjets' ON or OFF position, thus can be expressed as the following:

$$\frac{1}{f} = \frac{n}{R} + P_1 + P_2$$

where n is the number of steps per one pulsing period, which is fixed by the ratio of the diameters of rotating cap to the motor connected each other via pulley belt. P_1

would be zero if the desired duty cycle (DC) is less than the duty cycle of rotating cap (D_0), since there is no need to stop the rotating cap at ON position; similarly, P_2 is zero if the desired duty cycle is larger than the duty cycle of rotating cap. Also, the desired duty cycle can be achieved by the following relation:

$$DC = \frac{D_0 \cdot \frac{n}{R} + P_1}{\frac{n}{R} + P_1 + P_2}$$

By further algebras, the following relations could be achieved:

$$P_{1[2]} = \frac{1}{f} - \frac{n}{R}$$

$$R = \frac{f \cdot (1 - D_0)n}{1 - DC}$$

or

$$= \left(\frac{f \cdot D_0 \cdot n}{DC} \right)$$

By these final relations between parameters, if desired pulsing frequency (f) and duty cycle (DC) are chosen for each test, with fixed duty cycle of rotating cap (D_0) and n, then the step rate (R) can be calculated. Thereafter, P_1 or P_2 could be calculated by f, n, and R. Therefore, pulsing frequency and duty cycle could be controlled via a single program followed by the logic described above (by calculating R and P_1 or P_2). Step rate, R, however, is limited by the performance of motor, to be $2 < R < 2000$. This limitation of step rate determines upper bound of pulsing frequency; f should be less than 62 Hz (with rotating cap of $D_0 = 56\%$). Since it was found, as it is stated in section 3.3.1 - (2), that varying pulsing frequency does not affect on noise reduction, given with enough supply pressure, this limitation does not make any restraint. Therefore, in this way, one could vary duty cycle with a stepper motor, without changing rotating cap. This method was implemented via LabView^{TM} program to control pulsing frequency and duty cycle in a single program. The detailed result of the implementation is described in section 3.3.1 - (3).

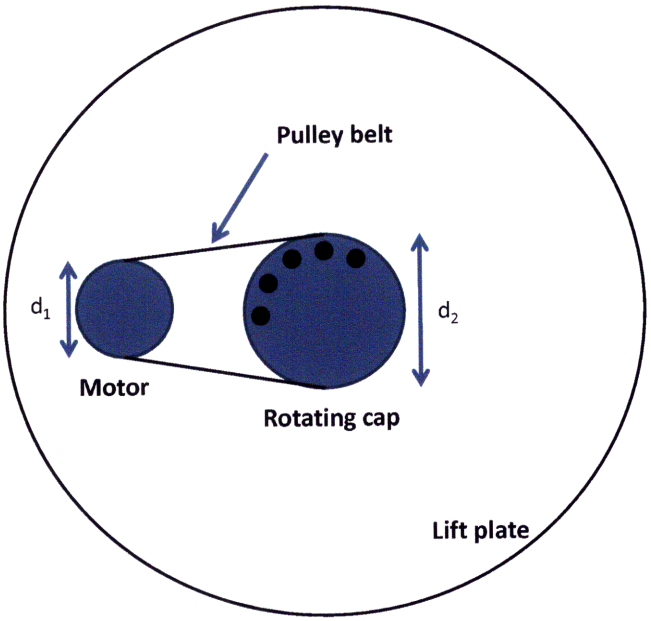

Figure 3.2: Schematic of pulsing configuration: motor and rotating cap connected to each other via pulley belt

3.2 Baseline Case

Since the present study focuses on the noise reduction in supersonic impinging jet problem, it is necessary to estimate a noise level of each case, with and without control. As discussed in section 2.2.3, OASPL is a good indication to present the level of noise magnitude. When the main jet is turned on without any control, this is referred to as *baseline case*. The OASPL value of baseline case will be the standard value which will be compared to OASPL's measured with microjet control activated. The difference of OASPL values (ΔdB) between baseline case and the case with microjet control is referred to as noise reduction. Since OASPL is nonlinearly dependent on jet operating conditions such as NPR, jet temperature, height [26], as shown in Figure 3.3, the noise level of baseline case for each condition (h/d, TR) should be measured for an accurate comparison. Moreover, since the noise level of impinging jet flow field is very sensitive to a slight change of operating condition, the noise level of baseline case should be measured first in each run before microjet control is applied, in order to get a reliable ΔdB and confirm repeatability. The

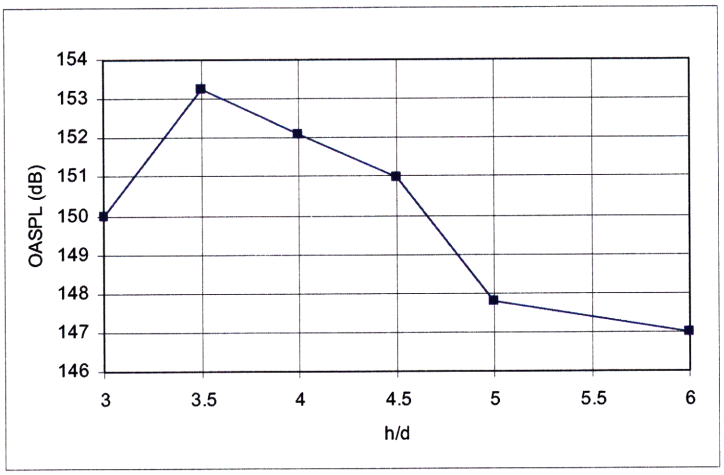

Figure 3.3: OASPL values of baseline cases for different heights [4]

amount of noise reduction can be accurately computed in this way, comparing the noise level of baseline and microjet control cases measured in the same run, which can minimize the error due to the sensitiveness of OASPL value to the slight, if any, change of operating conditions. As seen in Figure 3.4, spectra plots of two baseline cases for the same condition of h/d = 4.0, TR = 1.0, and NPR = 3.7, recorded in different runs show a good repeatability.

In addition, the most interests of the present study concerns finding optimal pulsing conditions to achieve maximum and consistent noise reduction, steady microjet control case was also measured for the sake of comparison; to better-estimate the effect of pulsed microjet. Since the main jet can be run for about 30 minutes at one time due to the limited capacity of air supply as described in section 2.1.1, it is important to measure each noise level of baseline case, steady microjet control and pulsed microjet control case in every single run, in order to accurately compare noise reduction between steady microjet control and pulsed microjet control.

3.3 Steady vs. Pulsed Microjets Control

In this section, the effect of pulsed microjet control is examined. Each pulsing parameter is varied to estimate its effect on suppression of impinging tones, by means of measuring the noise reduction for each condition. In addition, the effect of pulsed

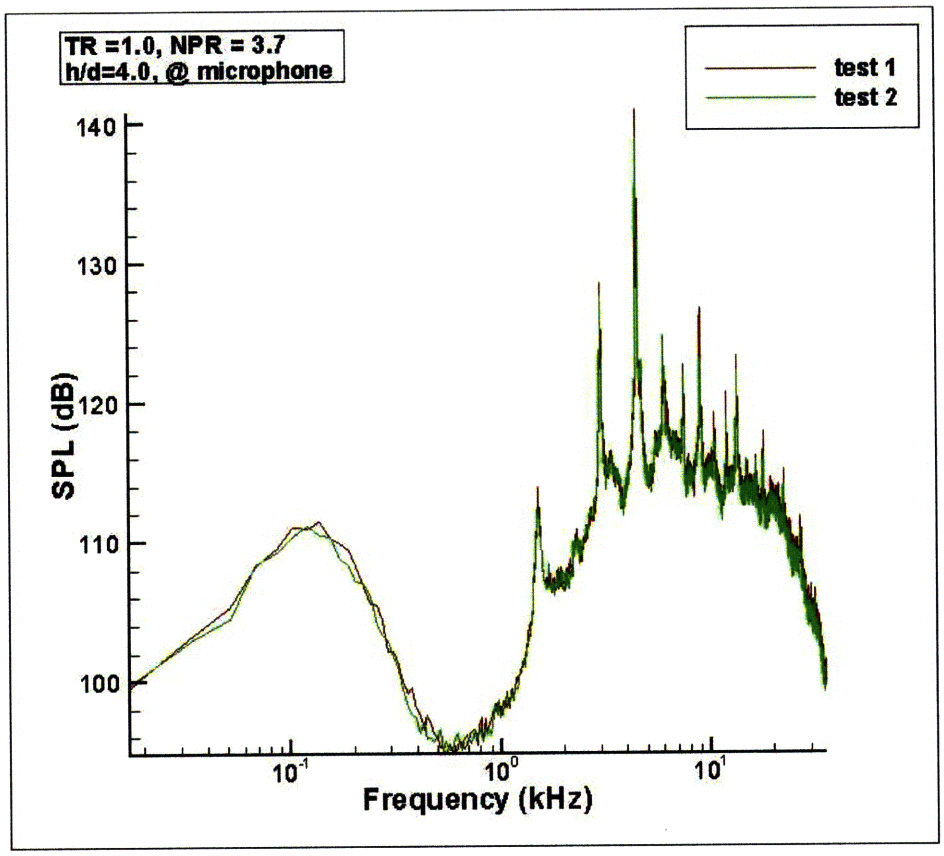

Figure 3.4: Spectra plots: baseline cases of the same condition in two different runs - repeatability

microjet on hot temperature jet is also examined. In order to carefully examine the effect of pulsed microjet on the impinging jet flow, a transient mode is investigated using the pressure response of the system in time domain plot.

3.3.1 Effect of pulsing parameters

(1) Supply pressure

Noise reduction is increased as supply pressure of microjets is increased, and gets saturated with beyond certain supply pressure [33]. This can be explained by that microjets need a minimum supply pressure to penetrate into shear layer of the main jet, and once the supply pressure is high enough for microjets to penetrate through the shear layer, noise reduction gets saturated. However, as described in section 2.4, noise reduction is not saturated yet at the supply pressure mostly used in [5]. Therefore, in order to realize maximum noise reduction by pulsed microjet control, supply pressure should be increased until noise reduction gets saturated; it is expected that pulsed microjet with higher supply pressure could generate more noise reduction than reported in [5]. Given that the diameters of microjets are very small compared to that of the main jet nozzle, and also that mass flow rate is directly proportional to the supply pressure, the increased mass flux needed for pulsed microjet control according to increased supply pressure may not be significant. In fact, it was mentioned in section 2.2.1 that the total mass flux of sixteen microjets (with supply pressure of 100psig = 115psi) is less than 1% of the mass flux of the main jet (only 0.05% for a single microjet). When the supply pressure of microjet is increased up-to 190psi, the mass flux of microjets increases by 0.5% than at 115psi which is still much less than that of the main jet. The detailed calculation is as follows: in general supersonic flow in a nozzle, maximum mass flow rate can be calculated by the following equation [35]:

$$\dot{m} = \frac{P_0 \cdot A^* \sqrt{\gamma}}{\sqrt{R \cdot T_0}} \left(\frac{2}{\gamma + 1} \right)^{\frac{\gamma+1}{2(\gamma-1)}}$$

where P_0 and T_0 are stagnation pressure and temperature, respectively, A^* is a cross sectional area of a throat, R is specific gas contant (287 J/kg·K, for dry air), and γ is specific heat ratio (1.4 for both air and nitrogen). With given stagnation pressure (NPR = 3.7 or 54.39psi for the main jet, and 115psi for the microjet) and temperature (300K for both the main jet and microjet), the mass flow rate of the main jet is 0.443 kg/s, and the mass flow rate of a single steady microjet is 0.228×10^{-3} kg/s which is about 0.05% of the main jet. When the supply pressure is increased up-to 190psi, the mass flow rate of a single steady microjet is 0.377×10^{-3} kg/s, thus to be 0.08% of the main jet. Total mass flow rate of microjets can be simply calculated multiplied by 16.

At first, as mentioned in section 2.4, saturated supply pressure should be higher for pulsed microjet than for steady microjet; since it is described in [5] that noise reduction gets saturated with the mass flow rate of $0.8\dot{m}_{100}$ for both steady and pulsed microjet. In other words, noise reduction gets saturated with steady microjet at certain pressure - which is the saturated supply pressure for steady microjet, whereas pulsed microjet could generate further more noise reduction at even higher supply pressure. Since the exact saturated supply pressure for pulsed microjet is not given in the literature, the effort to find the saturated supply pressure for pulsed microjet has been made; although the mass flow rate where noise reduction gets saturated is stated in [5], it is necessary to find an actual input pressure - saturated supply pressure - for pulsed microjet corresponding to saturated mass flow rate. Furthermore, a hypothesis can be made that pulsed microjet with higher supply pressure may produce even more noise reduction (see Figure 3.5).

In order to confirm noise reduction is saturated with mass flow rate of $0.8\dot{m}_{100}$ for microjets as stated in [5], and to clarify the exact saturated supply pressure for pulsed microjet, the experiments varying supply pressure for both steady and pulsed microjet were conducted. Supply pressure was varied from 40psi to 190psi. Figure 3.6 shows the relation between noise reduction (ΔdB) and supply pressure for microjets at the condition of $h/d = 4.0$, TR = 1.0. It can be seen that noise reduction gets saturated between 110 psi and 120 psi for steady microjet, where pulsed microjet

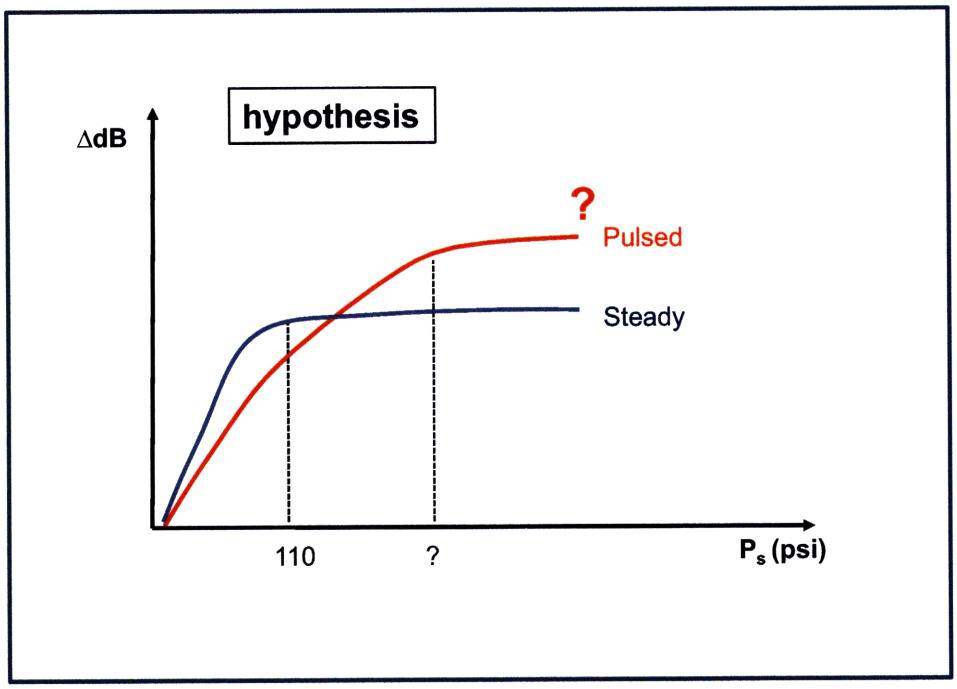

Figure 3.5: A hypothesis: pulsed microjet may generate more noise reduction with higher saturated supply pressure than steady microjet.

control results in saturation at about 140 psi. It should be noted that when one determines saturated supply pressure, the margin of error by ± 0.5 dB should be taken into account as well as whether noise reduction keeps increasing or not. Therefore, saturated supply pressure is higher for pulsed microjet as expected. However, the actual mass flow rate where the noise reduction gets saturated is not exactly the same as stated in [5]; saturation of noise reduction happened with larger mass flow rate for steady microjets, and with smaller mass flow rate for pulsed microjets, respectively, than reported in [5] - $0.8\dot{m}_{100}$; $0.8\dot{m}_{100}$ corresponds to 92 psi for steady microjet and 152 psi for pulsed microjet. Also, the maximum noise reduction was made by 6 dB with both steady and pulsed microjet, which is not consistent with the hypothesis; a hypothesis that pulsed microjet may produce even more noise reduction at higher pressure. Spectra plot shown in Figure 3.7 may explain why the hypothesis is not true; that is, once all impinging tones at several kilohertz are all eliminated, no more noise reduction may be made. In other words, OASPL can be reduced by until all impinging tones are eliminated, considering impinging tones are the primary source

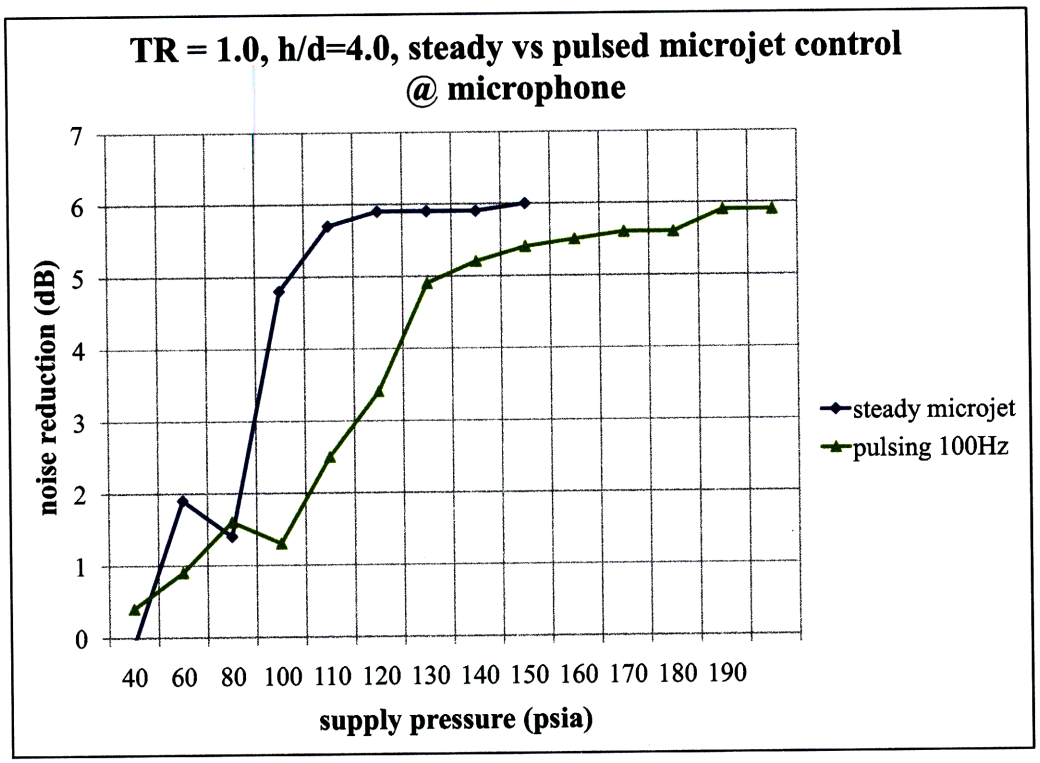

Figure 3.6: Noise reduction versus supply pressure of microjets, $h/d = 4.0$

of noise in supersonic impinging jet problem as stated in section 1.2. In this sense, if one could provide enough supply pressure (with enough mass of nitrogen gas) for either steady or pulsed microjet so that microjet (either steady or pulsed) is able to produce the maximum noise reduction, there may be no advantage of using pulsed microjet control. However, if there is limited mass of nitrogen gas for microjets, then pulsed microjet would be the better choice in terms of mass flow rate needed for control.

Figure 3.8 shows the modified plots such that horizontal axis corresponds to the normalized supply pressure; which means the corresponding supply pressure of steady microjet with the same mass flow used in pulsed microjet at certain supply pressure. Therefore, supply pressure of steady microjet has no need to be normalized, where supply pressure for pulsed microjet is normalized for comparison in terms of mass flow rate; given that mass flow rate is directly proportional to supply pressure [5]. It can be clearly seen in Figure 3.8 that pulsed microjet produces more noise reduction than steady microjet in certain range of supply pressure, from 60 to 110 psi at $h/d =$

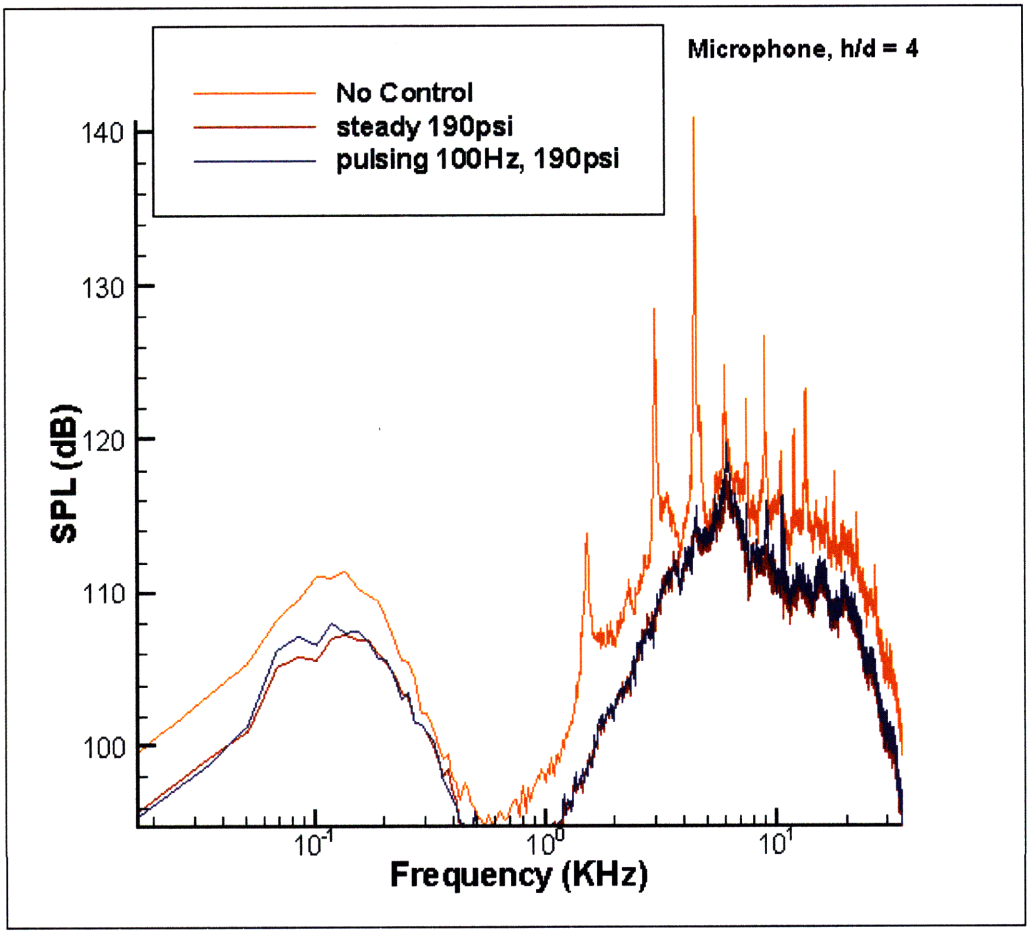

Figure 3.7: Spectra plots: baseline case, steady and pulsed microjet control

4.0. It is meaningful to notice that: 1) noise reduction with pulsed microjet control gets saturated at less mass flow rate than with steady microjet control, 2) the certain rage of supply pressure exists where pulsed microjet gives better noise reduction than steady microjet with the same mass flow rate, and 3) moreover, pulsed microjet is able to produce the same noise reduction (up-to 6 dB) as steady microjet with even less mass flow rate. In order to be more specific for 1) above, saturated supply pressure for pulsed microjet is 140 psi which is normalized to be 80 psi, where saturated supply pressure for steady microjet is 110 psi. Therefore it is clear that noise reduction with pulsed microjet gets saturated with less mass flow rate, and this fact could lead to 2) and 3) above. In reality, with limited mass of control (nitrogen) gas for microjets, this range of supply pressure could be the advantage of using pulsed microjet control. However, it should be also carefully noted that an actual input pressure for pulsed microjet is higher to deliver the same mass flux as steady microjet. If one could further develop (or modify) the design of microjet injection configuration for application to the reality (rather than using rotating cap to produce pulsed microjet), it can essentially save the mass of control gas by using pulsed microjets and thereby realize the advantage of pulsed microjet control; with current method of pulsing, there is loss of mass flow since control gas is still wasted, even though microjets are at OFF position, during the closing time of rotating cap. The microjet injector used in [3], for example, can be used to produce pulsed microjet without any loss of mass.

In addition, it should be noted that saturated supply pressure for pulsed microjet at $h/d = 3.5$ could not be estimated. As seen in Figure 3.9, using steady microjet at $h/d = 3.5$, the noise level is hardly reduced until supply pressure is increased by 180 psi. However, when supply pressure arrives at 180 psi, impinging tones are suddenly, extremely reduced or completely eliminated, and thereby noise reduction is made up-to 9.5 dB. Pulsed microjet control is hardly effective for $h/d = 3.5$ since input pressure cannot exceed 190 psi and thus it cannot reach an effective threshold of mass flow rate to penetrate into the shear layer of the main jet. In order to provide enough supply pressure for pulsed microjet to exceed the threshold (as seen in Figure 3.10), the actual input pressure should be increased by 300 psi or so, which exceeds

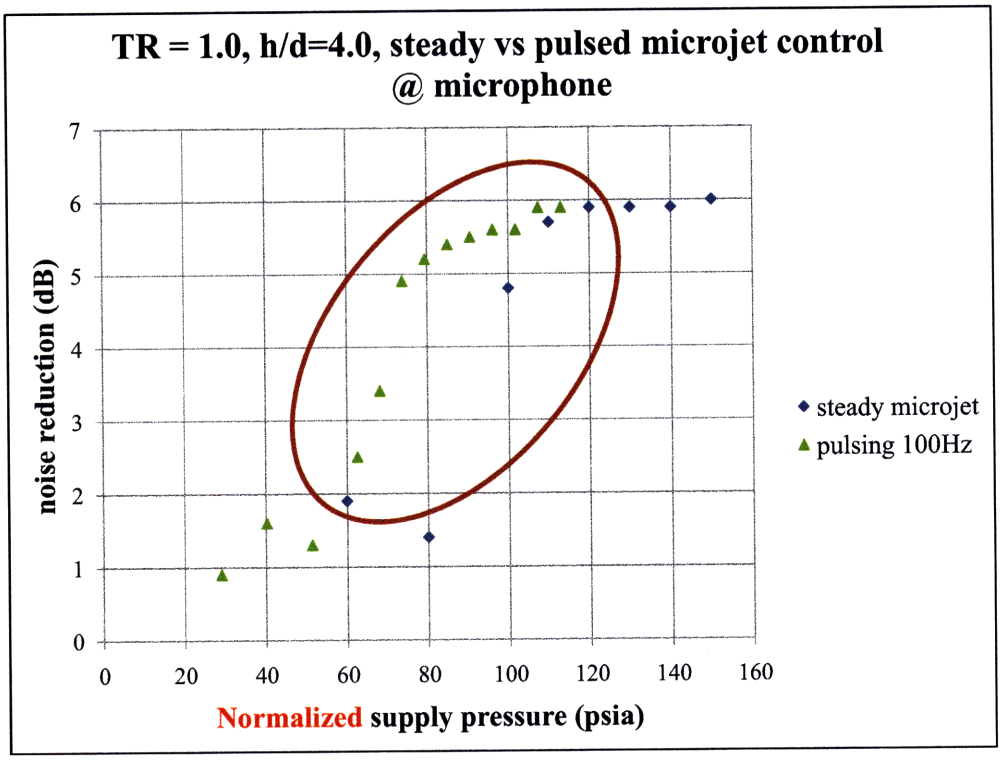

Figure 3.8: Noise reduction versus normalized supply pressure (mass flow rate) of microjets, $h/d = 4.0$

the limitation of current experimental set up; both pressure regulator which controls the input amount of nitrogen gas and pressure transducer at stagnation chamber are able to operate at up-to 200 psi. Since these modifications need major changes of experimental set up, resulting in much time consumption, the experiment with higher supply pressure than 200 psi could not be conducted due to the limited time for the present study.

In this section, the effect of supply pressure for microjets was examined. It was found that: 1) noise reductions with steady [pulsed] microjet control were saturated with larger [smaller] mass flow rate, respectively, than reported in [5] - $0.8\dot{m}_{100}$, 2) even more, noise reduction with pulsed microjet is saturated with less mass flow rate than steady microjet (by comparing normalized saturated supply pressure), 3) maximum noise reduction by either steady or pulsed microjet may be the same, since

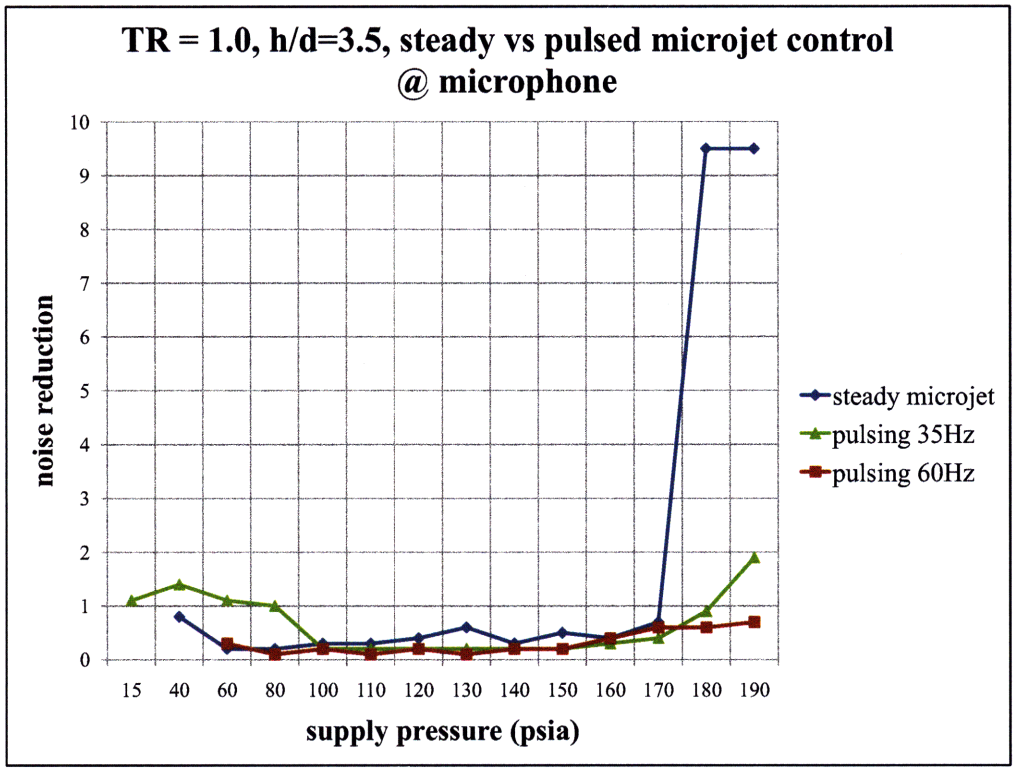

Figure 3.9: Noise reduction versus supply pressure of microjets, $h/d = 3.5$

OASPL is reduced by until all impinging tones are eliminated, 4) pulsed microjet is more effective than steady microjet in terms of mass flow rate; that is, pulsed microjet could produce more noise reduction with the same mass flow rate at certain range of supply pressure, or pulsed microjet could give the same noise reduction even with less mass flow rate. In the following sections, the effect of other pulsing parameters are described.

(2) Pulsing frequency

In order to examine the effect of pulsing frequency, frequency sweep test was conducted. The frequency was varied from 16 Hz up-to 100 Hz with an increment of 5 or 10 Hz, at the saturated supply pressure found in section 3.3.1-(1), for each condition. Figures 3.11~3.13 show the relation between noise reduction and pulsing frequency for different condition of h/d, TR, and duty cycle. For most cases, no dependence was found between noise reduction and pulsing frequency regardless of other conditions,

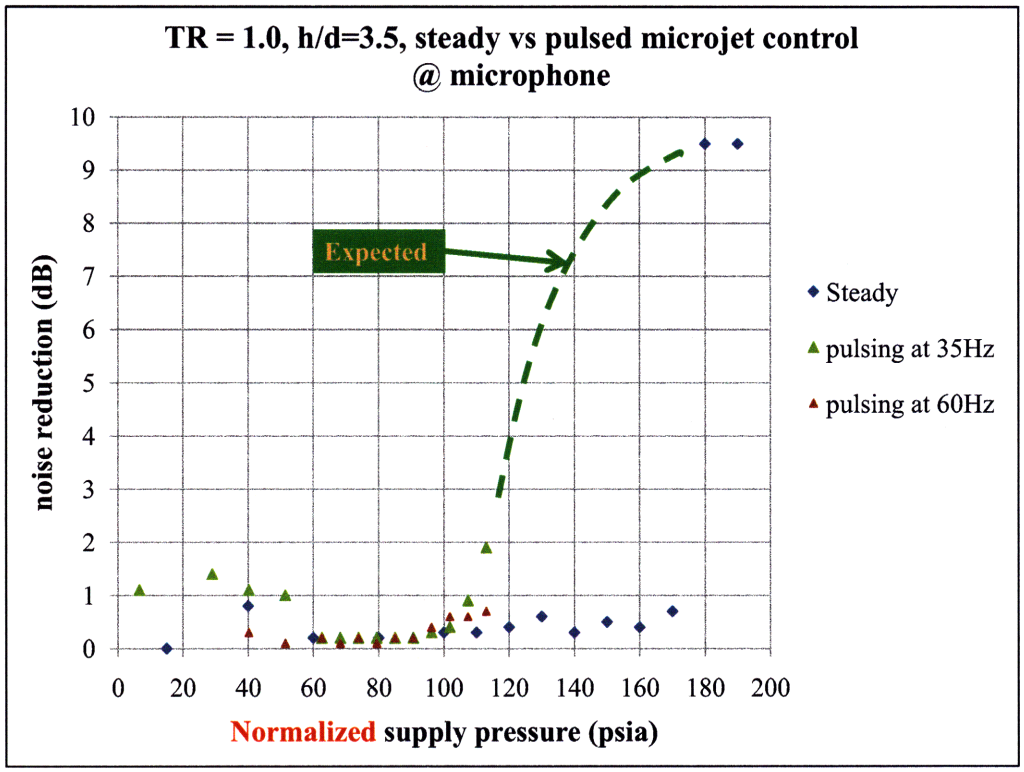

Figure 3.10: Noise reduction versus normalized supply pressure (mass flow rate) of microjets, $h/d = 3.5$

which is coherent with [5] where it stated that varying pulsing frequency does not have much effect on noise reduction beyond certain frequency. For some particular cases, noise reduction was increased as pulsing frequency increases at relatively lower supply pressure (120 psi); where at higher supply pressure (190 psi), no dependence of noise reduction on pulsing frequency was observed. In other words, when mass flow rate is not enough, noise reduction is increased as pulsing frequency becomes higher. If supply pressure is high enough and thereby is enough mass flow rate, almost the same amount of noise was reduced regardless of pulsing frequency. In addition, however, Choi [5] also stated that very low frequency pulsing (around 20 Hz) could produce more noise reduction by 1$\sim$2 dB which is referred to as low frequency mode. In fact, in the present study, the advantage of low frequency pulsing was never found. More details regarding the low frequency mode can be found in section 3.4.

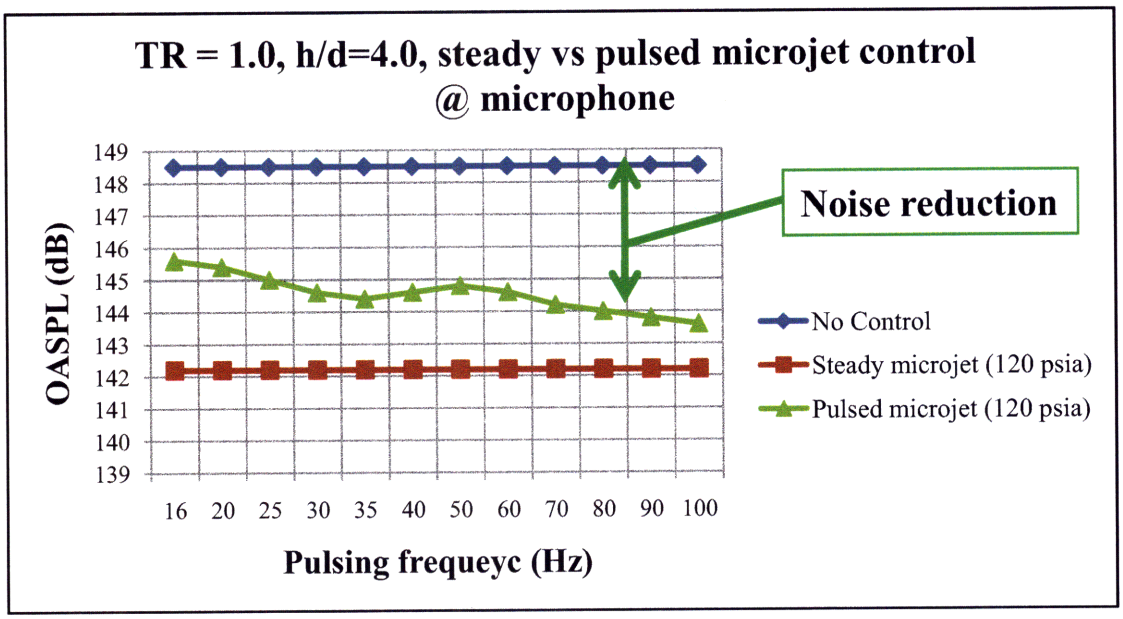

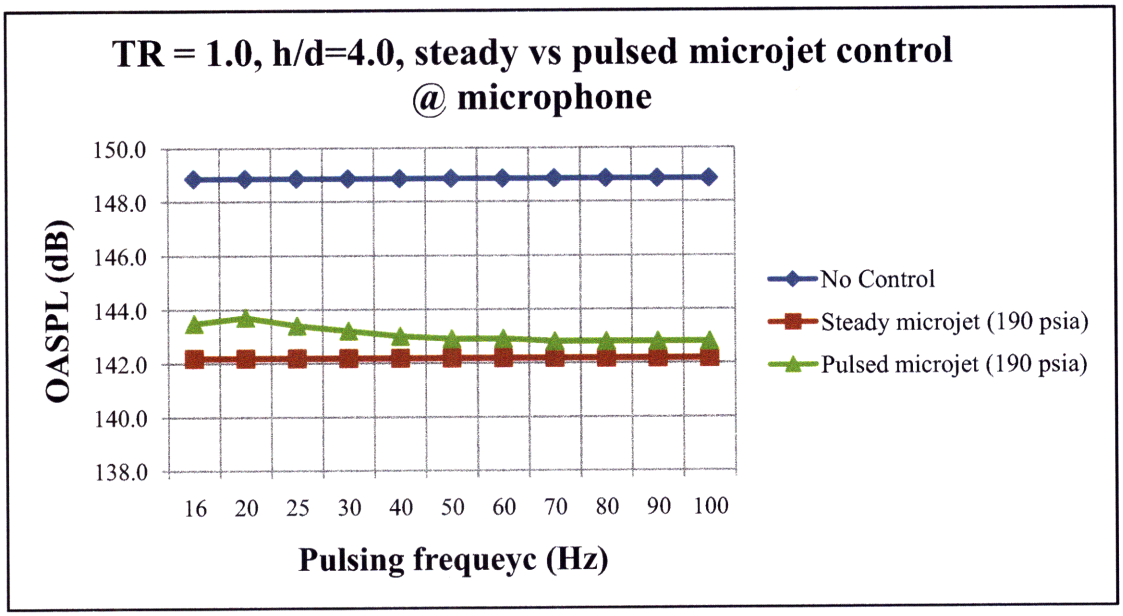

Figure 3.11: OASPL values versus pulsing frequency, TR = 1.0, $h/d = 4.0$

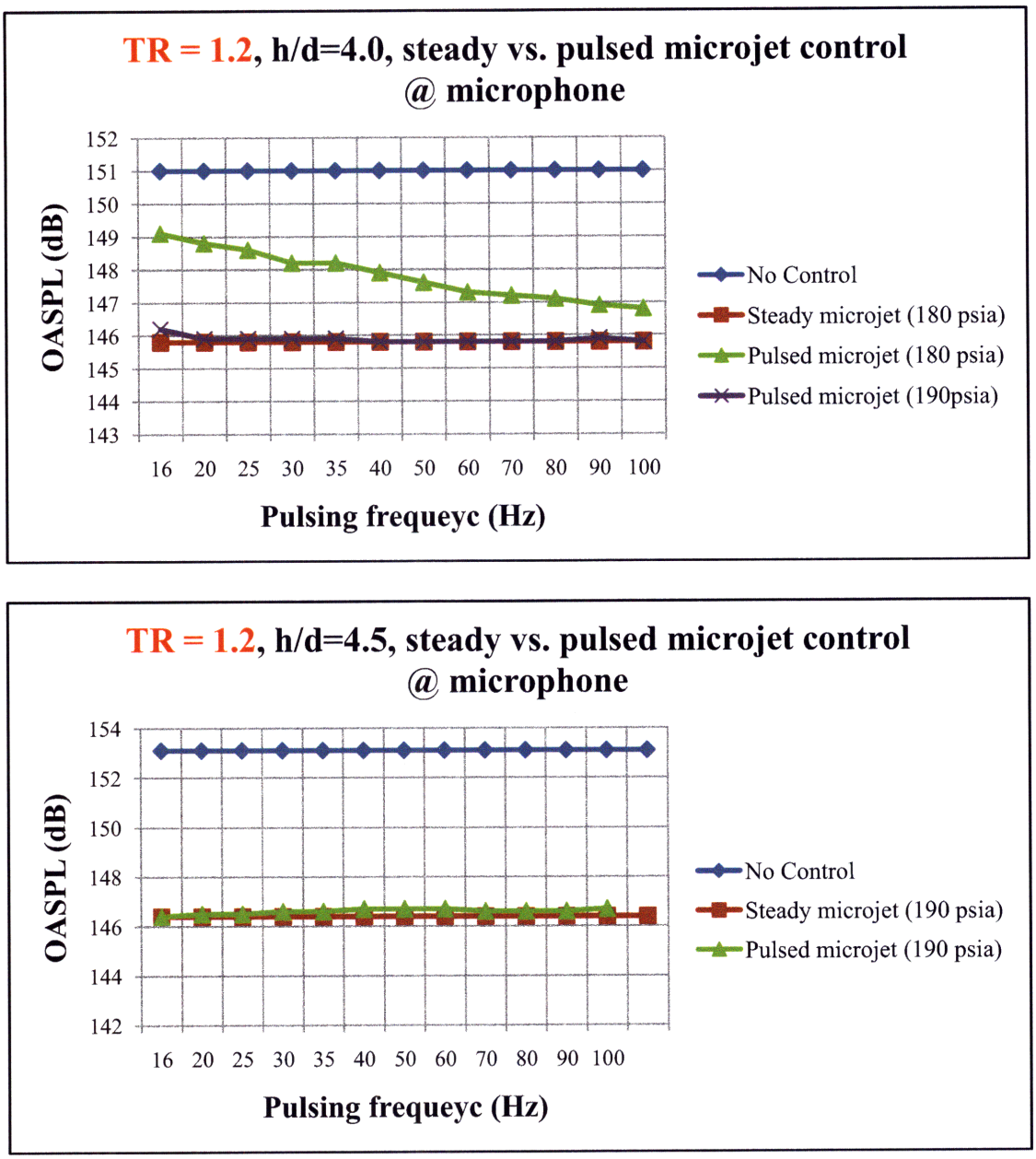

Figure 3.12: OASPL values versus pulsing frequency, TR = 1.2, $h/d = 4.0, 4.5$

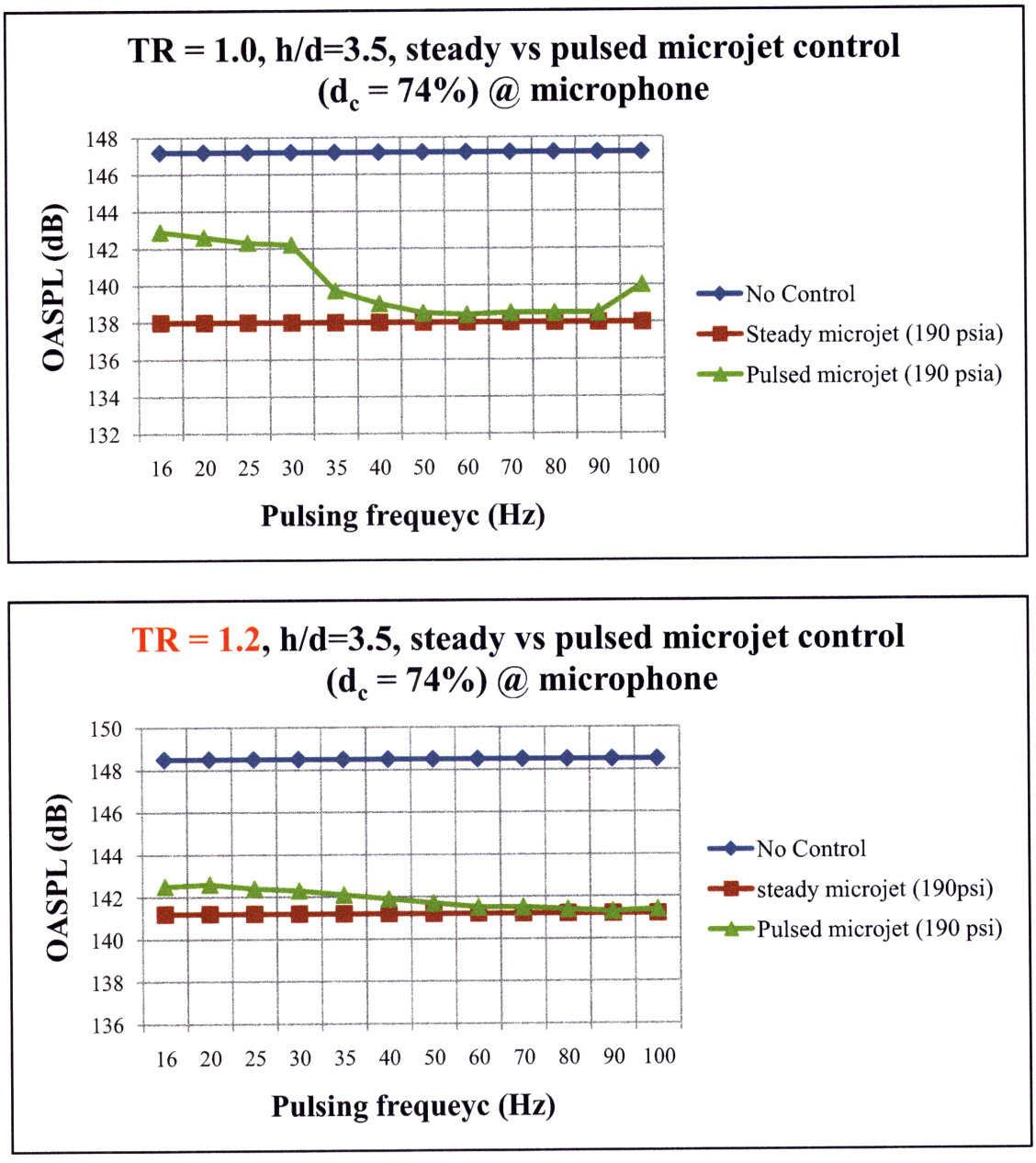

Figure 3.13: OASPL values versus pulsing frequency, TR = 1.0, 1.2, $h/d = 3.5$

(3) Duty cycle

As described in section 3.1, the primary purpose of changing hardware (motor and controller) is to vary duty cycle more efficiently. However, although this method described in section 3.1 is useful logically, when implemented, it did not work out as expected due to the physical restraint in reality. The reason is that the inertia of stepper motor is too large to follow the command in real time; since the motor is rotating fast (for example, one pulsing period is $\frac{1}{16}$ second when pulsing at 16 Hz), when the motor stopped momentarily at ON position of microjets and tried to start to rotate again, the motor jammed up. In order to resolve this problem, the motor should be replaced to the appropriate one with much better performance - that is, for example, the one with higher torque enough to overcome its inertia. However, due to the time constraint of this study, this trial was interrupted and rotating cap was changed in order to vary duty cycle.

Noise reduction by pulsed microjet control with duty cycle of 56% and 74% is shown in Figure 3.14. Since the lift plate was removed first from the main nozzle to change the rotating cap, and reassembled to the nozzle, OASPL of the baseline case was carefully checked if there is any change. In fact, OASPL of baseline case measured from microphone was changed by 0.6dB which is within the margin of the error of $\pm$0.5dB. However, with steady microjet control, noise reduction in second run suddenly happened at 160psi, where it previously happened at 180 psi. Also, pulsed microjet with duty cycle of 74% produced more noise reduction than with duty cycle of 56%. This may be due to larger mass flow rate with duty cycle of 74%, and thereby larger mass flux could deliver more momentum into the shear layer of the main jet. If we normalize supply pressure as previously to compare noise reduction between steady and pulsed microjet in terms of mass flow rate, as seen in Figure 3.15, it can be observed that duty cycle of 74% gives us the extension of plot so that noise reduction with pulsed microjet control can be seen in larger range of normalized supply pressure. Since the noise reduction by pulsed microjet (by 8dB) is almost the same as steady microjet (by 9dB) in available range of supply pressure,

pulsed microjet is effective from the point of view of mass flow rate; pulsed microjet generates more noise reduction with the same mass flow rate in the range of 130-140 psi, or almost the same noise reduction with even less mass flow rate.

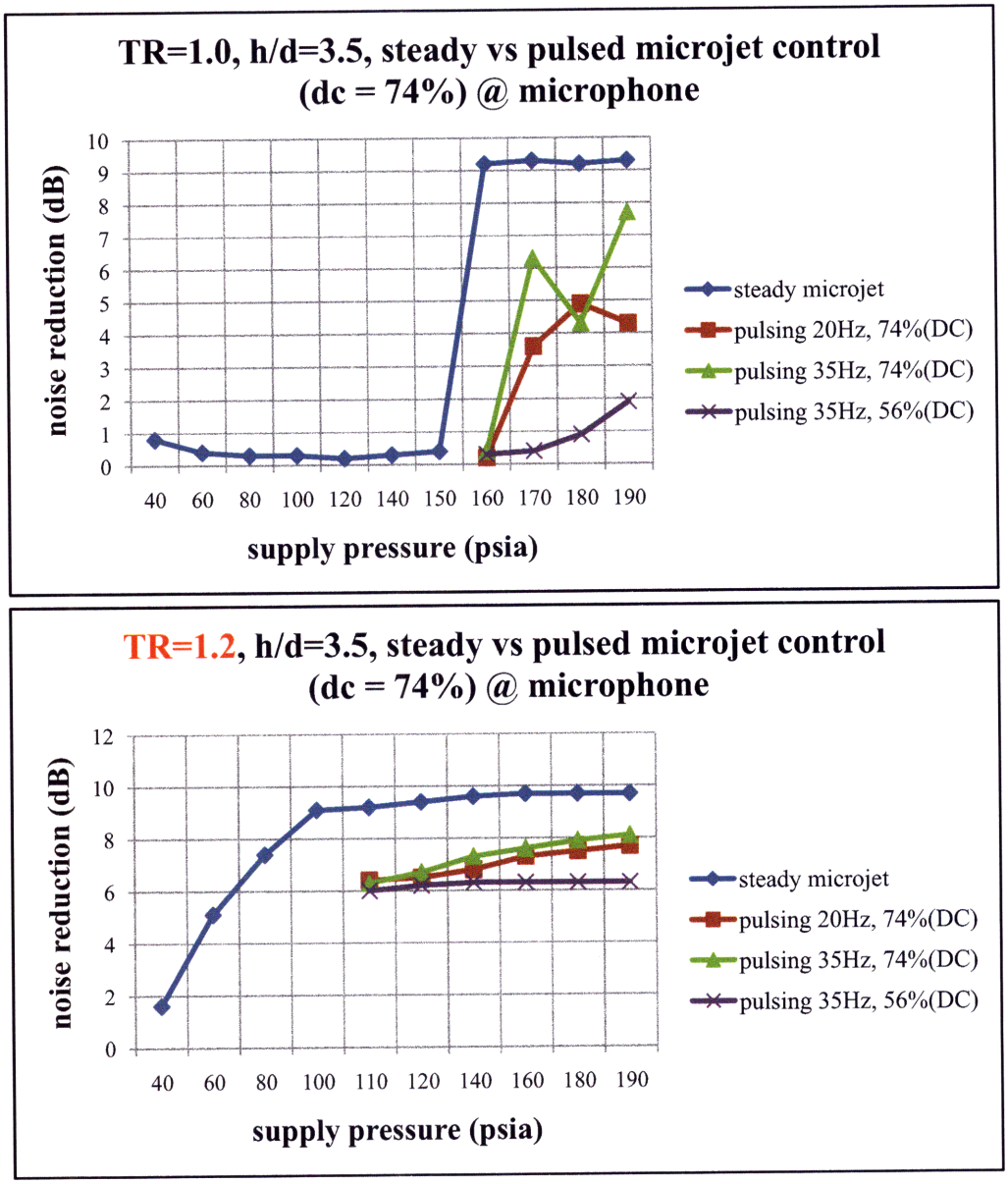

Figure 3.14: Noise reduction versus supply pressure of microjets, TR = 1.0, h/d = 3.5, with duty cycle of 74%

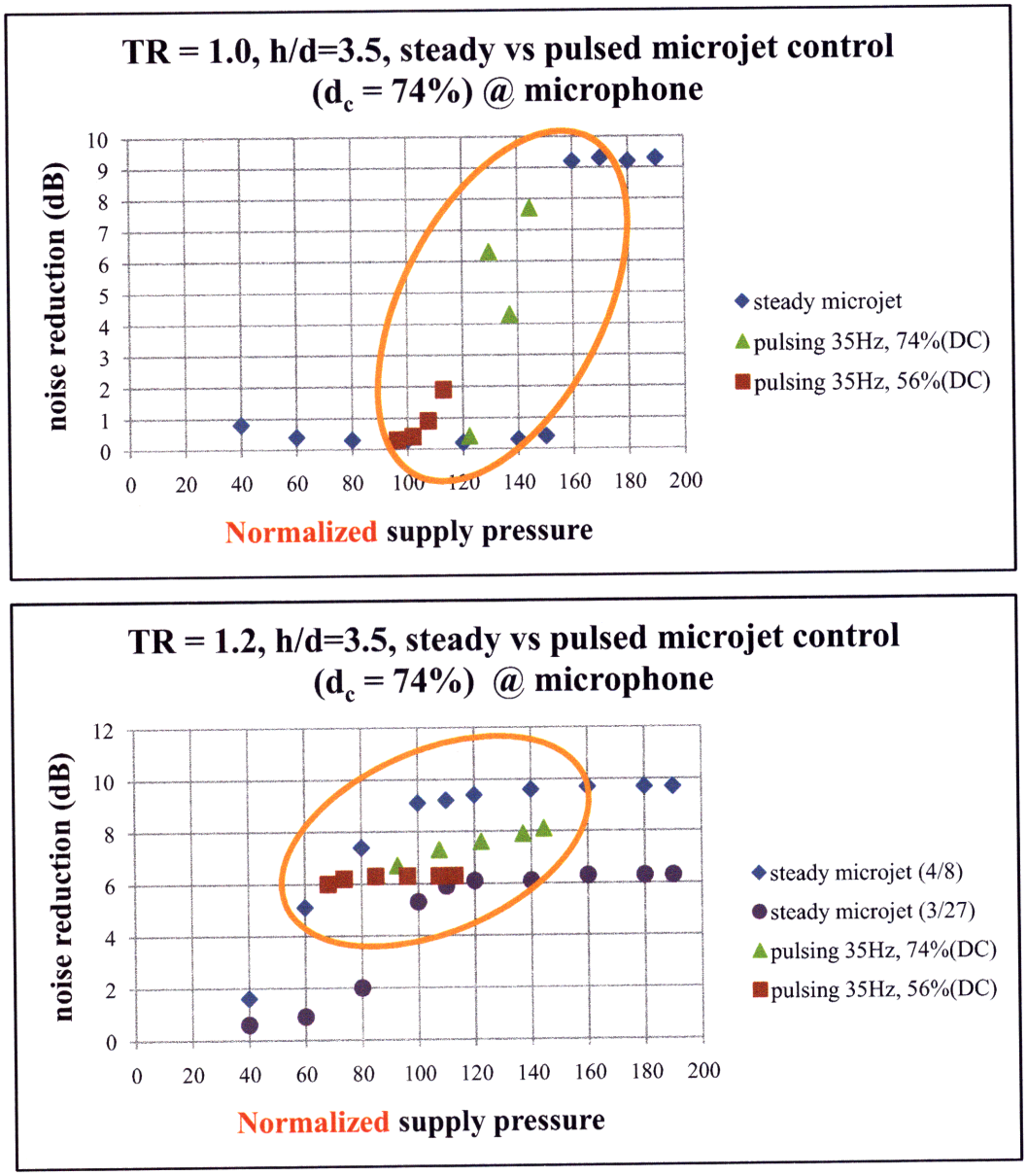

Figure 3.15: Noise reduction versus normalized supply pressure (mass flow rate) of microjets, TR = 1.0, $h/d = 3.5$, with duty cycle of 74%

3.3.2 Effect of pulsed microjet on hot temperature jet

In reality, since STOVL aircraft experiences hotter impinging jet than the ambient air, it is necessary to examine the effect of pulsed microjet on hotter main jet. In [5] and [34], it is stated that steady microjet is more effective on hotter main jet; in hot temperature impinging jet, the feedback loop is more resistive, and thereby the amplitude of impinging tone is higher and also impinging tone remains longer than cold (TR = 1.0) impinging jet. Therefore, microjet control could have more capability to suppress impinging tones in the case of hot temperature impinging jet. In the present study, pulsed microjet control was used for hotter temperature main jet. It should be noted that temperature ratio was increased only by up-to TR = 1.2 due to the limitation of motor operating condition (see section 2.4). Although it is not hot enough as the reality, the effect of pulsed microjet on hotter temperature jet may be inferred from the test result.

Figure 3.16 shows the effect of pulsed microjet at TR = 1.2 for different heights. In most cases, for hot temperature jet, pulsed microjet gets more effective than for TR = 1.0 in that pulsed microjet produces more noise reduction than steady microjet in much broader range of supply pressure. For the case of TR = 1.0, the range of supply pressure where pulsed microjet is more effective than steady microjet with the same mass flow rate is 60 $\sim$ 110psi, N/A, 90 $\sim$ 110psi, for h/d = 4.0, 3.5, 4.5, respectively (see Figures 3.8 and 3.10). However, for TR = 1.2, the range of supply prssure where pulsed microjet is more effective than steady microjet, is 60 $\sim$ 90psi, 60 $\sim$ 115psi, 20 $\sim$ 115psi, for h/d = 4.0, 3.5, 4.5, respectively (see Figure 3.16). Therefore, it can be inferred that pulsed microjet gets more effective in terms of mass flow rate than steady microjet on hotter temperature main jet, and thereby it can be more useful for application to the reality.

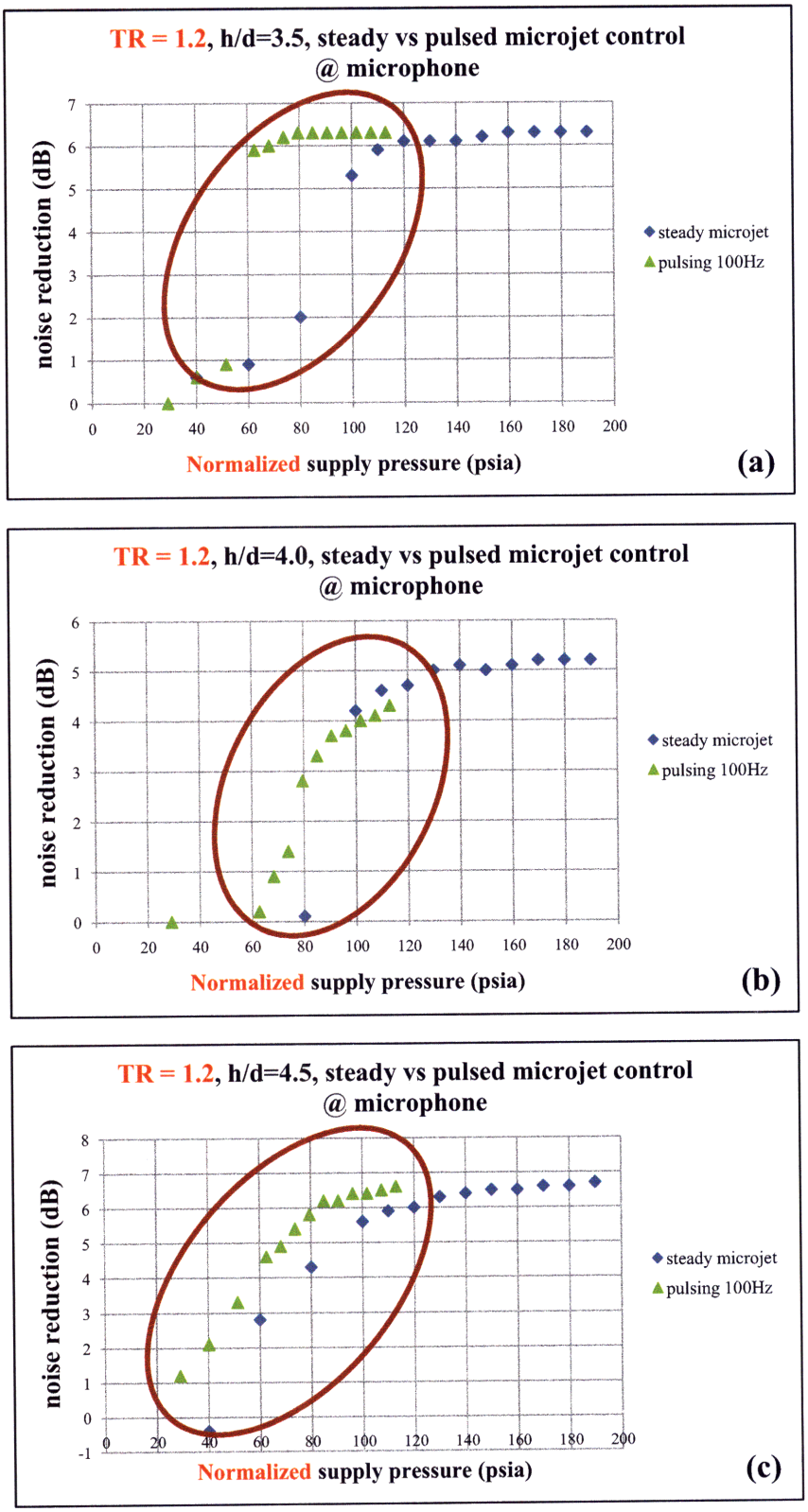

Figure 3.16: Noise reduction versus normalized supply pressure (mass flow rate) of microjets; the effectiveness of pulsed microjet on hot temperature jet (TR = 1.2)

3.3.3 Transient mode

When pulsed microjet is activated, even though the control input signal is a form of square wave (with certain pulsing frequency and duty cycle), the actual response of the system would not follow exactly as the input signal; that is, the pressure response of the system would not be an exact form of square wave. The reason is - which one could easily guess in common engineering sense - time delay exists when the system responses as the microjets penetrate into the shear layer and thus try to modify the flow structure; this is referred to be as *transient mode* , and the time needed for the system to observe in itself the effect of microjets could be referred to be as *time constant* .

In order to estimate the effect of pulsed microjet on the overall impinging jet flow system, it is necessary to compare the time scales of one puling period (1/pulsing frequency) and time constant of system. The raw voltage data in time domain are shown in Figures 3.17 $\sim$ 3.21.[1] For the sake of comparison, baseline case is plotted together with the case of pulsed microjet control in each plot, and the case of steady microjet control is also shown in Figures 3.20 and 3.21. Since the minimum and maximum value of pulsing frequency in this study are 16Hz and 100Hz, respectively, in order to look at the transient mode, the case of pulsing at 16Hz (the slowest pulsing) was examined first and the case of pulsing at 100Hz is followed. As seen in Figures 3.17 $\sim$ 3.21, the effect of (either steady or pulsed) microjet control can be clearly confirmed by looking at the amplitudes in time domain plots. As shown in Figure 3.17, the imprint of pulsed microjet (pulsing at 16Hz) can be clearly observed in the time domain plot. By a simple calculation, pulsing frequency of 16Hz can be coverted to the pulsing period of $1/16$ sec $= 0.0625$ sec. Observation of a pulsing period shown in Figure 3.17 is consistent with the calculation. The transient mode of the system response can be also clearly seen in Figure 3.17; the amplitude increases and decreases gradually during the transient mode. In order to look at the transient mode more

[1]The raw voltage data is the original data in Volt recorded by microphone, which can be converted into the pressure, if divided by a proper gain value (0.00316V/psi for the microphone used here). This raw pressure data is then processed by FFT analysis in order to obtain spectra in frequency domain.

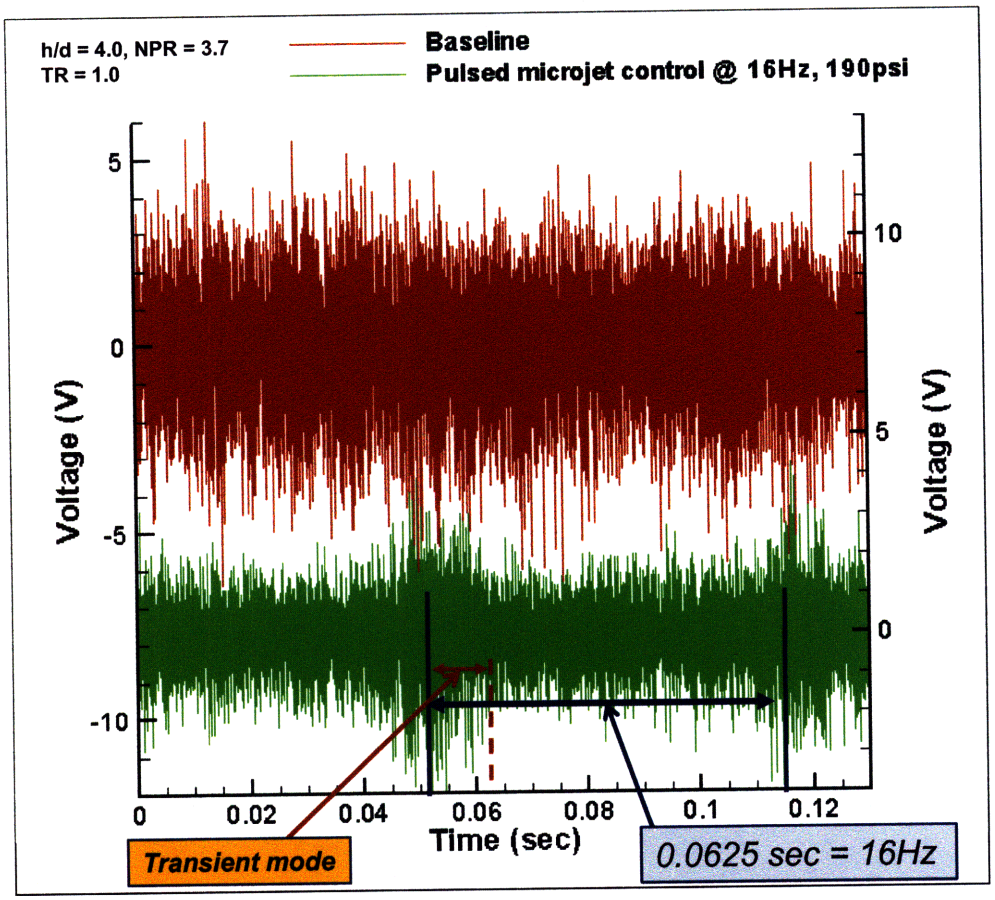

Figure 3.17: Observation of transient mode - raw voltage data versus time, for pulsing at 16Hz

in specific, horizontal axis is re-scaled to zoom in on the transient mode (see Figure 3.18). As seen in Figure 3.18, the time period at the transient mode (time constant) is estimated to be 0.0085 sec. It should be noted that this time constant implies that it takes 0.0085 sec for the impinging jet flow to completely recognize the presence of the microjet, thereby the effect of microjet control becomes valid. Considering the duty cycle of rotating cap is 56%, the opening time of microjets pulsing at 16Hz is $0.0625 \times 0.56 = 0.035$ sec. The opening time is about 4 times longer than the time constant. Therefore, for each pulsing period (at 16Hz), there is enough time for the system to recognize ON/OFF of microjet activation.

On the other hand, when pulsed microjet is activated at 100Hz, one pulsing period is 0.01 sec, which is close to the time constant of the system (= 0.0085 sec). Figure 3.19 shows the time domain plot for the case of pulsing at 100Hz. In this case, the effect of

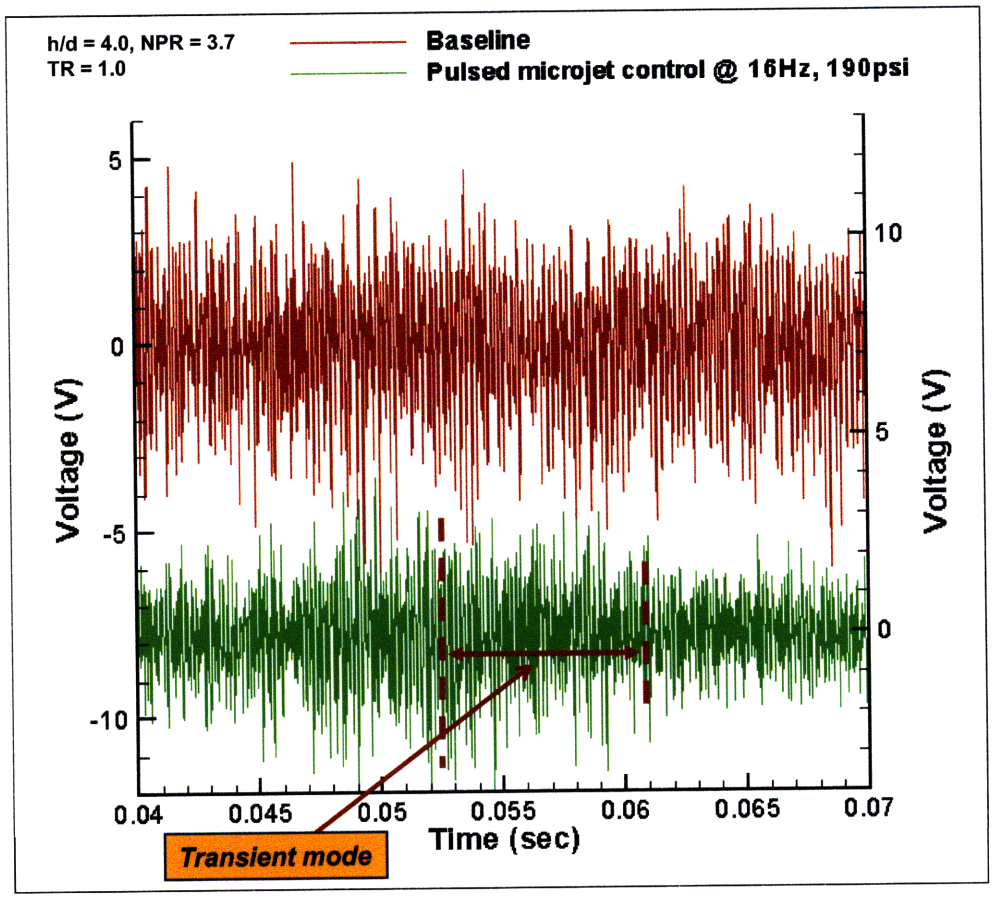

Figure 3.18: Observation in detail of transient mode - raw voltage data versus time, for pulsing at 16Hz

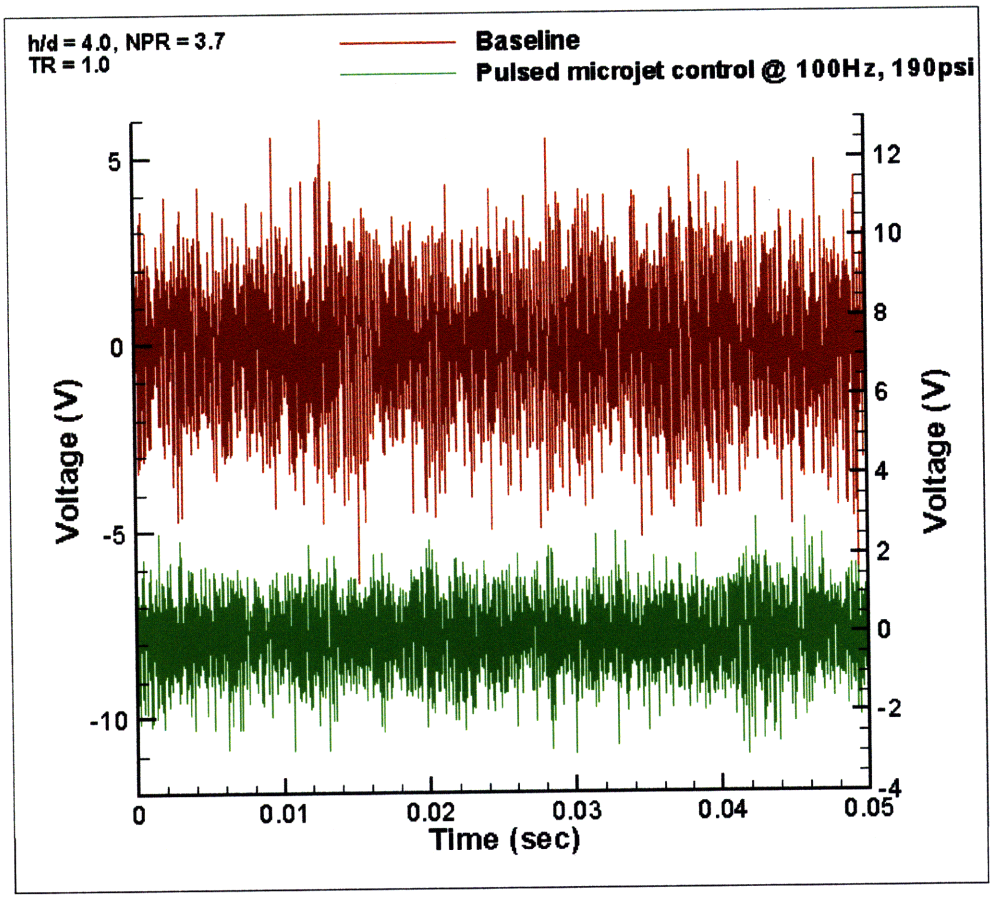

Figure 3.19: Observation of transient mode - raw voltage data versus time, for pulsing at 100Hz

pulsed microjet control (compared to the baseline case) is obviously seen, however, it is hard to clearly observe a pulsing period. The opening time of microjets pulsing at 100Hz (with duty cycle of 56%) is $0.01 \times 0.56 = 0.0056$ sec. The opening time in this case is shorter than the time constant of the system (0.0085 sec), therefore, there is not enough time for the impinging jet flow system to recognize ON/OFF of microjets. Rather, before the system completely recognize the microjets when microjets are activated, microjets go to OFF position and vice versa; before the system completely recognize the microjets are gone to OFF position, microjets are again at ON position. This might be the reason why a pulsing period (at 100Hz) cannot be clearly observed as seen in Figure 3.19. In addition, for the sake of comparison, time domain plots for steady microjet control are also shown in Figures 3.20 and 3.21; it is obvious that there is no transient mode observed in the case of steady microjet control.

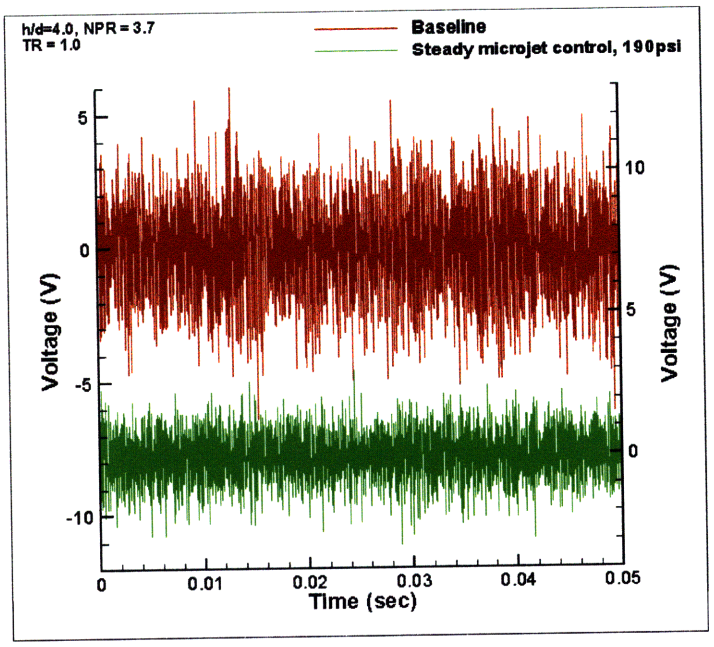

Figure 3.20: Raw voltage data versus time, steady microjet control for the sake of comparison

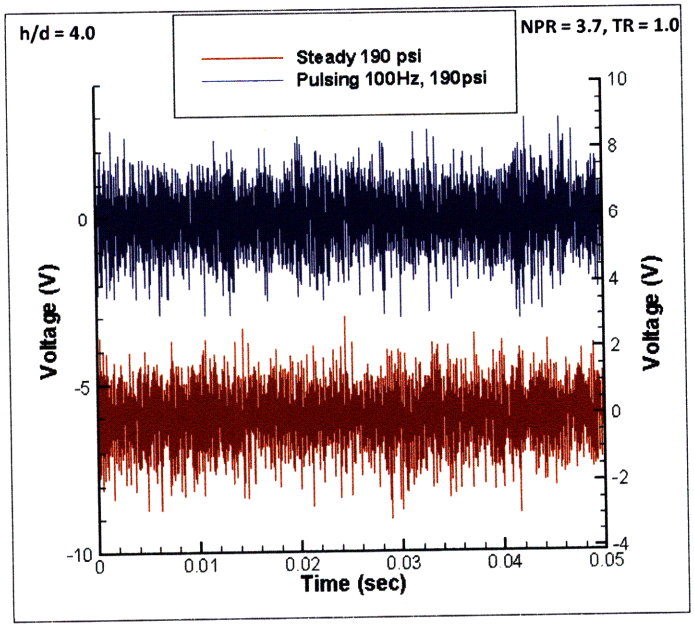

Figure 3.21: Raw voltage data versus time, steady microjet control vs. pulsed microjet control (at 100Hz) for the sake of comparison

Last, another careful observation of time domain plot is followed in this section. If one look at the raw data response, not the amplitude but the shape inside the time series plot, it can be carefully inferred that another time scale can be observed. As seen in Figure 3.22, even though it is hard to observe the imprint of pulsed microjet (at 100Hz) by looking at the amplitude, one can observe the time scale of 100Hz (pulsing period = 0.01 sec) inside the plot itself. Similarly, in the baseline case, certain time scale could be observed inside the time series plot itself, which is about the same as time constant mentioned above (0.0085sec). If this observation is meaningful - that is, impinging jet flow structure has some sort of mechanism in itself corresponding to the time scale of 0.0085 sec, one could relate the time scale observed inside the plot to the time constant. Moreover, one could relate the time constant of the system (0.0085 sec = 117Hz) to the reason why noise reduction increases as pulsing frequency is increased at relatively lower supply pressure (see section 3.3.1-(2)). If pulsed microjet could operate at the frequency of a principal mode of the system, it may effectively excite the flow structure; this argument is not a conclusion from the observation, but it is proposing a possible mechanism of impinging jet flow structure. More investigation on this observation is needed.

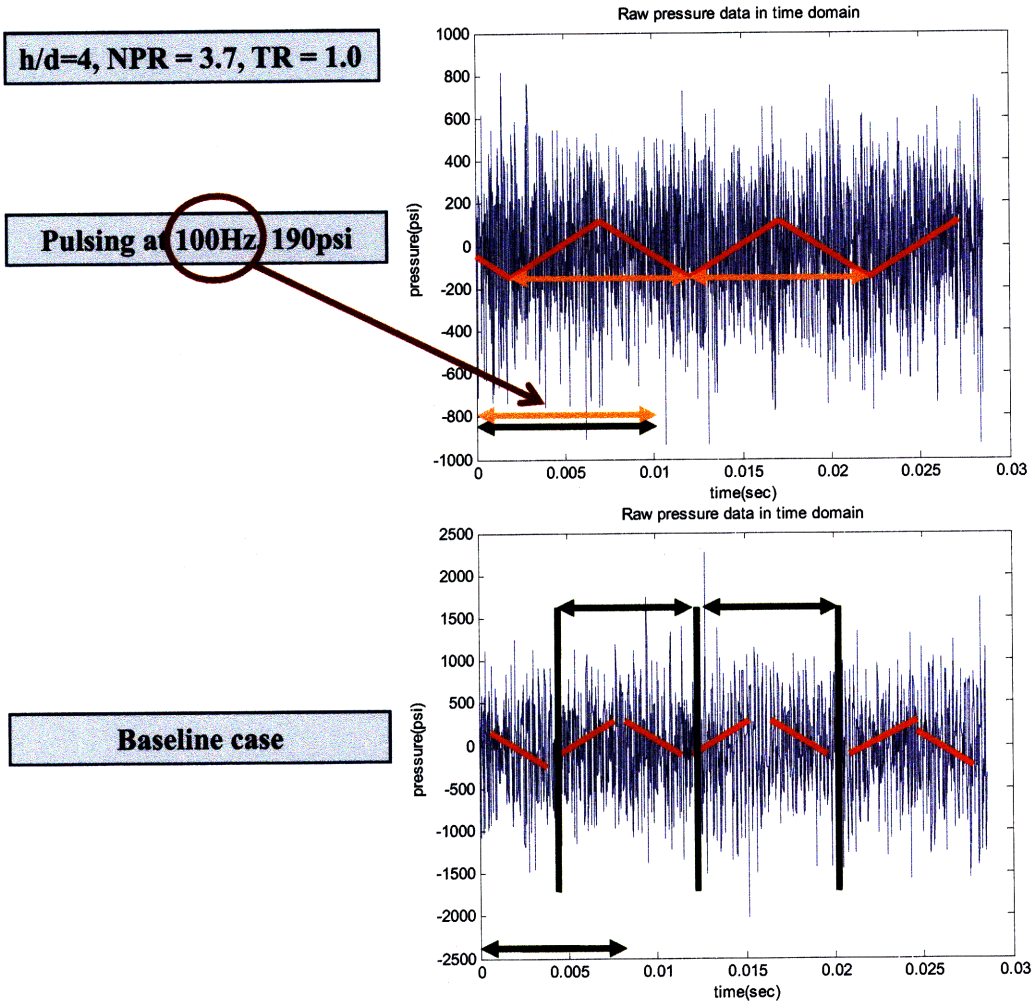

Figure 3.22: Additional observation of raw voltage data versus time, for pulsed microjet control (at 100Hz) and baseline

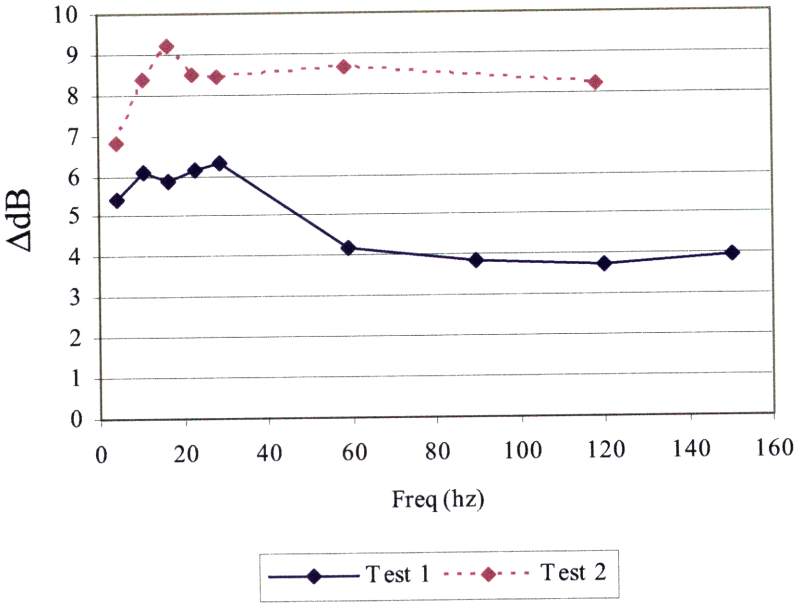

Figure 3.23: OASPL reduction obtained using pulsed microjet, as a function of pulsing freuqency [5]

3.4 Low Frequency Mode

3.4.1 Comparison with previous research

As described in sections 2.4 and 3.2.1 - (2), Choi [5] stated that very low frequency pulsing at around 20 Hz generates more noise reduction than other pulsing frequency, by 1 $\sim$ 2dB (see Figure 3.23). He also found a low frequency peak at around 20Hz in all sensors at ground plane, lift plate and microphone as seen in Figure 3.24; which is referred to as the low frequency mode. Choi [5] also performed analyses to rule out other possibilities for the reason of low frequency mode, such as surrounding noise, vibration of ground plane or lift plate, and natural frequency of each part of facilities, thus concluded the low frequency mode is highly related to the impinging jet flow structure [5].

As stated in section 2.4, clarifying the low frequency mode has been one of the main objectives of the present study. In order to examine the low frequency mode, pulsing frequency sweep tests were conducted for several conditions as described in section 3.3.1-(2), and also spectra plots were carefully examined to confirm the presence of

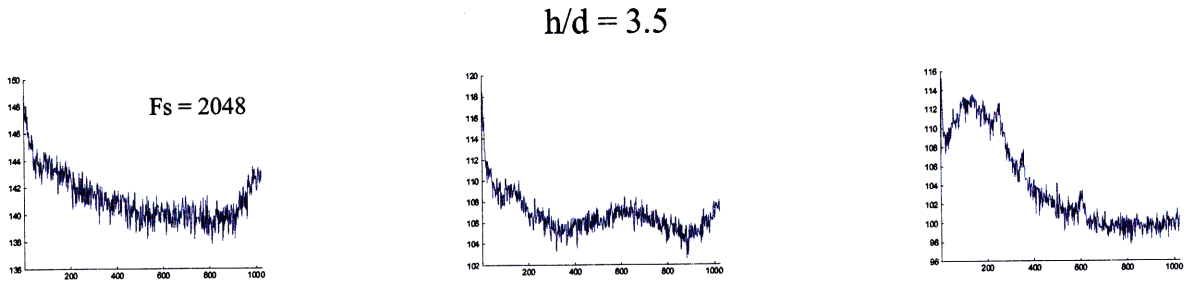

Figure 3.24: Spectra plot in low frequency region measured at ground plane, lift plate and microphone [5]

the low frequency peak around 20Hz. The result of frequency sweep tests were seen in Figures 3.11~3.13, and also spectra plots of baseline case and pulsed microjet control case are shown in Figure 3.25. As seen in Figures 3.11~3.13, 3.25, and 3.26, any test result was not coherent with [5]. Noise reduction was not dependent on pulsing frequency in most cases, and thereby low frequency pulsing at 20 Hz did not make any additional noise reduction. Also, low frequency peak at 20 Hz was not observed in any spectra plot. The conditions of sampling the data and FFT processing for [5] and present study are described in the following. In [5], 40960 points were recorded at the sampling frequency of 2048Hz in order to get a high resolution of 2Hz with FFT size of 1024, where in the present study, total 1638400 points were sampled at the frequency of 70,000Hz with FFT size of 4096, and thus the resolution was about 4Hz, which is enough to capture the low frequency mode at around 20Hz. In other words, the difference in processing the data between [5] and the present study is that low frequency was used for sampling in [5] to get a high resolution, where the present study maintained the sampling frequency (as for all other data set), and recorded much more points to get a high resolution. Since oversampling (which means sampling at higher frequency than Nyquist frequency) must be more accurate than lower sampling frequency, the difference of sampling frequency and FFT size should not affect the appearance of low frequency mode. In Figure 3.27, spectra plots of [5] and recent test results were shown for comparison. The overall shapes of spectral plot are consistent in both cases. However, in very low frequency range, the peak was

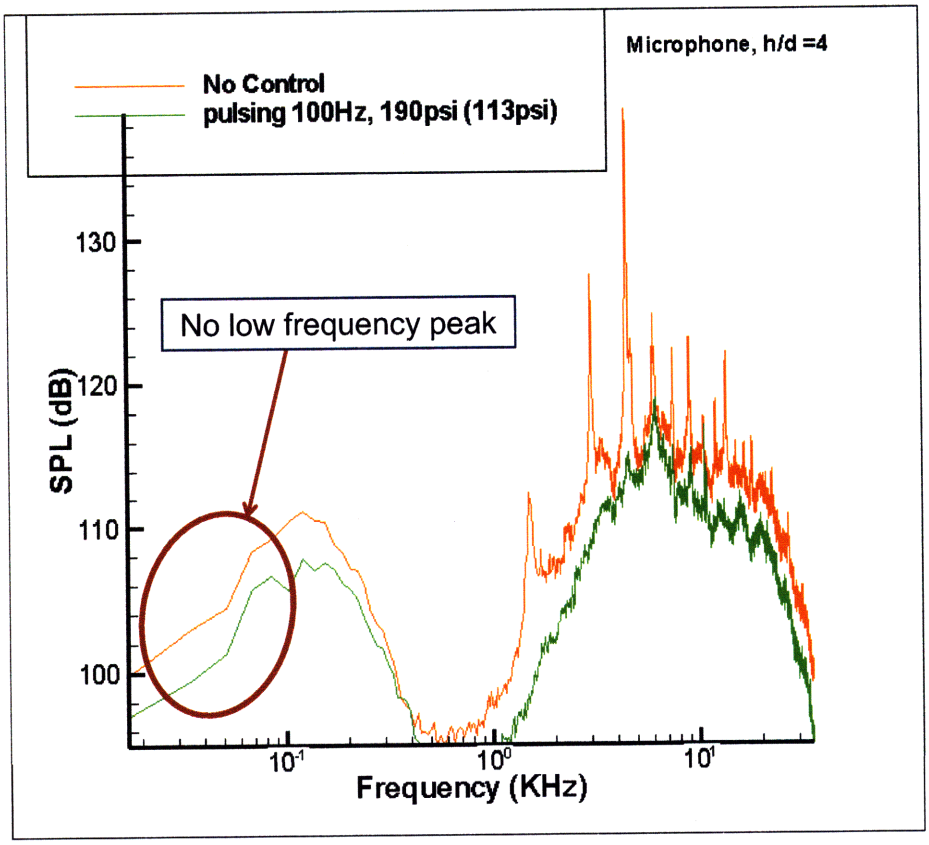

Figure 3.25: Spectra plots of baseline case and the case of pulsed microjet control @ microphone

observed only in [5], not in the recent test result. The experiment was repeated over all again in order to find any low frequency peak; however, it was never repeated as in [5]. Some of possible reasons for why low frequency peak is not repeated may be the following: for example, different ground plate was used, and the motor for pulsing injection was replaced to the new stepper motor. However, if the low frequency mode is coming from the impinging jet flow structure as stated in [5], it should be observed regardless of the change of experimental set up. This may imply that the low frequency peak observed in [5] is not from the main jet flow structure, rather, it might be due to a particular experimental set up, as yet unknown. On the other hand, the broadband hump in low frequency range ($50 \sim 350$Hz) is common between two plots - it is referred to as low frequency hump, which will be discussed in the next section.

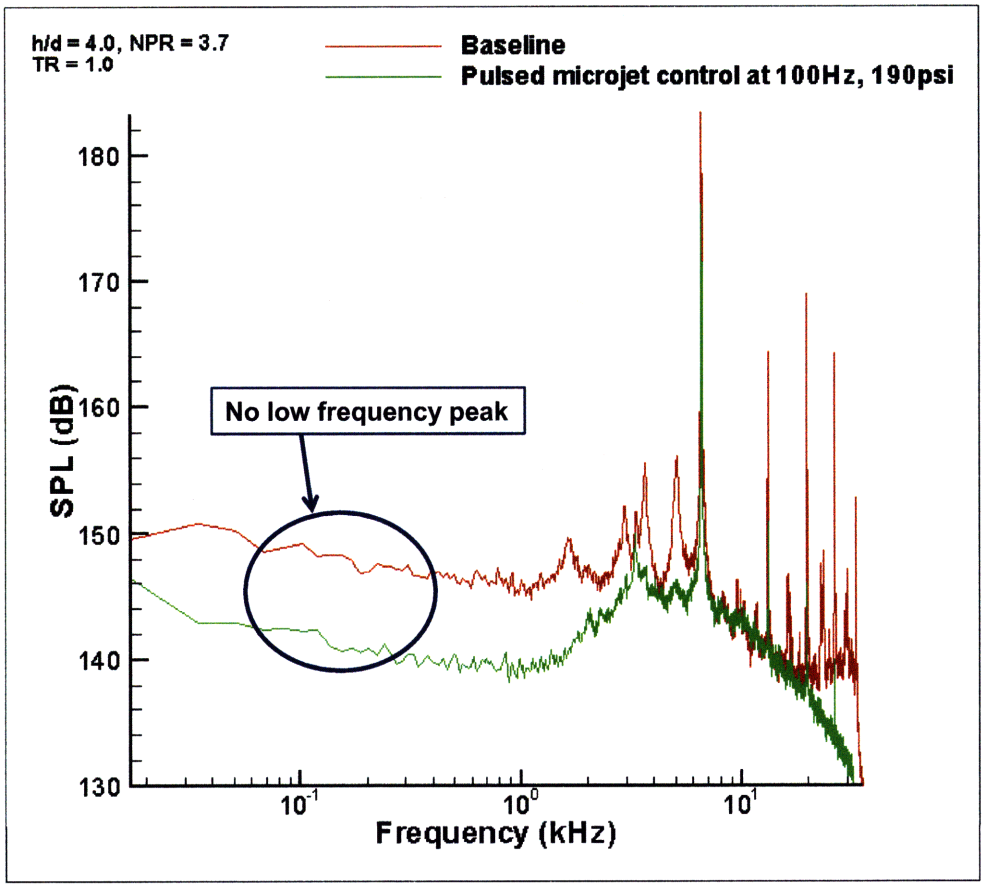

Figure 3.26: Spectra plots of baseline case and the case of pulsed microjet control @ Kulite on the ground plane

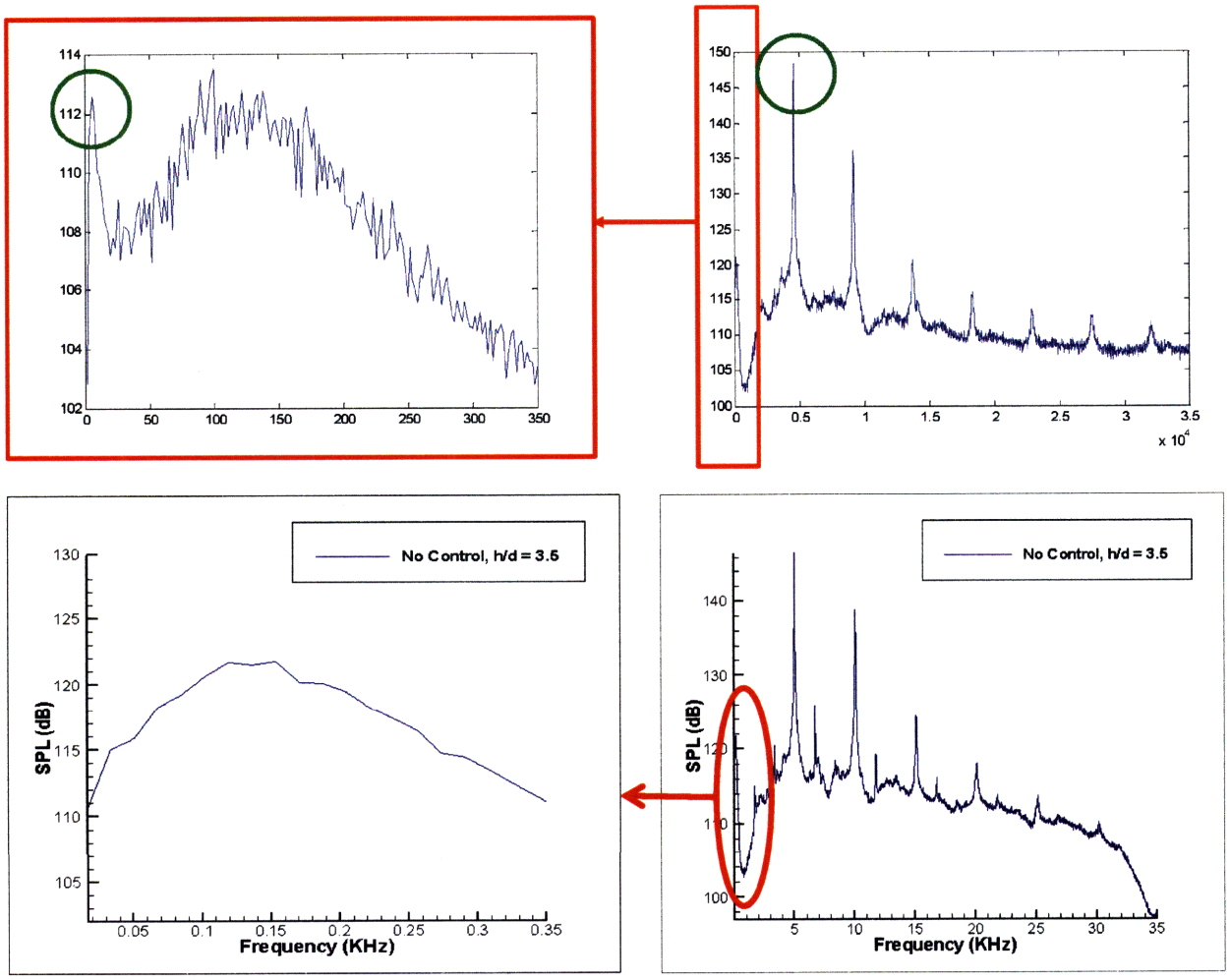

Figure 3.27: Comparison of spectra plot between [5] and the present study; the presence of low frequency peak

3.4.2 Low frequency hump

As seen in Figure 3.27, low frequency hump is common for both [5] and the present study, instead of the low frequency peak. One could observe two broadband humps in the spectra plot. One is the low frequency hump in the range of $50 \sim 350$Hz, another is in higher frequency range of $1 \sim 10$kHz. It is well known that the broadband hump in the frequency range of several kilohertz is due to turbulent mixing noise, where turbulent mixing refers to that small vorticity structure in the impinging jet (turbulent) flow field evolves into large scale vortical structure [21]. However, the low frequency hump is not mentioned in any literature.

It should be also noted that low frequency hump is observed only from the microphone data, but not from the Kulite^{TM} data on the ground plane (see Figures 3.25 and 3.26). If low frequency hump is caused by impinging jet flow structure, although the exact mechanism is not clearly known yet, it should be also observed from the Kulite^{TM} measurement on the ground plane, which is not the case. Therefore, it can be carefully inferred that the low frequency hump is not due to the flow structure of impinging jet. Rather, it could be an acoustic effect, in that the hump is observed only from the microphone. Since nearby metal surfaces were covered by thick acoustic foam in order to minimize acoustic reflection, a hypothesis can be made such that low frequency hump is a result of the acoustic reflection by a room; since all other possible reasons have already been ruled out [5]. In order to confirm this hypothesis, rough analysis was conducted as following.

For the analysis of the effect of reflection by STOVL room, it should be first noted that: 1) the room is assumed to be an exact rectangular with flat surfaces (see Figure 3.28), 2) all surfaces are assumed to be perfectly rigid, thus a normal velocity of particle is zero, 3) the room surfaces are the only causes of acoustic reflection, where other possible reflection by the experimental set up such as beams, nozzle, ground plane, and lift plate are all assumed to be negligible. With appropriate boundary conditions based on the assumptions as stated above, the following three-dimensional

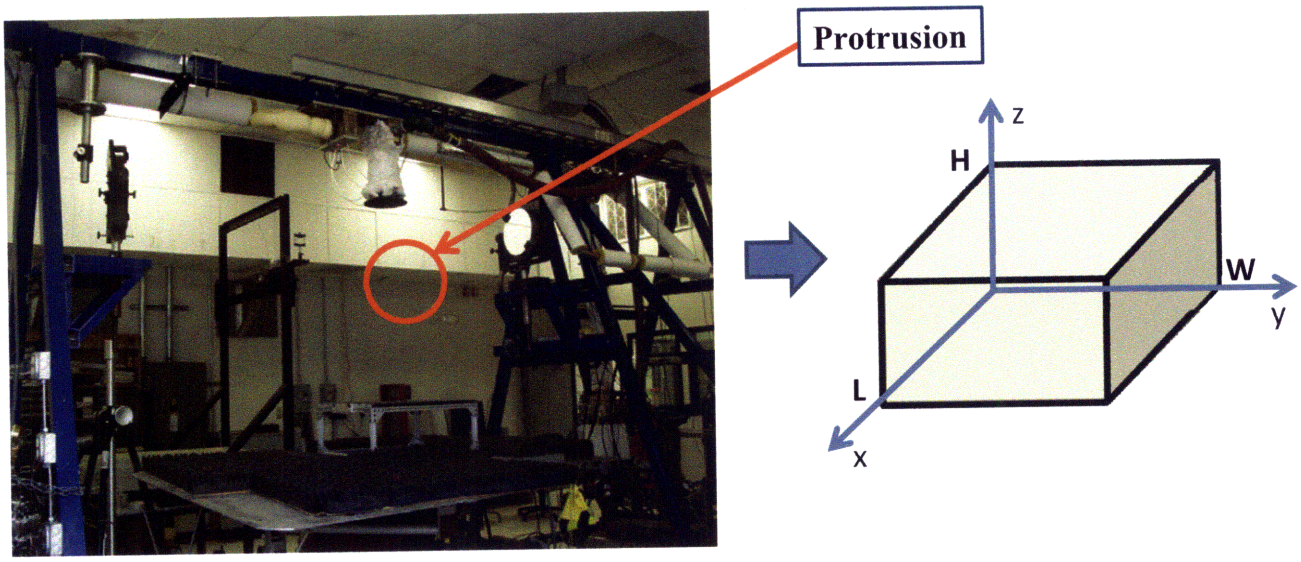

Figure 3.28: Schematic model of the STOVL room

wave equation was solved:

$$\phi_{xx} + \phi_{yy} + \phi_{zz} - \frac{1}{c^2}\phi_{tt} = 0$$

where ϕ is the velocity potential and c is the speed of sound. All subscripts stand for second order partial differentiation. Boundary condition on the surfaces is that all normal velocities are zero; that is, $\phi_x = 0, \phi_y = 0, \phi_z = 0$ at $x = L, y = W, z = H$, respectively. By separation of variables as a typical method to solve a partial differential equation, the following is obtained:

$$\phi = (\cos qx + \sin qx)(\cos ry + \sin ry)(\cos sz + \sin sz)(\cos \omega t + \sin \omega t)$$

with the condition of: $q^2 + r^2 + s^2 = \frac{w^2}{c^2}$, where q, r, s are constants. By substituting boundary conditions, one could further get the form:

$$\phi = \cos\frac{l\pi x}{L}\cos\frac{m\pi y}{W}\cos\frac{n\pi z}{H}(A\cos\omega_{lmn}t + B\sin\omega_{lmn}t)$$

where, $q = \frac{l\pi x}{L}$, $r = \frac{m\pi y}{W}$, $s = \frac{n\pi z}{H}$, and l, m, n, are integers $(= 0, 1, 2, 3, \cdots)$. It should be also noted that A and B are constants which can be determined by appropriate

initial conditions. However, initial conditions cannot be defined exactly in this case due to the complexity of the underlying physics of impinging jet problem. The final solution can be obtained by a proper superposition of each mode. It should be recalled that the main objective of this analysis is to clarify if the reflection by STOVL room results in a low frequency hump observed in a spectra plot. Therefore, the frequency of each mode by reflection should be further calculated. The frequency, f, can be obtained from ω above ($\omega = 2\pi f$):

$$f = \frac{c}{2}\sqrt{\left(\frac{l}{L}\right)^2 + \left(\frac{m}{W}\right)^2 + \left(\frac{n}{H}\right)^2}$$

where L, W, H are dimensions of STOVL room, $47ft$, $26ft$ (or) $20ft$, and $17.5ft$, respectively. It should be noted that since there is a protrusion of the wall as seen in Figure 3.28, in order to consider this effect, both of the two different dimensions are simply substituted into W. In this way, one could consider all effects of two different dimensions, although it may also include unnecessary modes - which is fine as long as all possibilities are taken into account. The calculated frequency of reflection is plotted in Figures 3.29 and 3.30, which represent all possible frequencies of the first ten modes and the first twenty modes from the room reflection, respectively. It can be observed that the frequency range of reflection by room matches exactly for the same range of low frequency hump. It should be noted that the amplitude of acoustic reflection cannot be determined here due to the uncertainty of the initial condition.

In addition, a slight change of boundary condition was applied for the case when the door of STOVL room is opened, thereby one of the wall representing a pressure release surface, not rigid surface (see Figure 3.31). It should be noted that the opened door changes the boundary condition only in a portion of one surface, however, it was assumed for simplicity that the surface as a whole represents the pressure release surface. As seen in Figure 3.31, there was little change - almost the same - of the frequency range by acoustic reflection.

In order to confirm the analysis above, an experiment is proposed. One may make a foam-wall around the ground plane, thus could remove the effect of reflection by

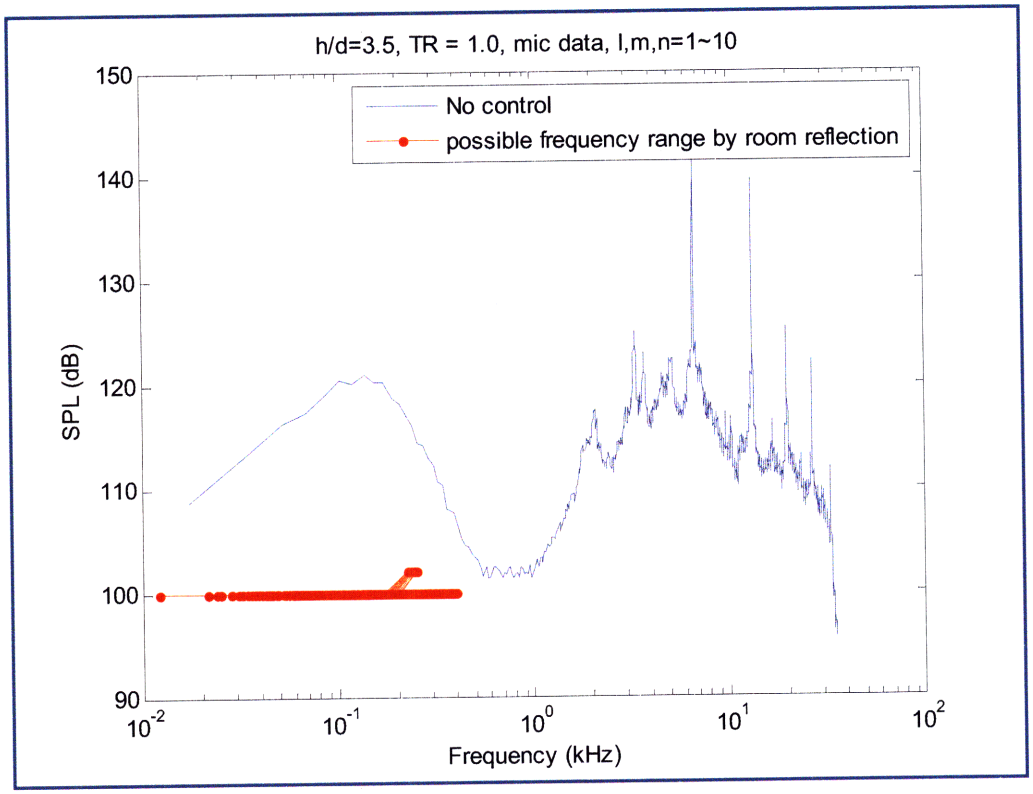

Figure 3.29: Frequency range of the reflected acoustic wave by STOVL room, mode 1~10 in each direction

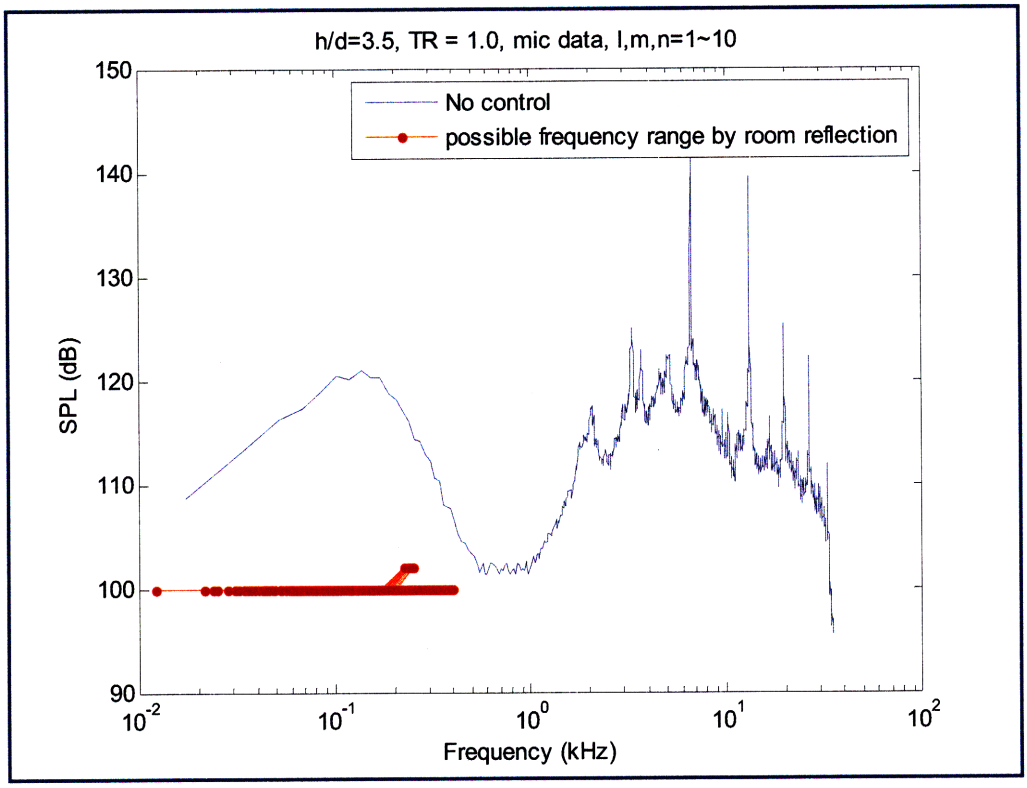

Figure 3.30: Frequency range of the reflected acoustic wave by STOVL room, mode 1~20 in each direction

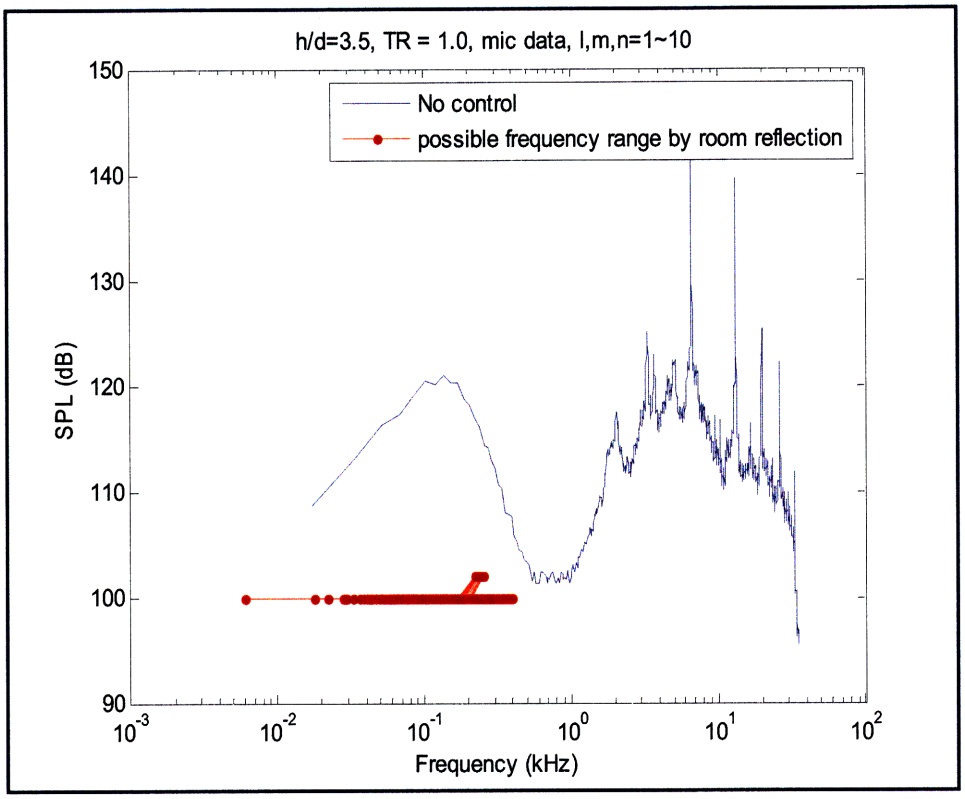

Figure 3.31: Frequency range of the reflected acoustic wave by STOVL room with the door open, mode 1~10 in each direction

a room. If spectra plot does not contain any low frequency hump then, it could be confirmed that the low frequency hump is due to the reflection by room. This thesis, however, does not include a result of proposed experiment due to the time constraint.

In this section, a rough analysis of acoustic reflection by room was described. Given that the low frequency hump is only observed in microphone data, it was assumed that this broadband hump in low frequency range is not coming from the impinging jet flow structure, but due to the acoustic reflection by STOVL room. A simple analysis led to a conclusion such that low frequency hump may be due to the reflection by a room, not due to the character of supersonic impinging jet flow, and also the experiment which could confirm this analysis is proposed.

3.5 Extremum Seeking Control

In this section, a particular control strategy to efficiently alter the control parameters to generate maximum and uniform noise reduction for overall jet operating condition is proposed. Since the OASPL of impinging jet flow field is a nonlinear function of h/d, NPR, TR, and so on, it is necessary to develop an adaptive feedback control strategy. Extremum seeking control - one of the feedback control method - is, in general, the way to achieve, if any, a desired extremum (maximum or minimum) output with the absence of the system model. Therefore, it would be a proper strategy for this study, in that supersonic impinging jet flow structure is hard to model exactly, and in that the desired output is a maximum noise reduction or a minimum OASPL value. The rationale of the extremum seeking control is very briefly described in this section, where further details can be found in [6]. This method employs a slow periodic perturbation added to the control input - starting from one's best guess, at the frequency much less than the dominant frequency range of control inputs by an order of magnitude. This perturbed input will create a periodic output signal which is in either in-phase or out-of-phase. In Figure 3.32, a positive slope indicates in-phase, where a negative slope corresponds to out-of-phase. Therefore, the control input (θ), fed back by output signal (y), is increased or decreased depending on if the output is in-phase or out-of-phase, respectively. The input signal (θ) is kept increased or decreased until the slope becomes zero, which means the output is an extremum value; the input signal at this time is referred to as θ^* in Figure 3.32. In order to employ this method in the current study, the output signal - Kulite^{TM} or microphone measurement - should be fed back to the control input, and also the control input should be perturbed periodically at very low frequency. It should be also noted that, in this study, the output is OASPL measured from the sensor which has to be a minimum value and the input is a pulsing parameter.

As described in section 2.3, there are total four control parameters associated with pulsed microjet, that is, pulsing frequency, duty cycle, supply pressure, and phase. Pulsing frequency, supply pressure and duty cycle are the parameters of our interest

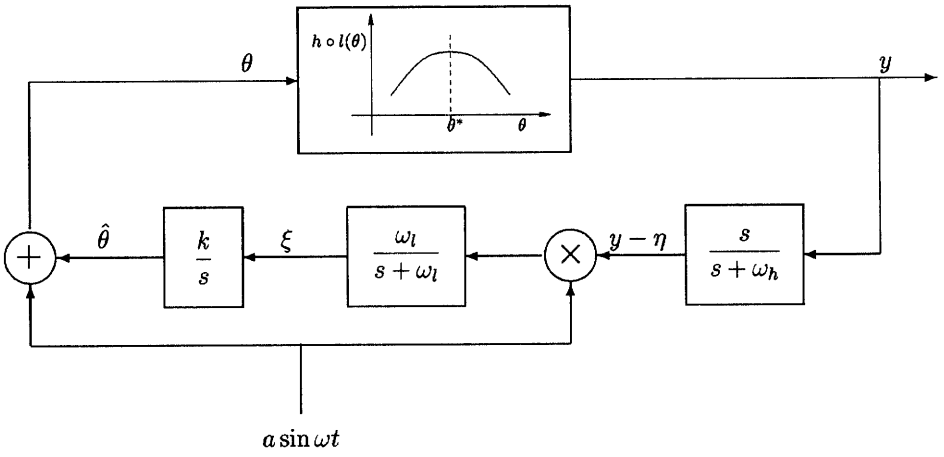

Figure 3.32: Schematic block diagram of extremum seeking control method [6]

amongst all. As stated in section 3.3.1, noise reduction is mostly dependent on a mass flow rate of microjets, since the key is the momentum which microjets deliver. It should be noted that supply pressure and duty cycle are the ones related to the mass flow rate of microjets; mass flow rate is directly proportional to the supply pressure, and higher duty cycle delivers larger mass flow rate at the same supply pressure for pulsed microjet. As stated in section 3.3.1, noise reduction is increased as supply pressure is increased by until certain supply pressure - which is referred to as saturated supply pressure. However, as described in section 3.3.1 - (1), since saturated supply pressure varies for each jet operating condition such as h/d or TR, and since a clear relation between duty cycle and noise reduction has not been clarified yet, therefore, an extremum control strategy would be useful for applications to these two parameters.

In order to implement this method in STOVL facility, the algorithm should be developed such that the input is increased or decreased automatically depending on whether the fed-back-output signal is in-phase or out-of-phase. However, implementation of this rationale into STOVL facility could be complicated since it would need some modifications of hardware. First, microjets should be replaced to the ones used in [3] so that they can be controlled all individually. In this way, pusling frequency and duty cycle could be altered via one single Labview^{TM} program; even the motor

is no more necessary to produce pulsing injection, thereby no more concerns about the inertia of the motor (see section 3.3.1-(3)). However, it may be still hard to perturb the supply pressure by low frequency excitation, since supply pressure is currently controlled manually by a pressure regulator of wheel-valve type; a modification of supply system of nitrogen gas is needed. Even if the supply pressure could be controlled electronically and thereby could be perturbed as desired, actual response at microjet exit should be carefully double-checked if microjet output follows the command signal.

As described in this section, the extremum control strategy, although some difficulties of implementation are expected, can be a sophisticated, elegant and efficient way to find optimal conditions of pulsed microjet in order to produce a maximum and uniform noise reduction in overall jet operating conditions.

Chapter 4

Active Control using High Frequency Actuator

4.1 Overview

In the previous sections, pulsed microjet using a rotating cap was used as the actuator. Since the pulsed microjet generated by rotating cap can operate in very limited, low frequency range (from 16Hz up-to 100Hz) compared to the impinging tone frequency which is in the range of several kilo-hertz, it is necessary to develop an actuator which can operate in high frequency range, that is, the one with high-bandwidth [36]. In this section, the actuator pulsing at high frequency range (which matches impinging tone frequency range) is described.

Solomon et al.[37] demonstrated the supersonic microjet actuator pulsing at 5∼10kHz range, based on the concept of Hartmann tube. As shown in Figure 4.1, the supersonic microjet - that is, supersonic jet coming out of small diameter tube - flows into a primary cavity, and impinges on the bottom of the cavity which is directly connected to four columns of micro-scale cylinder; and this is referred to as microjets. Since the flow is supersonic and underexpanded, shock structures can be observed [7]; which provides a fundamental mechanism of pulsing at high frequency in the resulted microjet flow. This *high frequency actuator* produces pulsed microjets at the frequency range of about 5 $\sim$ 10kHz, depending on the design parameters as well as other pa-

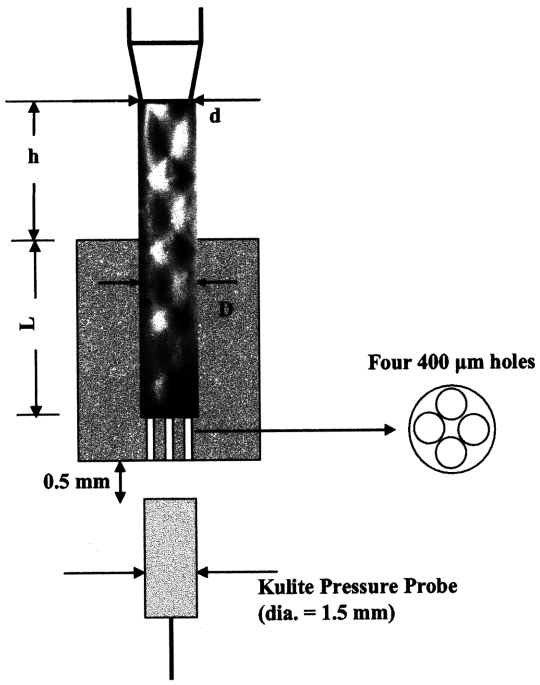

Figure 4.1: Schematic of micro-actuator [7]

rameter such as supply pressure. Since the pulsing frequency range is close to the impinging tone frequency, the expectation was that it could be applied to the STOVL facility, thereby to actively suppress impinging tones; therefore, it was expected that microjets pulsing at the same frequency range as the impinging tone frequency could result in more efficient control [36].

In the following sections, the design and control parameters of the actuator is described, and some of initial test results are shown. Since the description of the high frequency actuator in this thesis is yet only the initial step, further careful investigation is necessary in the future by means of more experiments, in order to analyze the effect of high frequency actuator on impinging jets and thus to develop the appropriate control strategy using this actuator.

4.2 Actuator Description: Realization of Control Parameter

4.2.1 Overview

Since the mechanism of producing pulsed action in the high frequency actuator differs from the one with rotating cap, the control method of pulsing parameters would be different. Pulsing frequency is determined by several parameters such as design parameters of h, L (which represents the distance from the primary jet exit to the entrance of first cavity, the height of the first cavity, respectively - as shown in Figure 4.1), as well as supply pressure, and so on [7]; for example, if h or L is increased, pulsing frequency is decreased. It should be also noted that the supply pressure of microjets and pulsing frequency in this actuator are not independent from each other. For instance, pulsing frequency can be varied by increasing or decreasing supply pressure; if supply pressure is increased, pulsing frequency is increased as well, and vice versa. Therefore, control strategy using this high frequency actuator should be very carefully determined. Also, in order to maximize supply pressure at the appropriate pulsing frequency, the design parameters of h and L should be carefully chosen, since once the actuator is designed and fabricated for the experimental set up, it can not be easily modified. In what follows, the initial choice of design parameters and some of the test results are demonstrated.

4.2.2 Particular design of the actuator

For the initial test, the actuator was designed and fabricated with certain parameter values: h=1.65mm, L=8mm, the space between microjets is 1.66mm (thus, with four microjets, the width of second cavity is 6.64mm), the height of second cavity is 1mm, the diameters of primary jet and first cavity are 1mm and 1.6mm, respectively (see Figures 4.2 and 4.3). Figure 4.2 shows the schematic of the modified design of high frequency actuator to be incorporated with the lift plate. Total four modules, each of which has four microjets, are incorporated with the lift plate; thus total sixteen

microjets are used. In order to distribute microjets as uniformly as possible at the periphery of the nozzle exit, microjets are arranged in linear array. Each microjet has the same diameter as the one with rotating cap - 400μm, and also has inclination angle of 60° from the main jet axis. It should be noted that the particular design parameter described in this section is one of possible choices, as the first step to develop a suitable actuator for active control of supersonic impinging jet; the optimal design of the actuator, with many design parameters such as h, L, the number of microjets per one module, microjet-spacing, and so on, should be further investigated. Also, in this particular set up, the differences between high frequency actuator and the one using rotating cap are as follow: first, sixteen microjets are not uniformly distributed as the one with rotating cap, rather, each module composed of four microjets is located at each corner on the plane by 90° with respect to each other (see Figure 4.3); also, the mass flow used for the high frequency actuator is smaller than the one with rotating cap. Four steel tubes are used for the primary jets of this actuator, where total sixteen of (the same diameter) steel tubes are used for microjets of the one with rotating cap. Moreover, the actual mass flow coming out of the microjet exit is only a fraction (maximum 64%) of the mass flow at the inlet of primary jet, thus the mass flow at given input pressure for high frequency actuator is less than before; rough calculation gives $0.25 \times 0.64 = 16\%$. Therefore, it should be taken into account when the noise reduction is compared between high frequency actuator and the one with rotating cap.

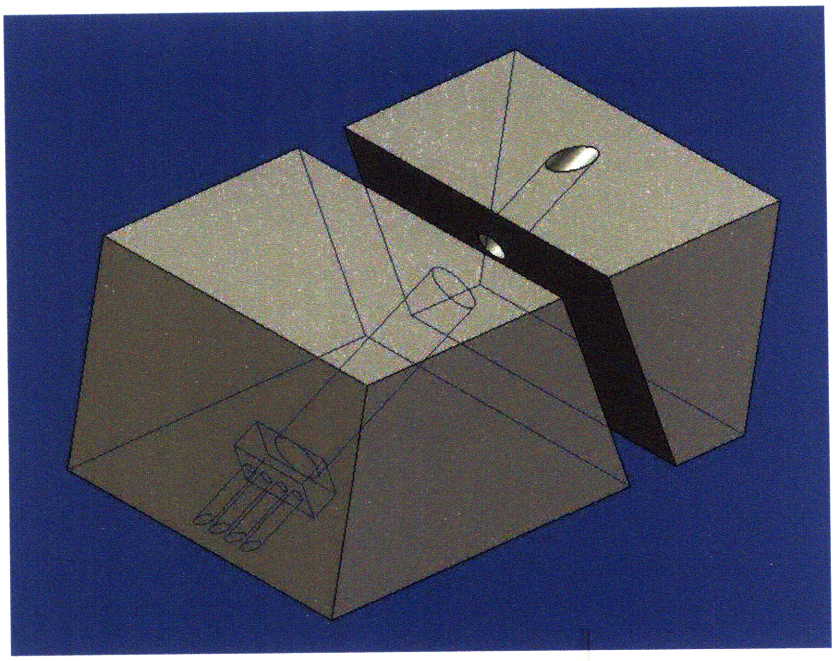

Figure 4.2: Schematic of the modified design of high frequency actuator

4.2.3 Characterization of the microjet parameters

As mentioned in 4.2, pulsing frequency can be varied by several parameters. However, once the design parameter is chosen and the actuator is fabricated, supply pressure is the main parameter that can vary pulsing frequency. Therefore, one need to clarify the relation between supply pressure and pulsing frequency before the actuator is applied to main experiment; in this section, the characteristic of the actuator is examined.

In order to incorporate the high frequency actuator with the lift plate, a small plate that includes four modules of high frequency actuator (one primary jet and four microjets per one module) as shown in Figure 4.4 is used; it is combined with the lift plate, and microjets were characterized with main jet OFF. Since every else set up is the same as when main jet is running, the same sensors (described in section 2.2.2) are used to characterize the microjets; since Kulite^{TM} pressure transducer on the ground plane records the pressure response in normal direction, microphone was used to capture pulsing frequency. Supply pressure was increased from 50psig up-to 160psig, and the followings are found: 1) by up-to 70psig, nothing could be distinguished, and as seen in spectra plot in Figure 4.5, microjets were not pulsing,

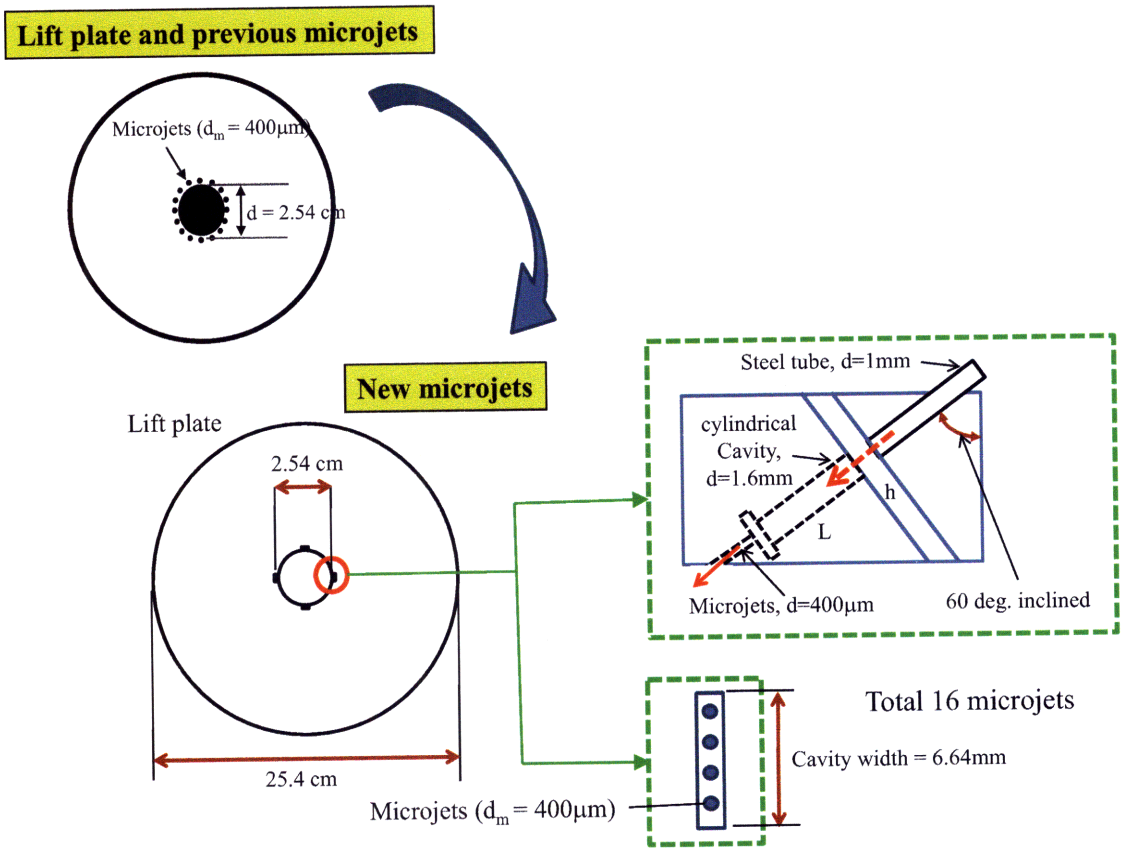

Figure 4.3: Schematics of actuator configurations: the one with a rotating cap and high frequency actuator

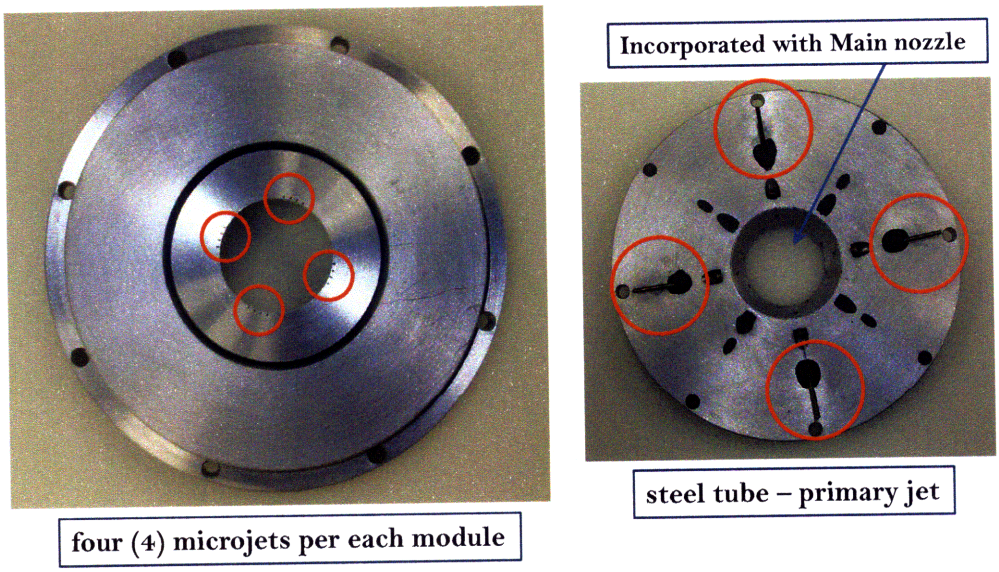

Figure 4.4: High frequency actuator incorporated with lift plate: four primary jets (1mm-diameter) and sixteen microjets (0.4mm-diameter)

but to be just unsteady flow; 2) between 70 and 80psig, the sound of microjets were cracking, although it does not contain any peak in the spectra plot yet (see Figure 4.5); 3) at about 85psig, microjets started pulsing at 4.4kHz; 4) as the supply pressure is increased by 1psig, pulsing frequency is increased by 0.1kHz; 5) pulsing frequency was increased up-to 6.1 $\sim$ 6.2kHz, which was realized by supply pressure of about 102psig, and above this pressure, pulsing frequency was kept at 6.1kHz, where the amplitude of the peak keeps increasing; and also, the shape of spectra becomes more clear with a high amplitude-peak at 6.1kHz and its harmonics (see Figure 4.5); 6) when supply pressure was kept increased, above 120psig, pulsing sound was gone, which is now the same as below 70psig. However, the spectra plot in Figure 4.6 shows it has somewhat high amplitude tone over 20kHz, which is not an audible frequency for human; 7) this high amplitude peak over 20kHz is gone as well when supply pressure is increased above 130psig, and there is no high amplitude peak observed any more for the highest supply pressure range. Therefore, with this particular high frequency actuator, available pulsing frequency range is from 4.4kHz to 6.1kHz by increment of 0.1kHz via increasing supply pressure by 1psig. As seen in Figures 4.5 and 4.6, the shape of spectra plot is different for each range of supply pressure; before cracking

(~70psig), cracking (70~84psig), pulsing (85~102psig), after pulsing frequency is saturated (102~120psig), after pulsing sound is gone (120psig and above), and the highest supply pressure range (above 130psig). It should be noted that as the tests are repeated, certain supply pressure does not give the same pulsing frequency all the time; pulsing frequency sometimes shifts up or down by 0.1~0.4kHz. This may be due to the lack of high accuracy of supply system for nitrogen gas to the microjets. Since nitrogen gas is supplied to microjets via manual wheel-valve pressure regulator, it is hard to repeat the exact same supply pressure as desired. Therefore, in the main experiments, microjets were always characterized before and after the main jet running, in order to clarify the exact control parameters and check the repeatability. In the test result which will be shown in the next section, pulsing frequency and supply pressure are specified for each case.

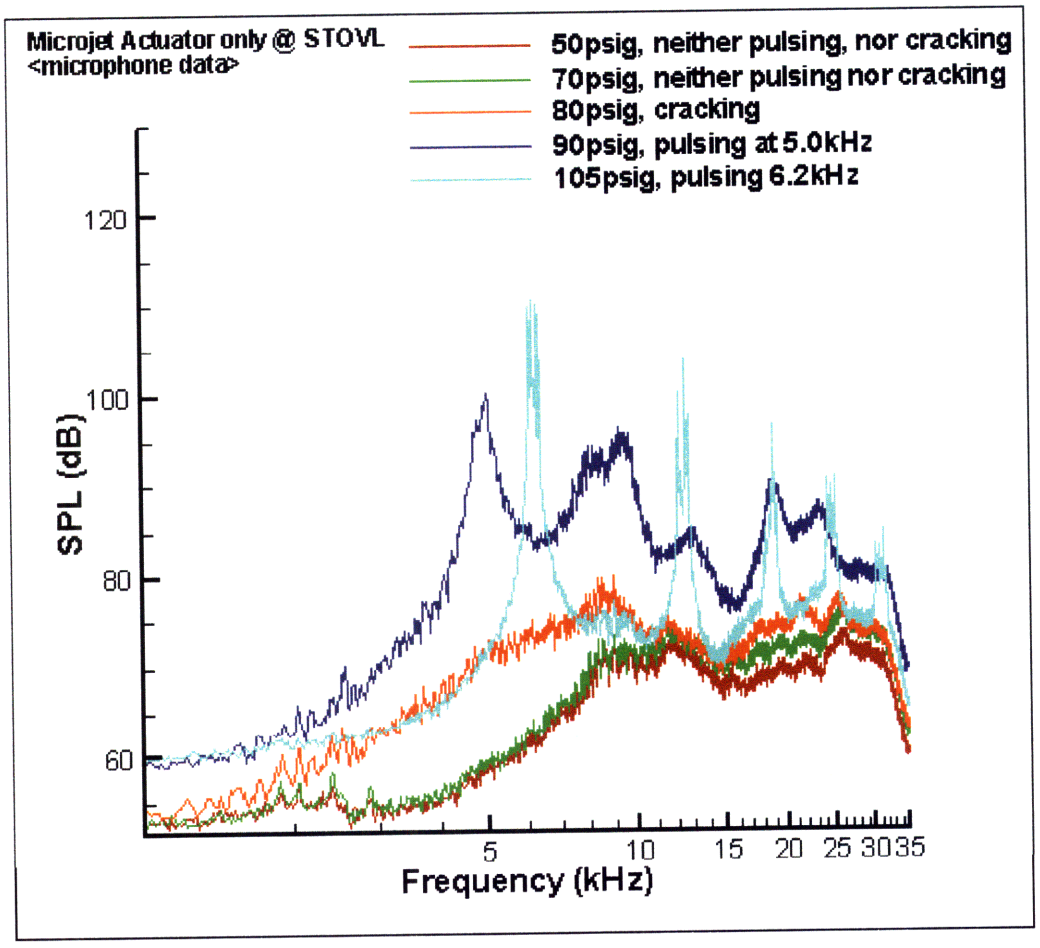

Figure 4.5: Spectra plots of high frequency actuator; measured at the microphone

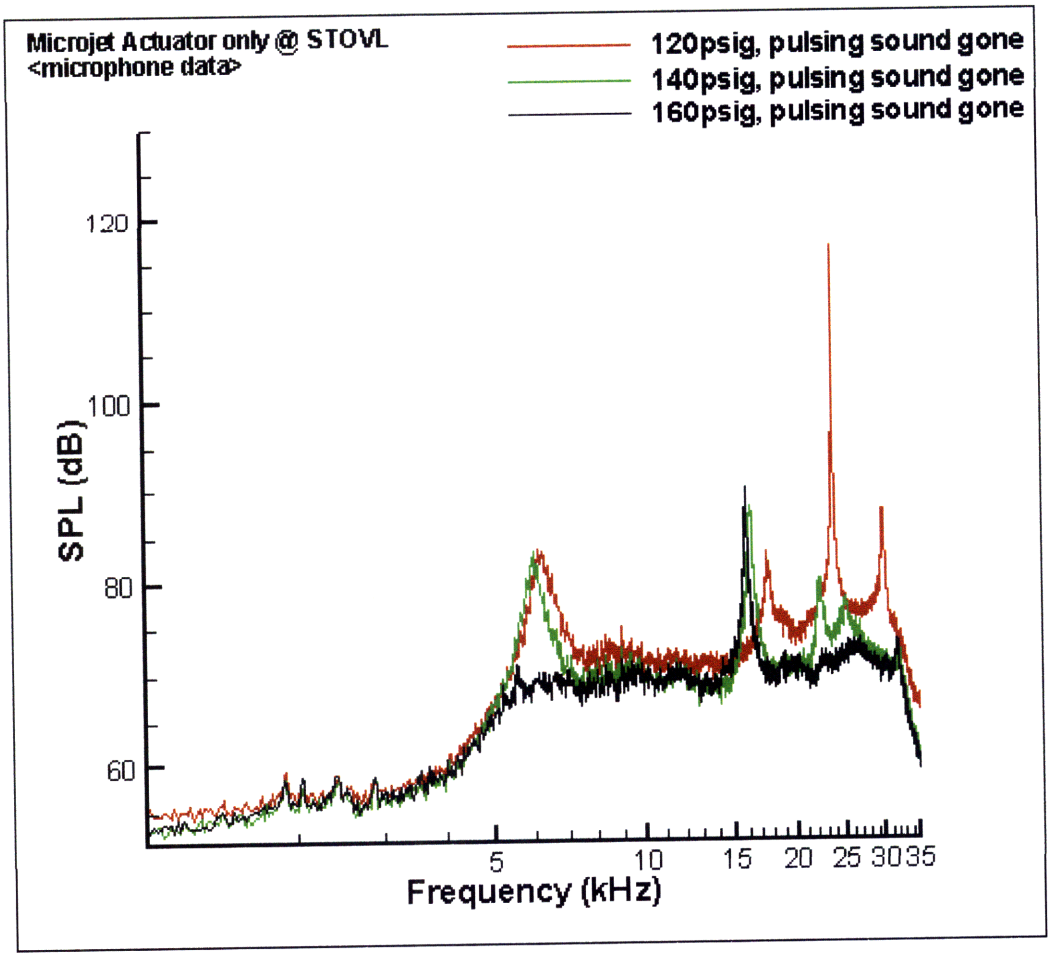

Figure 4.6: Spectra plots of high frequency actuator; measured at the microphone

4.3 Observations from Initial Test: Effect of High Frequency Actuator

4.3.1 Overview

As stated in section 4.1, it was expected that high frequency actuator could lead to overall noise reduction as well as suppression of impinging tones. As will be shown in this section, the high frequency actuator has a strong impact on the impinging tones. However, significantly more work remains to be done in terms of realizing the full potential of this device as an effective noise suppressor. Suitable control strategies as well as associated hardware modifications have to be carefully investigated.

4.3.2 Experimental set up and test conditions

The same experiment set up as well as procedures (as described in section 2), except for a few changes described in this section, were used to examine the effect of high frequency actuator on supersonic impinging jet. In this case, only one Kulite^{TM} pressure transducer was mounted on the ground plane (at $x/d = 0$ from the center of the nozzle), where another 5-psid Kulite^{TM} pressure transducer (model XCS-062-5D) was mounted on the lift plate (at $x/d = 3$ from the center of the nozzle); when pulsed microjet was generated using rotating cap, unsteady pressure was not measured on the lift plate due to the vibration of the motor (which enabled rotating cap to produce pulsed microjet). Also, different model of data acquisition card (NI BNC-2090) was used in this experiment; by checking the background noise level and comparing it with the one recorded by previous data acquisition card, one could assume the change of data acquisition card would not make a big difference. The main jet was operated (as the same as described in section 2) at the following conditions: ideally expanded, NPR = 3.7 with Mach number = 1.5, and only cold jet (TR = 1.0) for $h/d = 3.5$, 4.0, 4.5 were tested at this time.

4.3.3 Results

In this section, only the test result for $h/d = 4.5$ is presented, since the most of observations described here are common with other height conditions. It should be also noted that the results presented in this section include only the microphone data, since the microphone could pick up the signal from any direction whereas the Kulite^{TM} pressure transducer measure the signal only from the normal direction; since spectra plots from any sensor (either microphone or Kulite^{TM}) represent mostly the same characters of the impinging jet flow, the microphone data may be enough to discuss the noise reduction by the actuator.

Before looking at the result, it should be again reminded that in the range of supply pressure from 50psig to 70psig, microjet is not yet pulsing; between 70 and 80psig, it starts cracking, and between 85 and 90psig, microjets starts pulsing; it produces pulsing until pulsing frequency is saturated at 6.1kHz with supply pressure of 105psig, and keeps pulsing at 6.1kHz until 120psig; above 120psig, microjet produces high amplitude peak at around 20kHz until the pressure of 130psig, and stops pulsing above then (see Figures 4.5 and 4.6). As seen in Figure 4.7, maximum noise reduction was generated at about 175psi (= 160psig); at 85psi (= 70psig), noise reduction is a little less than at 175psi, however, is larger than at supply pressure where pulsed microjet is produced. It should be noted that noise reduction gets larger as supply pressure goes up until before it starts cracking or pulsing. When microjets start cracking, noise is a little increased, and when microjets start pulsing, noise reduction is less than not-pulsing-case. When microjet stops pulsing at 6.1kHz (around 120psig), noise reduction gets larger as supply pressure is increased. Since as supply pressure is increased, the momentum that microjets deliver into shear layer gets bigger, one could easily expect that noise reduction will be larger; and this explains for the supply pressure range above 120psig. When microjets are pulsing, however, less noise reduction is made than the pressure of 70psig, even though supply pressure is higher for the range of pulsing (88~110psig); this may be clarified by looking at the spectra plots for each case, which will be discussed from the next paragraph. It should also

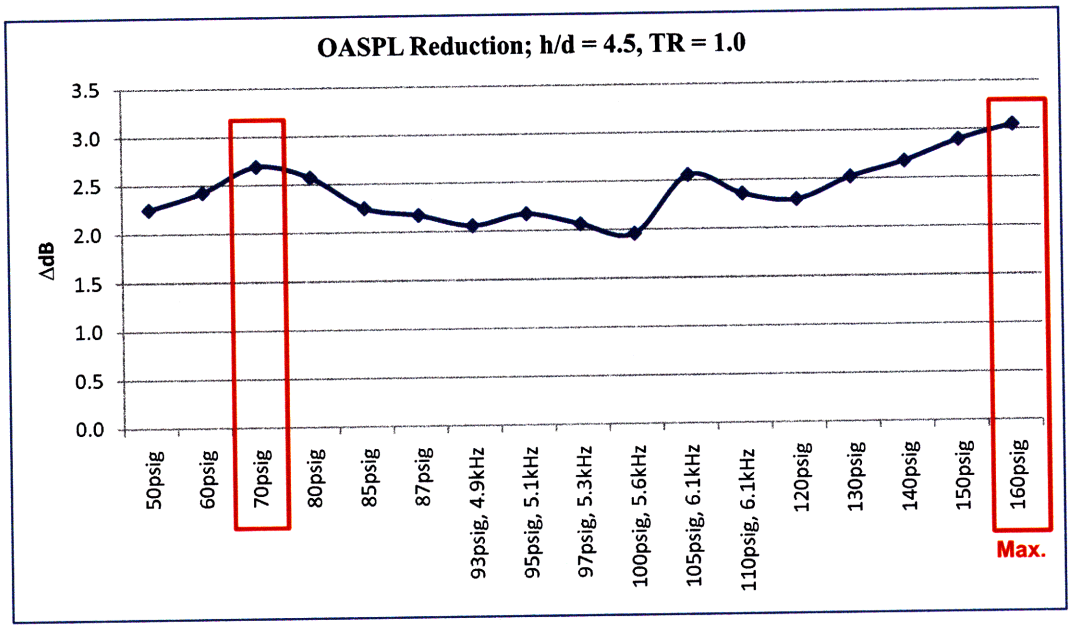

Figure 4.7: OASPL reduction versus supply pressure (pulsing frequency), TR = 1.0, $h/d = 4.5$

be worth noting that OASPL reduction is not large as the case using pulsed microjets with rotaing cap (maximum noise reduction is 3.0dB using high frequency actuator, and 5.3dB using pulsed microjet with rotating cap, for h/d=4.5, TR = 1.0). However, considering the mass flow used for high frequency actuator is much less than before as stated in section 4.2.2, less noise reduction than before is not a disappointing result, rather it is expected that using more modules (microjets) could be more effective.

In Figures 4.8 $\sim$ 4.10, spectra plots are shown for baseline case at h/d=4.5 as well as for controlled cases at certain supply pressures. As seen in Figure 4.8, when microjets are activated - not pulsing yet - original impinging tones are completely eliminated, where new peak and its harmonics are observed at different frequencies. Even though the amplitude of new peak is almost the same as the original impinging tones, one should compare the width of impinging tone with that of new tone; the bandwidth of new peak is more narrow than impinging tones, thus has less density in sound pressure level. This is consistent with why OASPL is reduced with microjet control. When pulsed microjet is applied, for example at 5.3kHz (with 97psig) which is the same as impinging tone frequency, it can be observed that the amplitudes of

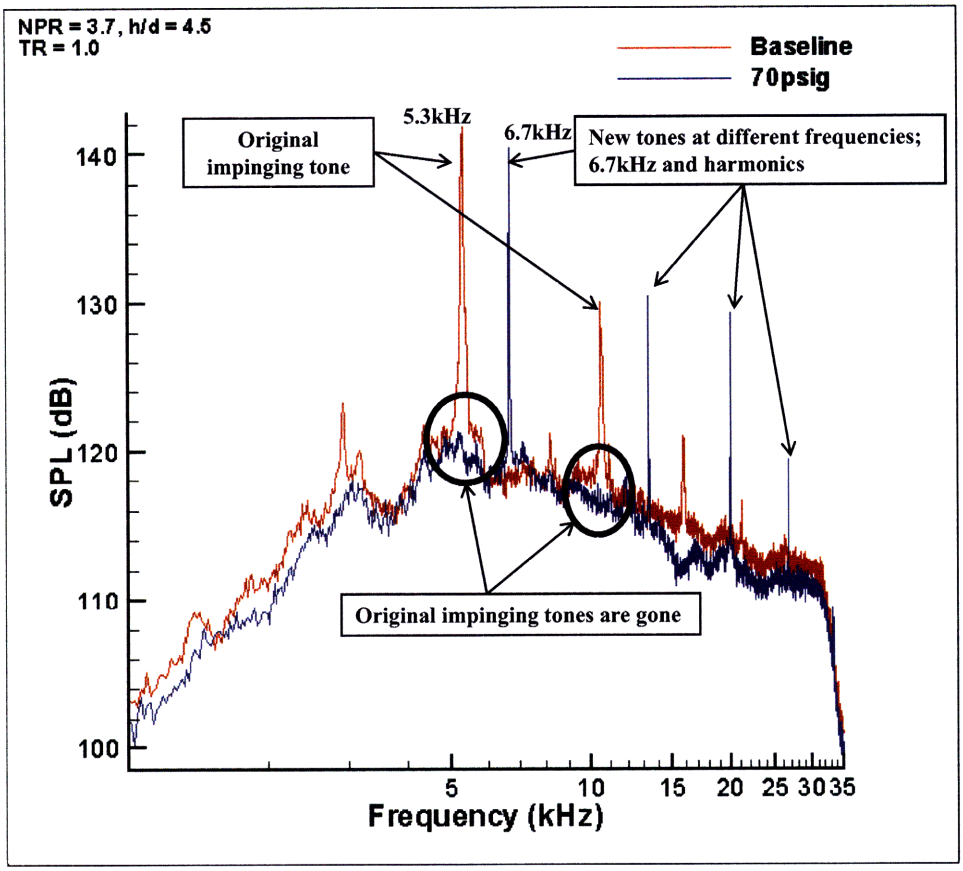

Figure 4.8: Spectra plots: baseline, and controlled case (70psig), TR = 1.0, h/d = 4.5, measured at the microphone

new tones are increased as supply pressure goes up (see Figure 4.9). This may be the reason why noise increased again even though supply pressure is increased (thus the momentum microjets deliver is increased). When supply pressure is increased further up-to 160psig, however, the amplitudes of new tones are suppressed, and thus larger noise reduction is achieved (as seen in Figure 4.10).

It should be noted that there is any peak observed, in neither spectra of baseline case nor spectra of actuators, at the frequency where new peak cropped up in controlled cases. Figure 4.11 clearly shows that there is no frequency match among the peaks in baseline case and the peak of the actuator and new peaks in controlled cases. It is also worth noticing that new peaks cropped up at the consistent frequency all the time no matter what supply pressure (and pulsing frequency for some cases) are given.

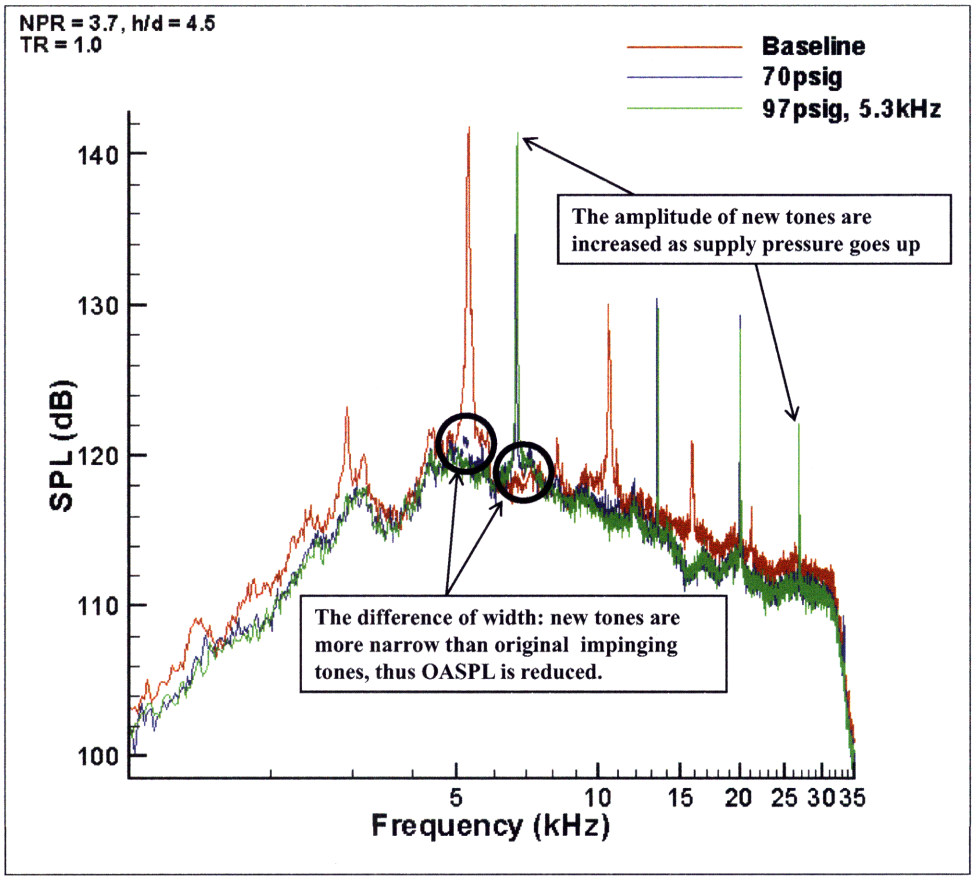

Figure 4.9: Spectra plots: baseline, and controlled case (70, 97psig - 5.3kHz), TR = 1.0, $h/d = 4.5$, measured at the microphone

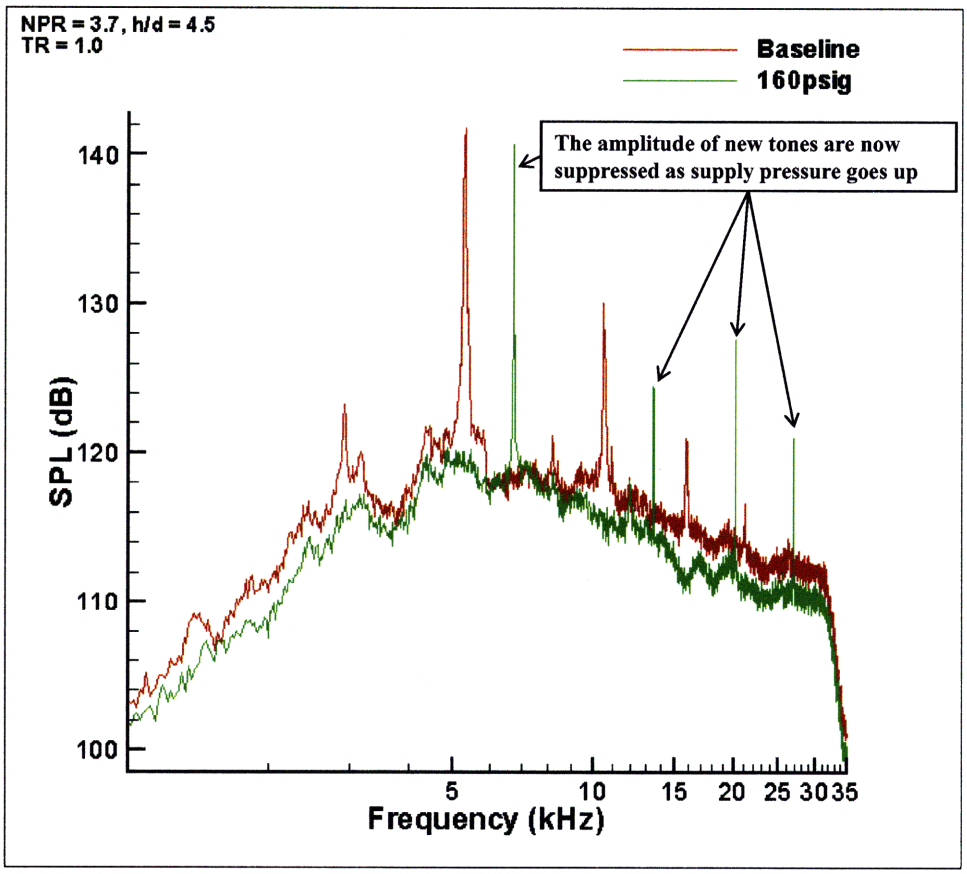

Figure 4.10: Spectra plots: baseline, and controlled case (160psig), TR = 1.0, h/d = 4.5, measured at the microphone

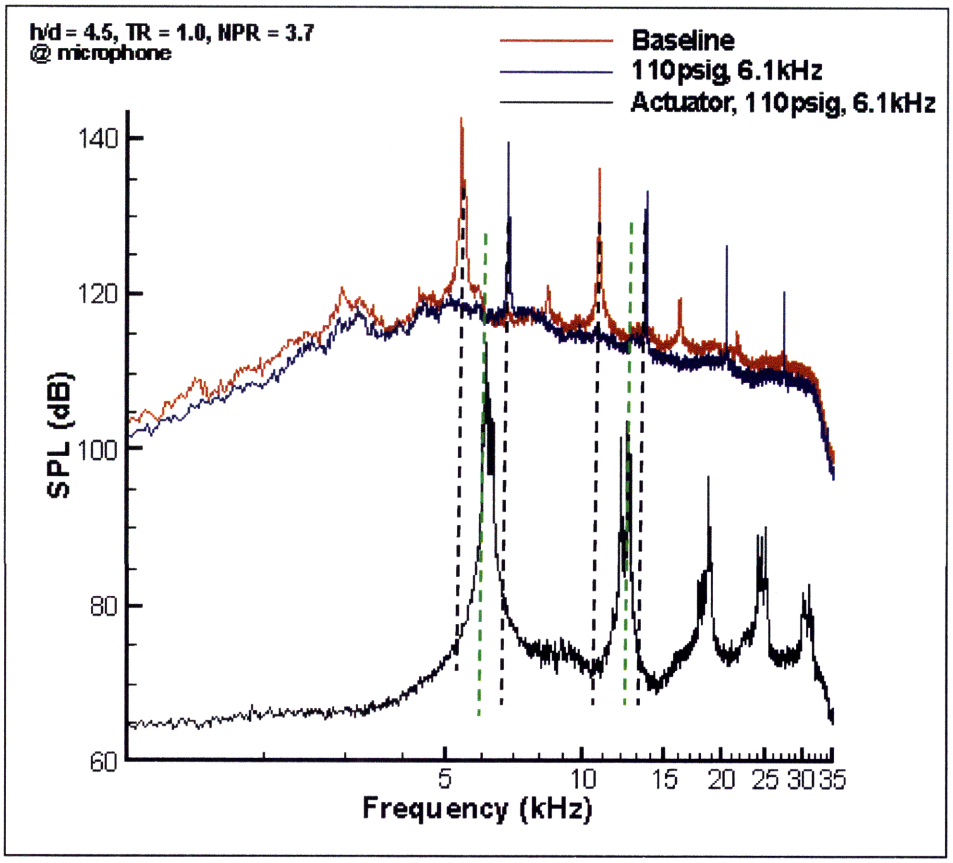

Figure 4.11: Spectra plots: baseline, controlled case (110psig), and the actuator only (110psig), TR = 1.0, $h/d = 4.5$

Based on these observations, the question is then raised such that where these new peaks are coming from; if they are shifted from impinging tones from the interaction between impinging jet and microjet, although the exact mechanism of interaction is yet unknown. Similar observation was demonstrated in other studies that original peak in cavity flow oscillations is split into two peaks when control is applied and this phenomenon is referred to as "peak-splitting" [38]; Fleifil et al. [39] also dealt with new peaks cropping up in combustor pressure spectra with active control and referred to it as *second peak* . This phenomenon is often known as "waterbed effect"; if the amplitude of certain frequency is reduced, then the amplitude of other frequency may have to get larger. In other words, when the amplitude of certain frequency is suppressed with a control applied, the amplitude of other frequency may be excited and increased. The observation, described in this section, of new peaks cropping up at different frequency may be along the same line with other references [38, 39]; although the exact reason and mechanism is yet unknown and may be further investigated in the future. In addition, as stated in section 3.5, if supply system of nitrogen gas for the microjets could be changed to be a way of electronic control, supply pressure (and pulsing frequency) would be more accurately and promptly varied, and thereby make it easier to implement a feedback control strategy (such as extremum seeking control strategy, described in section 3.5). With an appropriate control strategy, if one could clarify how to suppress impinging tones without new peaks cropping up using high frequency actuator, then it may be possible to achieve uniform and consistent noise reduction with less mass flow rate in overall jet operating conditions, which is a fundamental goal of this study.

Chapter 5

Conclusion

In this thesis, the active control of supersonic impinging jet flow using pulsed microjet injection is examined in order to achieve a consistent and robust performance of suppression of impinging tones at overall jet operating conditions. The pulsing action was accomplished by way of a saw-toothed rotating cap that was incorporated in the lift plate which periodically blocked and unblocked the microjet flow as it rotated.

The effect of pulsed microjet with a new motor and controller was investigated for each control parameter. These new devices were introduced in order to efficiently alter pulsing parameters via only software development. It was originally expected that a stepper motor and controller could efficiently vary duty cycle without changing a rotating cap. However, due to the inertia of the motor in the frequency range of operation, it did not work properly as expected. More experiments were conducted to find the effect of pulsing parameters. Supply pressure was increased up-to 190psi, which increases the total mass flux of microjets only by 0.5% (than 115psi), and the supply pressures for both steady and pulsed microjets where the noise reduction is saturated were found - which is referred to as saturated supply pressure. It was also found that pulsed microjet gives more noise reduction than steady microjet with the same mass flow rate, at certain range of supply pressure. Moreover, pulsed microjet was able to generate the same amount of noise reduction as steady microjet even with less mass flow rate. Therefore, pulsed microjet could be more effective than steady

microjet, in that it can save mass flow rate to have the same control ability. Using rotating cap corresponding to duty cycle of 74% confirmed pulsed microjet gives more noise reduction than steady microejt with the same mass flow rate. It should be also noted that in particular cases, duty cycle of 74% reduced more amount of noise level than the case with duty cycle of 56%. However, due to the limitation of the time, no further observation could be made on the effect of duty cycle. On the other hand, the noise reduction was hardly dependent on varying pulsing frequency. It was also found that there was no additional noise reduction at low frequency pulsing at 10~20Hz with new motor and controller. Since, moreoever, no low frequency peak was found in the spectra plot of even baseline case, no other investigations on the low frequency mode could be made. Instead, the low frequency hump was observed in both [5] and current study, the possible source of which is proposed - acoustic reflection by a room. When the temperature of the main jet was increased up-to TR = 1.2, pulsed microjet appeared to be more effective than for the main jet of TR = 1.0; the range of supply pressure where pulsed microjet gives more noise reduction than steady microjet with the same mass flow rate became broader for hotter main jet.

In addition, the concept of extremum control strategy was introduced, which could be an efficient and elegant way to find an optimal condition of pulsing parameter, and its expected effectiveness and difficulties in implementation were briefly described. Also, the high frequency actuator for active control of supersonic impinging jet is demonstrated. It is yet an initial step to develop an effective actuator to suppress impinging tones with least mass flow rate. With certain choices of design parameters, high frequency actuator was fabricated and tested in STOVL facility. The effect of high frequency actuator on noise reduction was examined, and observations from the spectra plot are demonstrated. It was found that high frequency pulsing is not yet found to be effective, since new peaks crop up at different frequencies other than original impinging tone frequency with microjet control. However, with further investigations, a suitable control strategy could be developed for this high frequency actuator.

Bibliography

[1] B. J. Greska. *Supersonic Jet Noise And Its Reduction Using Micorjet Injection.* PhD thesis, Florida State University, 2005.

[2] I. M. Choutapalli. *An Experimental Study of A Pulsed Jet Ejector.* PhD thesis, Florida State University, 2007.

[3] P. A. Ragaller. The reduction of supersonic jet noise using pulsed microjet injection. Master's thesis, Massachusetts Institute of Technology, 2007.

[4] A. M. Annaswamy, J. J. Choi, and F. S. Alvi. Pulsed microjet control of sueprsonic impinging jets via low-frequency excitation. *Journal of Systems and Control Engineering*, 222(5):279–296, 2008.

[5] J. Choi. *Active Noise Control in Supersonic Impinging Jets Using Pulsed Microjets: Actuator Design, Reduced-Order Modeling.* PhD thesis, Massachusetts Institute of Technology, 2006.

[6] K. B. Ariyur and M. Krstic. *Real-Time Optimization by Extremum-Seeking Control.* Wiley-Interscience, 2003.

[7] J. T. Solomon, R. Kumar, and F. S. Alvi. Development and characterization of high bandwidth micro-actuator. *Proceedings of FEDSM*, (2008-55032), 2008.

[8] M. Gad-el Hak. *Flow Control : Passive, Active, and Reactive Flow Management.* Cambridge University Press, 2000.

[9] W. Linke. *Über* den strömungswiderstand einer beheizten ebenen platte. *Luftfahrt-forschung*, 19:157–160, 1942.

[10] C. W. Frick and C. B. McCullough. Tests of a heated low drag airfoil. *NACA ARR*, 1942.

[11] H. W. Liepmann and G. H. Fila. Investigations of effects of surface temperature and single roughness elements on boundary layer transition. *NACA Report*, (890), 1947.

[12] L. Lees. The stability of the laminar boundary layer in a compressible fluid. *NACA Report*, (876), 1947.

[13] G. B. Schubauer and H. K. Skramstad. Laminar boundary-layer oscillations and transition on a flat plate. *NACA Report*, (909), 1948.

[14] F. G. Collins and J. Zelenevitz. Influence of sound upon separated flow over wings. *AIAA Journal*, 13:408–410, 1975.

[15] K. K. Ahuja, R. R. Whipkey, and G. S. Jones. Control of turbulent boundary layer flows by sound. *AIAA Paper*, (83).

[16] S. S. Papell. Vortex generating flow passage design for increased film-cooling effectiveness and surface coverage. *NASA TM*, (83617).

[17] R. G. Bradley and W. O. Wray. A conceptual study of leading-edge-vortex enhancement by blowing. *Journal of Aircraft*, 11:33–38, 1974.

[18] J. Johnston and M. Nishi. Vortex generator jets - a means for passive and active control of boundary layer separation. *AIAA paper.*

[19] A. Powell. The sound-producing oscillations of round underexpanded jets impinging on normal plates. *Journal of the Acoustical Sciety of America*, 83(2):515–533, 1988.

[20] G. Neuwerth. Acoustic feedback of subsonic and supersonic free jet which impinges on an obstacle. *NASA TT*, pages F–15719, 1974.

[21] C. K. W. Tam and K. K. Ahuja. Theoretical model of discrete tone generation by impinging jets. *J. Fluid Mech.*, 214:67–87, 1990.

[22] A. Powell. On edge tones and associated phenomena. *Acoustica*, 3:233–243, 1953.

[23] M. Sheplak and E. F. Spina. Control of high-speed impinging-jet resonance. *AIAA Journal*, 32(8):1583–1588, 1994.

[24] C. Shih, F. S. Alvi, and D. Washington. Effects of counterflow on the aeroacoustic properties of a supersonic jet. *Journal of Aircraft*, 36(2):451–457, 1999.

[25] R. Elavarasan, A. Krothapalli, L. Venkatakrishnan, and L. Lourenco. Suppression of self-sustained oscillations in a supersonic impinging jet. *AIAA Journal*, 39(12):2366–2373, 2001.

[26] F. S. Alvi, C. Shih, R. Elavarasan, G. Garg, and A. Krothapalli. Control of supersonic impinging jet flows using supersonic microjet. *AIAA Journal*, 41(7):1347–1355, 2003.

[27] J. Choi, Annaswamy A. M., Egungwu O., and F. S. Alvi. Acive noise control of supersonic impinging jets using pulsed microjets. *AIAA Paper*, (2005-0798), 2005.

[28] J. Choi, A. M. Annaswamy, F. S. Alvi, and H. Lou. Active control of supersonicm impingingement tones using steady and pulsed microjets. *Experiments in Fluids*, 41(6):841–855, 2006.

[29] J. Choi, Annaswamy A. M., and F. S. Alvi. Pulsed microjet control of supersonic impinging jets: A reduced-order model. *AIAA Paper*, (2006-2601), 2006.

[30] K. G. Iyer. Experimental investigation of supersonic impinging jets in stovl configuration. Master's thesis, Florida State University, 1999.

[31] G. Garg. Unsteady flow properties of a supersonic impinging jet. Master's thesis, Florida State University, 2001.

[32] A. Krothapalli, E. Rajakuperan, F. S. Alvi, and L. Lourenco. Flow field and noise characteristics of a supersonic impinging jet. *Journal of Fluid Mechanics*, 392:155–181, 1999.

[33] H. Lou. *Control of supersonic impinging jets using microjets.* PhD thesis, Florida State University, 2005.

[34] R. Kumar, S. Lazic, and F. S. Alvi. Active control of high temperature supersonic impinging jets. *AIAA Paper*, (2008-360), 2008.

[35] S.M. Yahya. *Fundamentals of Compressible Flow.* Halsted Press, a Division of John Wiley and Sons, Inc., New York, 1982.

[36] A. M. Annaswamy, M. Fleifil, J. W. Rumsey, R. Prasanth, J. P. Hathout, and A. F. Ghoniem. Thermoacoustic instability: model-based optimal control designs and experimental validation. *IEEE Transactions on Control Systems Technology*, 8(6):905–918, 2000.

[37] J. T. Solomon, R. Kumar, and F. S. Alvi. High bandwidth micro-actuators for active flow control. *AIAA Paper*, (2008-3042), 2008.

[38] C.W. Rowley, D.R. Williams, T. Colonius, R.M. Murray, and D.G. Macmynowski. Linear models for control of cavity flow oscillations. *Journal of Fluid Mechanics*, 547:317–330, 2006.

[39] M. Fleifil, J. P. Hathout, A. M. Annaswamy, and A. F. Ghoniem. The origin of secondary peaks with active control of thermoacoustic instability. *Combustion Science and Technology*, 133:227–260, 1998.